63-3 5

405041

405041

MEMORANDUM
RM-3531-PR
APRIL 1963

MONTE CARLO CALCULATIONS OF THE TRANSPORT OF 14 MEV NEUTRONS IN THE ATMOSPHERE

J. I. Marcum

PREPARED FOR:
UNITED STATES AIR FORCE PROJECT RAND

The RAND Corporation
SANTA MONICA • CALIFORNIA

MEMORANDUM
RM-3531-PR
APRIL 1963

MONTE CARLO CALCULATIONS OF THE TRANSPORT OF 14 MEV NEUTRONS IN THE ATMOSPHERE

J. I. Marcum

This research is sponsored by the United States Air Force under Project RAND—contract No. AF 49(638)-700 monitored by the Directorate of Development Planning, Deputy Chief of Staff, Research and Development, Hq USAF. Views or conclusions contained in this Memorandum should not be interpreted as representing the official opinion or policy of the United States Air Force.

The RAND Corporation
1700 MAIN ST • SANTA MONICA • CALIFORNIA

PREFACE

RAND was one of the first to make use of the Monte Carlo method for the solution of complicated problems involving nuclear radiation. This method has been used chiefly when solution by other means was prohibitively complicated. This report gives the solution to a number of problems involving the transport of 14 Mev neutrons in air, and is one of a continuing series. It should be useful as a guide for those offices and research organizations that now have copies of the RAND Monte Carlo neutron transport code.

SUMMARY

This report presents new results for the transport of 14 Mev neutrons in the atmosphere. Two corrections have been made to the RAND neutron Monte Carlo transport code, and curves from several previous reports are presented along with the new results given by the corrected code so that comparisons can be made and the previous incorrect results can be changed.

For the first time, results are given for the transport of 14 Mev neutrons near an air-ground interface and also in an infinite homogeneous air medium.

An auxiliary smoothing and graphing code has been developed for use in conjunction with the Monte Carlo transport code. This code is described and sample results are shown.

CONTENTS

I. INTRODUCTION

Some years ago RAND developed a neutron transport code primarily for use in the upper atmosphere where the vertical inhomogeneity was thought to play a decisive role in the propagation. Subsequently, this code was modified by the introduction of a compressed air-ground so that problems involving a density interface could be run. The density of the second medium is a variable so that the code is also able to run problems in an infinite homogeneous air medium. When the density below an arbitrary plane, usually taken at sea level, is made about 1600 times that of the air immediately above that plane, that model represents the air-ground interface. When the density below the ground plane is made equal to the sea level air density, that model represents an infinite homogeneous air medium provided the source height is near sea level or below.

In recently changing this code to FORTRAN so that it could be run on the IBM 7090, an error was uncovered. This error had persisted despite a prodigious code checking effort at the time of the development of the original code. The error exists only when the energy of the initial neutron source is exactly 14 Mev. Thus, the original code is still satisfactory for all neutron energies other than 14 Mev, and even this error can easily be avoided by the simple expedient of making the source energy 13.99 Mev. This will give results not significantly different from 14 Mev and will avoid the coding error which involved the use of the same random number twice in succession. The result of the successive use of the same random

number was that when a 14 Mev neutron made an elastic collision the angular distribution of the scattered neutron was suppressed in the forward direction and accentuated in the other directions. This occurred because of the correlation which arose from the concurrent use of the same random number and could happen only when the neutron energy corresponded exactly to a table entry rather than using interpolation in the table.

The original code could give results either in neutron flux or in tissue dose at the surface of a phantom. While the flux results are totally unambiguous, the presentation of dosage as tissue rads at the surface of a phantom can be quite misleading and ambiguous. Therefore, the code has also been changed so that dosage is now presented as first collision rads rather than phantom surface rads.

II. DESCRIPTION OF CODING ERROR

The error in the code could make itself felt only if the neutron had the possibility of making an inelastic collision. The threshold for inelastic collisions was taken to be 3.9 Mev, and therefore this error could not occur for source energies below 3.9 Mev. Above 3.9 Mev, a random number was generated to determine whether the collision of a neutron was an elastic collision or an inelastic collision. If the random number (between 0 and 1) was less than $\frac{\sigma_{el}}{\sigma_{el} + \sigma_{in}}$, the neutron was determined to have made an elastic collision. If the collision was elastic, the subsequent angular probability density was determined by drawing another random number and by using a table which gave the emergent angle as a function of this random number and of the energy of the neutron. Everything was done correctly if interpolation on the neutron energy was necessary in the table. However, if the neutron energy was an exact entry in the table, the previous random number used to determine whether the collision was elastic or inelastic was reused to determine the emergent angle from the elastic collision.

There were only two table entries above the inelastic threshold of 3.9 Mev. These were 10.0 Mev and 14.0 Mev. Thus if a neutron made an elastic collision and had an energy of exactly 14.0 Mev or 10.0 Mev, a correlation error was made, since the random number used in the angular distribution is automatically a low random number and not a "random number" between 0 and 1 as it should be.

For practical purposes, this error could occur only when the source energy itself was one of these two table entries, namely 14.0 or 10.0 Mev. The probability that a neutron with energy greater than 10.0 Mev will be moderated to exactly 10.0 Mev is so tiny that it can have no practical effect on the results. We have run no problems for a source energy of 10.0 Mev; therefore all of the errors which have been made due to this mistake in coding have been in problems where the source energy of the neutrons was exactly 14.0 Mev.

Since one can see by an examination of the angular distribution function that this coding error tended to suppress forward scattering at the expense of scattering in other directions, one would expect that the effect of the error would be to increase fluxes or dosages at close distance and to decrease them at further distances, with a cross-over at some intermediate distance from the source. This prediction has in fact been verified and the comparison of the new results with the old results for 14 Mev neutrons shows precisely this effect.

III. CHANGE IN METHOD OF PRESENTING DOSAGES

At the time that the neutron transport code was originally written, it was believed that the best way to convert from neutron flux to dosage was by means of surface body dosage conversion factors calculated by means of an auxiliary Monte Carlo calculation. The conversion factors were obtained from the results of a Monte Carlo calculation done at Oak Ridge National Laboratory.[1] Calculated depth dose curves were obtained for broad beams of fast neutrons. Monodirectional sources of various neutron energies perpendicularly incident on an infinite plane slab of tissue material 28 cm in thickness were run on the ORNL code. Dosages were calculated not only at the surface but also as a function of depth in this tissue phantom. However, only the surface dosages were taken from this report, and a numerical fit was made so that interpolation could be used between the various source energies calculated in the ORNL report. (Extrapolation was also used to extend the results from 10 to 14 Mev.)

Although the motivation for the use of this dosage conversion method (rather than using the first collision dosage as a conversion unit) was the desire to give a more accurate description of the dosage that would be received by a human being in a nuclear environment, subsequent study has shown that the results presented in this way actually led to confusion.

III. CHANGE IN METHOD OF PRESENTING DOSAGES

At the time that the neutron transport code was originally written, it was believed that the best way to convert from neutron flux to dosage was by means of surface body dosage conversion factors calculated by means of an auxiliary Monte Carlo calculation. The conversion factors were obtained from the results of a Monte Carlo calculation done at Oak Ridge National Laboratory.[1] Calculated depth dose curves were obtained for broad beams of fast neutrons. Monodirectional sources of various neutron energies perpendicularly incident on an infinite plane slab of tissue material 28 cm in thickness were run on the ORNL code. Dosages were calculated not only at the surface but also as a function of depth in this tissue phantom. However, only the surface dosages were taken from this report, and a numerical fit was made so that interpolation could be used between the various source energies calculated in the ORNL report. (Extrapolation was also used to extend the results from 10 to 14 Mev.)

Although the motivation for the use of this dosage conversion method (rather than using the first collision dosage as a conversion unit) was the desire to give a more accurate description of the dosage that would be received by a human being in a nuclear environment, subsequent study has shown that the results presented in this way actually led to confusion.

In the field of x-ray dosimetry, it has been the practice to quote dosages as first collision roentgen (or later rad) dosage. First collision dosage means simply that dosage which would be delivered to a dosimeter or phantom which is very tiny compared to the removal mean free path of the radiation in the material of the dosimeter. This method was adopted despite the realization that the deposition of energy in a specimen such as a human being which was large compared to the mean free path could be very nonuniform, particularly for low energy x-rays. Not only can the deposition be nonuniform, but the total integral dose to the specimen can be considerably less than that which would be calculated using the first collision dosage.

A very crucial point is that if first collision dosage is used as the measure of dosage, then all the effects of nonuniform deposition of energy in a large specimen such as a human being may be taken into account in the RBE* ascribed to the radiation in question, (applied, of course, only to the specimen in question). Also, included in the RBE in this method of usage is any effect of the radiation which differs from that of the base radiation, usually taken to be cobalt^{60} gamma radiation. Thus, the RBE used here, and as is now commonly used in the field of military applications,

*The radiobiologists prefer to reserve the term RBE, or Relative Biological Effectiveness, for use only in those cases where the deposition of the radiation is uniform within the specimen. The term potency is used for those cases where the radiation is nonuniformly deposited.[2] Nonetheless, in the field of military applications, the term RBE has generally been accepted for the case of nonuniform deposition where the radiobiologists would prefer to use the term potency. Here we use the term RBE in the latter context.

combines two factors. These are (a) the geometrical factors or depth dose considerations, and (b) the basic difference in effectiveness of the radiation as compared to a standard radiation. At first, it may seem that this system is just as complicated as the one first used with the RAND Monte Carlo code, which was to attempt to take the geometrical considerations into account in the dosage itself, reserving the RBE only for defining the differences in radiation effectiveness of the neutrons and the standard radiation.

However, this has not proven to be the case. A basic error was made in equating the unilateral radiation assumption of the Oak Ridge calculations with the quasi-isotropic radiation field due to atomic explosions. Field measurements in atomic explosion environments have clearly shown that the surface dosage in a human phantom is about 60 per cent as large as the first collision dosage at that point, whereas the Oak Ridge calculations show an average surface dosage which is about 20 per cent greater than the first collision dosage for a normal weapons air moderated neutron spectrum. Thus, although a factor of two discrepancy has appeared, it is readily explained by the fact that the field radiation is essentially isotropic rather than monodirectional. Since it generally fails to penetrate the phantom, the result is that each side of the phantom receives only about one half of the dosage. That rather tricky point was completely neglected in the original thinking, illustrating the pitfalls that one can encounter in this sort of problem.*

*An additional reason for having used the ORNL calculations was that they included the dosage to the phantom given by the capture γ rays. In the method where first collision dosage is used, the effect of the capture γ rays is included in the RBE.

Figure 1 shows a graph of the first collision tissue dosage now used in the RAND neutron code. It was obtained from "Radiation Dosimetry"[3] (page 676) and has been verified by an independent calculation. Figure 2 is a graph showing the ratio of first collision rads (given in Fig. 1) to the surface tissue rads which were originally used in the code. The curve shown in Fig. 2 is the ratio of the actual empirical fits which were made to the two sets of data for use in the code. This accounts for the two rather sharp discontinuities. These discontinuities are the points where the piecewise exponential fits to the ORNL data join in the original code.

In the original scheme of things, it was tacitly assumed that the RBE could be obtained from experiments in which small mammals such as mice were exposed to neutron radiation. Such experiments had given RBE's in the neighborhood of 1.7, and this RBE was recommended in the 1957 version "Effects of Nuclear Weapons"[4] (page 363). It was stated that a neutron RBE of 1.7 obtained in experiments with mice might also be applied to man in the LD_{50} range of 100 to 1000 rem in the absence of other data. Since 1957, the tendency has been to lower this number considerably. In the 1962 edition of the same reference, the recommended RBE for acute effects of neutron radiation is 1.0. It is also more clearly recognized now that there are considerable species differences in the neutron RBE. The appendix, which is reproduced from Ref. (8),*

*Reference (8) is a classified document but its unclassified appendix is reproduced here not only because it is relevant to the subject matter, but also to make the content available in an unclassified document.

gives some experimental evidence that the RBE including the geometrical factor may be about 0.5 for man. Reference (17) also reaches similar conclusions.

The RBE of neutrons is certainly nonlinear, i.e., dependent on the dosage level. In the very low dosage range, up to a hundred rads or so, it seems that the RBE may be considerably greater than 1. This is due primarily to the effects on lens opacity in the eye. The appendix gives arguments for an RBE around 0.5 in the range 100 to 1000 rads. In the supralethal range above 1000 rads, there is not much experimental evidence, but the RBE probably tends to rise again and may approach 1.0 at very high dosage levels.

Figure 3, showing the possible RBE dependence on incident neutron energy, is taken from Ref. (8). It is to be used in the 100 to 1000 rem region and is based on depth dose considerations only. It assumes that at 14 Mev, where the neutron energy is deposited almost uniformly, the intrinsic RBE is 1.0. The fall-off in the curve toward the lower energy range is simply a result of the rapidly decreasing penetrability of the lower energy neutrons.

IV. CORRECTIONS TO HIGH ALTITUDE DOSAGE RESULTS

In a previous, classified document,[5] Monte Carlo results were given for the dosage from a point isotropic source of 14 Mev neutrons at altitudes of 100,000 and 200,000 feet as well as for a source of 0.45 Mev neutrons at an altitude of 200,000 feet. Figures 4 through 15 show the original results presented in that report along with the new results obtained at this time for the source of 14 Mev neutrons at 100,000 and 200,000 foot altitudes in the atmosphere.* Both changes previously discussed (i.e., the correction due to the repeated use of the random number and the change from surface phantom rads to first collision rads) have been simultaneously incorporated in the new results. Therefore, one cannot determine the individual contribution of each change from these curves. In comparisons presented elsewhere in this report, however, problems will be shown where each effect is treated separately.

It was not thought worthwhile to rerun the problem for the 0.45 Mev source, since the dosage was originally quite small compared to the higher energy neutrons. Furthermore, one can see from Fig. 2 that the relative rad dosage is reduced by a further factor of about 2 when change over to first collision rads is made. From Fig. 3, one notes that the RBE in this energy range is in the neighborhood of 0.2 compared to 1.0 for 14 Mev so that the rem dosage contributed by neutrons in this range are altogether insignificant compared to the dosages contributed by higher energy neutrons.

*Various details of these and succeeding problems are presented in notes opposite the figures which give the individual problem results.

The results of Figs. 4 through 15 presented originally in RM-1928[5] were used again in RM-2191,[6] and the results in that report should be changed in accordance with these new results. No new runs have been made for the 2.9 and 1.5 Mev cases shown in RM-2191. Since the random number error does not have any effect at these energies, the only difference is due to the new method of presentation involving first collision rads rather than phantom surface rads. An approximation to this correction can easily be made by reference to Fig. 2 which gives the ratio of the first collision rads to the phantom surface rads as a function of energy. The energy in Fig. 2 refers to the energy of the arriving neutrons and not of the source neutrons, so that one must make an assumption about the spectrum of the arriving neutrons in order to make this correction. If one assumes that the average energy of the arriving neutrons is 1.0 Mev from a 2.9 Mev source and 0.75 Mev from a 1.5 Mev source, the correction factors as read from Fig. 3 are both about 0.62, and the results in RM-2191 can be reduced accordingly.

Figures 4 through 15 also show the exponent of the direct beam, or the number of source energy mean-free-paths, from the source to any particular radius.

V. COMPARISON OF RAND AND LOS ALAMOS RESULTS

In RM-2556[7] a comparison was made of Monte Carlo results using the RAND, LOS ALAMOS and Sandia codes. Two problems were compared, one with a source energy of 3 Mev and one of 14 Mev. The comparison was on the basis of flux so that no difference due to the dosage change treated in Sec. III is encountered. The 3 Mev comparison is presumed to be correct and not affected by the correlated random number error. The 14 Mev problem which was affected by this error has been rerun. The original results were given in Tables 13 through 21 of RM-2556. Tables 1 through 10 list the results of the old calculation as given in RM-2556, the new flux as presently calculated, and the ratio of these two quantities. One can best see the overall change by consulting Table 1, which gives the ratio of the new calculations to the old for the total flux rather than for the various sub-energy fluxes presented in the succeeding tables where the fluctuations are more severe. At close distances, the new calculations are about 20 per cent less than the old, becoming equal at a range of about 800 feet, and finally rising monotonically to one and one half times the old calculations at the most distant range of 5000 feet. This behavior is in accordance with that to be expected from the nature of the error as explained in Sec. II.

VI. COMPARISON OF DOSAGES NEAR AN AIR-GROUND INTERFACE

Problems have previously been run with the RAND Monte Carlo code for a source energy of 14 Mev where the source was located at 0, 750 and 3000 feet above a density interface which represented schematically the boundary between the atmosphere and the ground. Results for the 750 foot case and the 3000 foot case were presented in Figs. 6 and 7 of RM-2829-PR[8] Figures 16 and 17 of this report show those results along with results now obtained with the corrected code for the dosages on the interface.

When these problems were originally run, the conversion to first collision rads in the code had not yet been made. However, it is possible to obtain dosage subdivided on energy with the Monte Carlo code. This means that not only can one obtain the dosage at a particular point due to neutrons arriving with all possible energies, but also the individual contributions to the dosage can be obtained for neutrons arriving in many prescribed energy subdivisions. The dosage was automatically subdivided on arrival energy in the above prescribed manner in many problems, in case one would be interested in the energy spectrum of the dosage. Therefore it was possible to convert, approximately, the results from surface phantom rads to first collision rads by using the appropriate conversion factor at the middle of each sub-energy group. Figures 16 and 17 show the original results using surface phantom rads as well as the approximately corrected results for first collision rads which were used in RM-2829.

Figure 18 gives new results, not included in RM-2829, for a source on the density interface. Shown also in Fig. 18 are the results of the old code with neither of the two corrections made. A similar approximate correction to first collision rads was subsequently made to the old results of Fig. 18, and they were then used in preparing Fig. 1 of RM-2908.[9]*

Since publication of the reports mentioned above, a reciprocity theorem has been discovered, making it unnecessary to run three separate problems to obtain the results which were originally wanted. This theorem states that the dosage at any altitude and radius from a point source on the density interface is the same as the dosage from a source at that altitude and measured at the same radius on the interface. For instance, to obtain the dosage on the interface for a source at 3000 feet altitude, one can put the source on the interface and look at the dosage on the 3000 foot plane. Likewise, for the 750 foot case, one looks at the dosage on the 750 foot plane. Since any number of dosage observation planes can be used in a single problem, this allows the simultaneous solution of several different problems as well as a large saving of machine time.

---

*It was not thought worthwhile to prepare new curves of the type shown in Figs. 1 through 4 of RM-2908. Since a large part of the dosage shown in these figures came from gamma rays, the resultant change in the total dosages would be quite small and comparable to, or less than, other uncertainties already present in the calculations.

VII. RESULTS FOR A 14 MEV SOURCE IN AN INFINITE HOMOGENEOUS ATMOSPHERE

By making the density of the compressed air-ground equal to the density of the atmosphere at the air-ground interface, it was possible to run this code for an essentially infinite homogeneous medium. A 14 Mev source was assumed to be at zero altitude, and dosage planes were put at altitudes of 0, $\pm$ 250 feet, $\pm$ 500 feet, $\pm$ 2000 feet and $\pm$ 4000 feet. The dosages on all of these planes were then plotted on a master graph as a function of the number of mean free paths from the source. An average curve drawn through all the points gave the dose build-up factor as a function of the number of mean free paths from the source. The concept of the build-up factor* has been seldom used in neutron transport problems although it is used frequently in the description of gamma ray transport. The dose build-up factor shown in the final smooth curve of Fig. 19 is the ratio of the total rad dosage at a particular point to the rad dosage from the unscattered flux, or so-called direct beam, at the same point.

It is useful to have this infinite homogeneous medium build-up factor so that comparisons can easily be made for cases where the medium is nonhomogeneous, such as in the exponential atmosphere or near a density interface. One can then calculate the ratio of the dosage at any point in a nonhomogeneous problem to the dosage that would obtain in a similar homogeneous problem where the number

*For a description of the build-up factors and their definitions see NYO-3075.(10)

of grams of air between the source and the receiver is the same. This ratio, designated by K, is usually a slowly varying function and not too far removed from unity. The use of these concepts is explained in greater detail in RM-3399-PR,[11] where they were applied to gamma ray problems.

VIII. THE SMOOTHING OF MONTE CARLO RESULTS BY MEANS OF A MOVING AVERAGE "K" CODE

One of the advantages of computing the K factor, i.e., the ratio of the dosage in an infinite homogeneous medium to that in a nonhomogeneous medium, is that it provides a method of easily smoothing Monte Carlo results. The method is as follows: The K factor is computed for every Monte Carlo point or bin along some particular axis in the nonhomogeneous problem. As stated before, this factor will often be close to unity and usually within an order of magnitude of unity.* It is then possible to average the K factor along this axis three points at a time. In other words, the first three values of K are added together and divided by three. The result is plotted at the same point as the middle value used in the average; then the second, third and fourth values of K are averaged and the results plotted at the third point, etc. This type of average is known as a moving average. The process may be repeated any number of times. An auxiliary 7090 machine code has been set up whereby the Monte Carlo results may be fed in and the K factor computed and averaged in the preceding manner any number of times. The results are both printed out and graphed by the printing machine simultaneously. Figures 20 through 59 show sample runs from this averaging code for many of the previous results presented in this report. Figures 20 through 25 show K averaged four times, called K_4 for the 200,000 foot source of 14 Mev neutrons. Figures 26 through 37 show results for the 100,000 foot

*In many cases the dosage itself might vary by many orders of magnitude over the range of interest.

source of 14 Mev neutrons. Figures 38 through 47 show K_4 on many observation planes for a 14 Mev neutron source at air-ground interface.

Figures 48 through 53 show K_0, K_1, K_2, K_4, K_6 and K_{10} for the ground observation level of this same problem. The ratio of the scattered dosage in the nonhomogeneous problem to the scattered dosage in the homogeneous problem is designated by K_{sc} and is computed, averaged and graphed in the same manner as K.

Figures 54 through 59 show K_{0sc}, K_{1sc}, K_{2sc}, K_{4sc}, K_{6sc} and K_{10sc} for the 14 Mev source on the air-ground interface and the observation level at the same altitude. Tables 11 through 14 give the numerical printout from which Figs. 48 through 59 were graphed. Prints of this type produced by the averaging code are particularly useful where a large amount of material is to be digested as the result of a particular Monte Carlo run. One rapidly gets an idea of the general trend of the results by quickly leafing through the printout of the code, whereas the laborious hand plotting of the dosages on various levels not only takes an inordinate amount of time but is difficult to interpret since it is not smoothed. By screening the various averaged K graphs one can quickly get a general idea of the results of the overall problem.

Appendix

RELATIVE BIOLOGICAL EFFECTIVENESS OF NEUTRON RADIATION

In a recent article,[12] Woodward et al., concluded from an analysis of data gathered from shot Wilson of Operation Plumbbob that the potency of the neutron radiation relative to the gamma radiation was 1.2. This conclusion was based on the production of lethality at 30 days in swine.

We have analyzed this same data and reached a substantially different conclusion, namely, that in this experiment the potency of the neutron radiation relative to the gamma radiation was 0.50 ± 0.22. Since this conclusion results in a significant difference as to the possible radiation effectiveness of neutrons, we believe it is important that reasons for this difference be elucidated.

The basic difference hinges on what value one assumes for the $LD_{50/30}$ of the gamma radiation from an atomic explosion. In the reference article, it is stated that the $LD_{50/30}$ of 486 total rads which was observed at the explosion is in good agreement with values reported for swine after roentgen or gamma irradiation. If one takes the $LD_{50/30}$ values obtained by laboratory irradiation of swine as cited by Woodward et al., the calculated mean value turns out to be 517 r or 481 rads, which indeed is almost identical with the $LD_{50/30}$ value of 486 rads of neutrons plus gammas obtained in the atomic explosion. Using this particular values as the $LD_{50/30}$ of gammas alone uniquely prescribes a value of 1.0 for the potency of the neutron component, regardless of the neutron-gamma ratio, and

not 1.2 as stated. However, in order to make a reasonable calculation of the potency of the neutron component, one must carefully correct free air entrance dosages as given in the cited article to the equivalent free air dosage for bomb gamma radiation. This means that corrections must be made for dose rate and depth-dose distribution. (No correction was deemed necessary for the different spectra of the radiations involved.) Admittedly there is no exact way to do this.

By making these corrections to the cited laboratory data as best we could, we obtained values for the converted dosages for each of the four experiments. These values--362, 355, 366 and 400 r--correspond to bomb gamma dosages needed to produce 30-day lethality. The average of these numbers is 371 r, considerably less than the uncorrected average of 517 r. The difference is mainly due to the fact that the bomb gamma radiation gives a much higher tissue dose than the laboratory experiments for the same entrance air dose. This happens because the bomb gamma radiation is more penetrating than the high-voltage x-radiation and also because there is no inverse square effect. The dose rate corrections are rather small except in the case of the cobalt irradiation data of Rust, which involved a dose rate of only 50 r per hour. In this case, a 33 per cent reduction was necessary to correct for the very low dose rate.

We have carefully examined two other sets of laboratory data: experiments of Bond et al.,[13] and of Andrews.[14] These data seem considerably more reliable and require less correction than the published data. The resulting $LD_{50/30}$ numbers, when converted to

equivalent bomb gamma conditions are 360 r and 336 r, respectively, A weighted average, after small corrections for age of the animals in the different experiments, gives 343 r as the best estimate of the $LD_{50/30}$ for the Plumbbob swine.

If we use Woodward's number of 486 rads for the total dosage received by the animals in the explosion and the stated gamma-neutron ratio of 1.2, we obtain 265 rads of gamma radiation and 221 rads of neutron radiation. The relative potency, P, of the neutron component is then obtained from the following equation:

$$265 + 221P = 343\ (.93).$$

We multiply the 343 r by .93 to convert to rads. The resulting number for the potency of the neutron component is 0.25.

In addition, we have carefully reevaluated all the dosimetry data for the atomic explosion in question, and we find that at the $LD_{50/30}$ point (1508 yards ground range), there were 221 ± 19 rads of gamma radiation and 196 ± 30 rads of neutron radiation. Using these estimates of the values for the nuclear radiation in an equation similar to the one above gives $0.50 \pm .22$ for the potency of the neutron component. The uncertainty in this figure derives from possible errors in the dosimetry and from statistical uncertainties due to the finite population of animals in both the field and the laboratory experiments.

Two laboratory experiments with dogs where the neutron radiation was delivered uniformly through the animal gave an RBE of 1.0.[15,16]

These results are consistent with the above RBE of 0.5 for the very nonuniform depth dose distribution in the swine, but they are completely at variance with estimates of 1.0 or more for the RBE for such large animals or humans.

It should be noted that the RBE or potency as used herein relates the first collision, or free field, dosage directly to the biological effect. Thus the RBE includes the effect of different depth dose characteristics of the measured radiation to the base line radiation. Radiobiologists prefer to reserve the term RBE to compare two radiations which are both uniformly absorbed in the specimen and to use the term potency to compare nonuniformly deposited radiations.

Conclusions substantially the same as given here are reached independently by Bond and Bateman.[17]

It should be clearly understood that the above discussion and results for the RBE apply only to the range of dosages in the vicinity of the $LD_{50/30}$ point; i.e., in the range of 100 to perhaps as much as 1000 rem.

SUPRALETHAL DOSAGE RANGE

In the supralethal dosage range above 1000 rem immediate incapacitating effects will begin to appear. A dosage of 2500 rem has been suggested as an immediate incapacitation dose for troops in the field. In this dosage range, the mechanism of damage is definitely different from that in the lower range;[18] here the primary effect is on the central nervous system rather than on the hemopoietic (blood) system.

In central nervous system damage, the only important region seems to be the head. The depth-dose degradation of the neutron dosage will be much less than with the trunk of the body, Thereby accounting for a higher potency (hence RBE) of the neutrons for this case. Experimental evidence is scanty. It is assumed in this report that this RBE for neutrons is 1.0.

There is an intermediate region, perhaps between 800 and 1500 rem, where the mechanism of damage and eventual death is centered in the gastrointestinal system. The RBE of neutrons for the intermediate gastrointestinal damage region of dosage is unknown, but perhaps it lies between the two values (0.5 and 1.0) used here. There is definite experimental evidence, obtained with dogs, that the neutron RBE for gastrointestinal damage is greater than the RBE for hemopoietic damage.[19]

Table 1

TOTAL SCATTERED FLUX, 14 MEV TO 0.25×10^{-7} MEV

r (feet)	Old Flux	New Flux	Ratio New/Old
66	1.84^{-9}	1.38^{-9}	0.75
583	5.31^{-10}	5.14^{-10}	0.97
937	2.25^{-10}	2.32^{-10}	1.03
1278	1.05^{-10}	1.18^{-10}	1.12
1613	5.44^{-11}	6.29^{-11}	1.16
2277	1.62^{-11}	1.86^{-11}	1.15
2937	5.36^{-12}	6.16^{-12}	1.15
3596	1.67^{-12}	2.08^{-12}	1.25
4255	4.55^{-13}	5.95^{-13}	1.31
4912	1.04^{-13}	1.51^{-13}	1.45

TOTAL FLUX, 14 MEV TO 0.25×10^{-7} MEV

r (feet)	Old Flux	New Flux	Ratio New/Old
66	2.29^{-9}	1.83^{-9}	0.80
583	5.76^{-10}	5.59^{-10}	0.97
937	2.35^{-10}	2.42^{-10}	1.03
1278	1.08^{-10}	1.21^{-10}	1.12
1613	5.52^{-11}	6.37^{-11}	1.15
2277	1.63^{-11}	1.87^{-11}	1.15
2937	5.37^{-12}	6.17^{-12}	1.15
3596	1.67^{-12}	2.08^{-12}	1.25
4255	4.55^{-13}	5.95^{-13}	1.31
4912	1.04^{-13}	1.51^{-13}	1.45

Table 2

SCATTERED FLUX, 14 > E > 9 MEV

r (feet)	Old Flux	New Flux	Ratio New/Old
66	4.30^{-10}	2.28^{-10}	0.53
583	6.70^{-11}	6.80^{-11}	1.01
937	1.88^{-11}	2.70^{-11}	1.44
1278	6.70^{-12}	1.13^{-11}	1.69
1613	2.75^{-12}	4.70^{-12}	1.71
2277	5.20^{-13}	7.40^{-13}	1.42
2937	1.15^{-13}	1.37^{-13}	1.19
3596	2.40^{-14}	3.03^{-14}	1.26
4255	4.30^{-15}	8.70^{-15}	2.02
4912	4.30^{-16}	3.30^{-15}	7.67

TOTAL FLUX, 14 > E > 9 MEV

r(feet)	Old Flux	New Flux	Ratio New/Old
66	8.80^{-10}	6.78^{-10}	0.77
583	1.12^{-10}	1.13^{-10}	1.01
937	2.85^{-11}	3.67^{-11}	1.29
1278	9.27^{-12}	1.39^{-11}	1.50
1613	3.55^{-12}	5.50^{-12}	1.55
2277	6.10^{-13}	8.30^{-13}	1.36
2937	1.27^{-13}	1.49^{-13}	1.17
3596	2.59^{-14}	3.22^{-14}	1.24
4255	4.60^{-15}	9.00^{-15}	1.96
4912	4.82^{-16}	3.35^{-15}	6.95

Table 3

SCATTERED FLUX, 9 > E > 7 MEV

r(feet)	Old Flux	New Flux	Ratio New/Old
66	5.90^{-11}	6.65^{-11}	1.13
583	1.60^{-11}	9.60^{-12}	0.60
937	4.50^{-12}	3.25^{-12}	0.72
1278	1.58^{-12}	1.43^{-12}	0.91
1613	7.20^{-13}	7.00^{-13}	0.97
2277	1.69^{-13}	1.68^{-13}	0.99
2937	3.60^{-14}	3.30^{-14}	0.92
3596	5.65^{-15}	2.25^{-15}	0.40
4255	4.60^{-16}	2.50^{-17}	0.05
4912	2.05^{-17}	1.70^{-20}	0.00

SCATTERED FLUX, 7 > E > 5 MEV

r(feet)	Old Flux	New Flux	Ratio New/Old
66	7.70^{-11}	8.90^{-11}	1.16
583	1.85^{-11}	1.55^{-11}	0.84
937	5.50^{-12}	4.80^{-12}	0.87
1278	1.98^{-12}	1.80^{-12}	0.91
1613	8.00^{-13}	7.70^{-13}	0.96
2277	1.80^{-13}	1.69^{-13}	0.94
2937	4.20^{-14}	3.70^{-14}	0.88
3596	8.25^{-15}	7.60^{-15}	0.92
4255	1.50^{-15}	1.36^{-15}	0.91
4912	1.78^{-16}	1.64^{-16}	0.92

Table 4

SCATTERED FLUX, 5 > E > 4 MEV

r(feet)	Old Flux	New Flux	Ratio New/Old
66	2.28^{-11}	2.64^{-11}	1.16
583	7.80^{-12}	9.60^{-12}	1.23
937	2.90^{-12}	3.15^{-12}	1.09
1278	1.00^{-12}	9.60^{-13}	0.96
1613	3.80^{-13}	3.45^{-13}	0.91
2277	6.20^{-14}	6.10^{-14}	0.98
2937	1.32^{-14}	1.47^{-14}	1.11
3596	3.05^{-15}	3.55^{-15}	1.16
4255	5.70^{-16}	8.30^{-16}	1.46
4912	8.20^{-17}	1.54^{-16}	1.88

SCATTERED FLUX, 4 > E > 3 MEV

r(feet)	Old Flux	New Flux	Ratio New/Old
66	7.80^{-11}	7.25^{-11}	0.93
583	1.60^{-11}	1.25^{-11}	0.78
937	4.40^{-12}	3.95^{-12}	0.90
1278	1.66^{-12}	1.40^{-12}	0.84
1613	7.25^{-13}	5.40^{-13}	0.74
2277	1.60^{-13}	8.40^{-14}	0.52
2937	4.10^{-14}	1.70^{-14}	0.41
3596	1.00^{-14}	4.10^{-15}	0.41
4255	2.00^{-15}	9.80^{-16}	0.49
4912	3.30^{-16}	1.90^{-16}	0.58

Table 5

SCATTERED FLUX, 3 > E > 1 MEV

r(feet)	Old Flux	New Flux	Ratio New/Old
66	2.30^{-10}	2.22^{-10}	0.97
583	7.60^{-11}	6.70^{-11}	0.88
937	3.00^{-11}	2.65^{-11}	0.88
1278	1.22^{-11}	1.18^{-11}	0.97
1613	5.25^{-12}	5.70^{-12}	1.09
2277	1.05^{-12}	1.42^{-12}	1.35
2937	2.65^{-13}	4.05^{-13}	1.53
3596	6.90^{-14}	1.15^{-13}	1.67
4255	1.98^{-14}	3.10^{-14}	1.57
4912	5.67^{-15}	7.30^{-15}	1.29

SCATTERED FLUX, 1 > E > .2 MEV

r(feet)	Old Flux	New Flux	Ratio New/Old
66	2.80^{-10}	2.02^{-10}	0.72
583	9.40^{-11}	9.30^{-11}	0.99
937	3.90^{-11}	3.50^{-11}	0.90
1278	1.80^{-11}	1.73^{-11}	0.96
1613	8.70^{-12}	9.40^{-12}	1.08
2277	2.50^{-12}	2.85^{-12}	1.14
2937	8.10^{-13}	9.50^{-13}	1.17
3596	2.50^{-13}	3.30^{-13}	1.32
4255	7.10^{-14}	1.20^{-13}	1.69
4912	1.70^{-14}	4.45^{-14}	2.62

Table 6

SCATTERED FLUX, .2 > E > .05 MEV

r(feet)	Old Flux	New Flux	Ratio New/Old
66	2.15^{-10}	8.60^{-11}	0.40
583	5.70^{-11}	5.20^{-11}	0.91
937	2.10^{-11}	2.55^{-11}	1.21
1278	9.00^{-12}	1.30^{-11}	1.44
1613	4.50^{-12}	6.60^{-12}	1.47
2277	1.50^{-12}	1.80^{-12}	1.20
2937	6.20^{-13}	5.95^{-13}	0.96
3596	2.35^{-13}	2.15^{-13}	0.91
4255	6.80^{-14}	7.30^{-14}	1.07
4912	3.90^{-15}	2.25^{-14}	5.77

SCATTERED FLUX, .05 > E > .01 MEV

r(feet)	Old Flux	New Flux	Ratio New/Old
66	8.70^{-11}	1.08^{-10}	1.24
583	4.15^{-11}	4.60^{-11}	1.11
937	2.40^{-11}	2.30^{-11}	0.96
1278	1.16^{-11}	1.28^{-11}	1.10
1613	6.30^{-12}	7.40^{-12}	1.17
2277	1.98^{-12}	2.42^{-12}	1.22
2937	6.90^{-13}	8.10^{-13}	1.17
3596	2.04^{-13}	2.63^{-13}	1.29
4255	4.30^{-14}	7.90^{-14}	1.84
4912	6.80^{-15}	2.00^{-14}	2.94

Table 7

SCATTERED FLUX, .01 > E > .001 MEV

r(feet)	Old Flux	New Flux	Ratio New/Old
66	1.46^{-10}	1.16^{-10}	0.79
583	4.60^{-11}	5.00^{-11}	1.09
937	2.16^{-11}	2.75^{-11}	1.27
1278	1.14^{-11}	1.50^{-11}	1.32
1613	6.80^{-12}	8.40^{-12}	1.24
2277	2.70^{-12}	2.60^{-12}	0.96
2937	1.04^{-12}	8.30^{-13}	0.80
3596	3.63^{-13}	2.58^{-13}	0.71
4255	1.11^{-13}	8.50^{-14}	0.77
4912	2.80^{-14}	2.60^{-14}	0.93

SCATTERED FLUX, .001 > E > .0005 MEV

r(feet)	Old Flux	New Flux	Ratio New/Old
66	2.02^{-11}	1.95^{-11}	0.97
583	9.70^{-12}	1.06^{-11}	1.09
937	5.60^{-12}	5.55^{-12}	0.99
1278	3.25^{-12}	3.00^{-12}	0.92
1613	1.84^{-12}	1.63^{-12}	0.89
2277	4.75^{-13}	4.50^{-13}	0.95
2937	1.17^{-13}	1.26^{-13}	1.08
3596	3.30^{-14}	3.25^{-14}	0.98
4255	1.18^{-14}	8.10^{-15}	0.69
4912	5.05^{-15}	1.80^{-15}	0.36

Table 8

SCATTERED FLUX, $.5(10^{-3}) > E > .5(10^{-4})$ MEV

r(feet)	Old Flux	New Flux	Ratio New/Old
66	5.50^{-11}	5.30^{-11}	0.96
583	3.04^{-11}	3.00^{-11}	0.99
937	1.80^{-11}	1.62^{-11}	0.90
1278	1.02^{-11}	8.90^{-12}	0.87
1613	5.65^{-12}	5.00^{-12}	0.88
2277	1.45^{-12}	1.72^{-12}	1.19
2937	3.85^{-13}	7.10^{-13}	1.84
3596	1.21^{-13}	3.00^{-13}	2.48
4255	4.25^{-14}	1.11^{-13}	2.61
4912	2.19^{-14}	2.20^{-14}	1.00

SCATTERED FLUX, $.5\ (10^{-4}) > E > .6\ (10^{-5})$ MEV

r(feet)	Old Flux	New Flux	Ratio New/Old
66	5.05^{-11}	4.00^{-11}	0.79
583	2.22^{-11}	2.32^{-11}	1.05
937	1.37^{-11}	1.46^{-11}	1.07
1278	7.40^{-12}	8.70^{-12}	1.18
1613	4.12^{-12}	5.15^{-12}	1.25
2277	1.32^{-12}	1.50^{-12}	1.14
2937	4.95^{-13}	4.40^{-13}	0.89
3596	1.38^{-13}	1.20^{-13}	0.87
4255	2.40^{-14}	2.80^{-14}	1.17
4912	2.70^{-15}	2.45^{-15}	0.91

Table 9

SCATTERED FLUX, $.6(10^{-5}) > E > .4(10^{-5})$ MEV

r(feet)	Old Flux	New Flux	Ratio New/Old
66	5.33^{-12}	7.30^{-12}	1.37
583	3.55^{-12}	4.00^{-12}	1.13
937	2.43^{-12}	1.68^{-12}	0.69
1278	1.60^{-12}	9.00^{-13}	0.56
1613	1.02^{-12}	6.20^{-13}	0.61
2277	3.28^{-13}	3.90^{-13}	1.19
2937	8.00^{-14}	2.60^{-13}	3.25
3596	1.55^{-14}	1.47^{-13}	9.48
4255	2.35^{-15}	6.90^{-15}	2.94
4912	3.10^{-16}	1.05^{-16}	0.34

SCATTERED FLUX, $.4(10^{-5}) > E > .5(10^{-6})$ MEV

r(feet)	Old Flux	New Flux	Ratio New/Old
66	6.00^{-11}	3.15^{-11}	0.53
583	1.55^{-11}	1.44^{-11}	0.93
937	8.00^{-12}	8.50^{-12}	1.06
1278	4.60^{-12}	5.30^{-12}	1.15
1613	2.83^{-12}	3.40^{-12}	1.20
2277	1.11^{-12}	1.37^{-12}	1.23
2937	4.00^{-13}	5.35^{-13}	1.34
3596	1.33^{-13}	1.83^{-13}	1.38
4255	4.05^{-14}	2.90^{-14}	0.72
4912	1.10^{-14}	2.50^{-19}	0.00

Table 10

SCATTERED FLUX, $.5(10^{-6}) > E > .25(10^{-6})$ MEV

r(feet)	Old Flux	New Flux	Ratio New/Old
66	1.24^{-11}	6.20^{-12}	0.50
583	4.85^{-12}	4.25^{-12}	0.88
937	2.10^{-12}	2.78^{-12}	1.32
1278	8.60^{-13}	1.77^{-12}	2.06
1613	4.75^{-13}	1.08^{-12}	2.27
2277	1.84^{-13}	3.45^{-13}	1.88
2937	7.10^{-14}	9.50^{-14}	1.34
3596	1.85^{-14}	2.33^{-14}	1.26
4255	1.85^{-15}	5.20^{-15}	2.81
4912	1.60^{-17}	9.00^{-16}	56.20

SCATTERED FLUX, $.25(10^{-6}) > E > .25(10^{-7})$ MEV

r(feet)	Old Flux	New Flux	Ratio New/Old
66	8.00^{-12}	6.25^{-12}	0.78
583	5.20^{-12}	4.75^{-12}	0.91
937	3.62^{-12}	3.40^{-12}	0.94
1278	2.42^{-12}	2.30^{-12}	0.95
1613	1.54^{-12}	1.50^{-12}	0.97
2277	4.90^{-13}	5.40^{-13}	1.10
2937	1.39^{-13}	1.68^{-13}	1.21
3596	4.05^{-14}	4.55^{-14}	1.12
4255	1.00^{-14}	7.20^{-15}	0.72
4912	1.90^{-16}	1.70^{-17}	0.09

NOTES FOR TABLE 11

This table gives the IBM printout for the unscattered flux and dosage for a 14 Mev source on the density interface. It is for the co-altitude observation level. The code which generates this information is not part of the main code, but is incorporated in the auxillary smoothing and graphing code described on page 17. The notation for this table is as follows:

Radius ------ Horizontal distance from the z axis to the midpoint of each radial bin in units of 100,000 feet.

Slant Range - Distance from the source to the midpoint of each radial bin in units of 100,000 feet.

Time ------ - Transit time for source energy neutrons from the source to the midpoint of radial bin in seconds.

Exponent ---- Number of mean free paths of air between the source and the midpoint of radial bin for source energy neutrons.

Flux -------- Unscattered neutron flux at the midpoint of a radial bin x 10^{15}. (Multiply column numbers by 10^{-15} to convert to flux for a source strength of 1.0 neutrons.)

New Rads ---- Dosage in first collision tissue rads from the unscattered flux at the midpoint of a radial bin x 10^{20}. (Multiply column numbers by 10^{-20} to convert to dosage for a source strength of 1.0 neutron.)

Table 11

PROBLEM 206 OBSERVATION LEVEL = 0.

RADIUS	SLANT RANGE	TIME	EXPONENT	FLUX (20)	NEW RADS (30)
0.49999999E-06	0.49999999E-06	0.29442343E-09	0.12449256E-03	0.34258325E 14	0.20828848E 16
0.15000000E-05	0.15000000E-05	0.88327031E-09	0.37347770E-03	0.38055330E 13	0.23137403E 15
0.24999999E-05	0.24999999E-05	0.14721172E-08	0.62246283E-03	0.13696508E 13	0.83273915E 14
0.34999999E-05	0.34999999E-05	0.20609640E-08	0.87144797E-03	0.69862745E 12	0.42476113E 14
0.45000000E-05	0.45000000E-05	0.26498109E-08	0.11204331E-02	0.42252126E 12	0.25689030E 14
0.55000000E-05	0.55000000E-05	0.32386578E-08	0.13694182E-02	0.28277440E 12	0.17192507E 14
0.64999999E-05	0.64999999E-05	0.38275046E-08	0.16184033E-02	0.20240937E 12	0.12306363E 14
0.74999999E-05	0.74999999E-05	0.44163515E-08	0.18673885E-02	0.15199408E 12	0.92411454E 13
0.84999999E-05	0.84999999E-05	0.50051983E-08	0.21163736E-02	0.11830503E 12	0.71928723E 13
0.95000000E-05	0.95000000E-05	0.55940453E-08	0.23653588E-02	0.94685990E 11	0.57568492E 13
0.10999999E-04	0.10999999E-04	0.64773155E-08	0.27388364E-02	0.70596859E 11	0.42922451E 13
0.13000000E-04	0.13000000E-04	0.76550093E-08	0.32368067E-02	0.50520515E 11	0.30716158E 13
0.14999999E-04	0.14999999E-04	0.88327030E-08	0.37347770E-02	0.37927628E 11	0.23059762E 13
0.16999999E-04	0.16999999E-04	0.10010397E-07	0.42327473E-02	0.29513730E 11	0.17944164E 13
0.19000000E-04	0.19000000E-04	0.11188090E-07	0.47307175E-02	0.23615572E 11	0.14358120E 13
0.22499999E-04	0.22499999E-04	0.13249055E-07	0.56021655E-02	0.16825275E 11	0.10229662E 13
0.27499999E-04	0.27499999E-04	0.16193289E-07	0.68470912E-02	0.11249188E 11	0.68394360E 12
0.32500000E-04	0.32500000E-04	0.19137523E-07	0.80920167E-02	0.80441317E 10	0.48907819E 12
0.37499999E-04	0.37499999E-04	0.22081757E-07	0.93369424E-02	0.60345194E 10	0.36689502E 12
0.42499999E-04	0.42499999E-04	0.25025991E-07	0.10581867E-01	0.46923100E 10	0.28528953E 12
0.47499999E-04	0.47499999E-04	0.27970226E-07	0.11826794E-01	0.37517740E 10	0.22810552E 12
0.54999999E-04	0.54999999E-04	0.32386577E-07	0.13694182E-01	0.27931066E 10	0.16981914E 12
0.64999999E-04	0.64999999E-04	0.38275046E-07	0.16184033E-01	0.19948252E 10	0.12128413E 12
0.74999999E-04	0.74999999E-04	0.44163515E-07	0.18673885E-01	0.14946094E 10	0.90871322E 11
0.84999999E-04	0.84999999E-04	0.50051983E-07	0.21163736E-01	0.11607296E 10	0.70571637E 11
0.94999999E-04	0.94999999E-04	0.55940452E-07	0.23653588E-01	0.92691598E 09	0.56355914E 11
0.12499999E-03	0.12499999E-03	0.73605858E-07	0.31123141E-01	0.53140248E 09	0.32308939E 11
0.17500000E-03	0.17500000E-03	0.10304820E-06	0.43572398E-01	0.26776934E 09	0.16280209E 11
0.24999999E-03	0.24999999E-03	0.14721172E-06	0.62246283E-01	0.12877957E 09	0.78297177E 10
0.34999999E-03	0.34999999E-03	0.20609640E-06	0.87144797E-01	0.64088131E 08	0.38965184E 10
0.45000000E-03	0.45000000E-03	0.26498109E-06	0.11204331E-00	0.37815981E 08	0.22991881E 10
0.55000000E-03	0.55000000E-03	0.32386578E-06	0.13694182E-00	0.24692311E 08	0.15012771E 10
0.64999999E-03	0.64999999E-03	0.38275046E-06	0.16184033E-00	0.17244361E 08	0.10484464E 10
0.74999999E-03	0.74999999E-03	0.44163515E-06	0.18673885E-00	0.12633917E 08	0.76813430E 09
0.84999999E-03	0.84999999E-03	0.50051983E-06	0.21163736E-00	0.95942142E 07	0.58332224E 09
0.94999999E-03	0.94999999E-03	0.55940452E-06	0.23653588E-00	0.74918102E 07	0.45549739E 09
0.11250000E-02	0.11250000E-02	0.66245272E-06	0.28010827E-00	0.51145294E 07	0.31096020E 09
0.13750000E-02	0.13750000E-02	0.80966444E-06	0.34235456E-00	0.32171559E 07	0.19560107E 09
0.16249999E-02	0.16249999E-02	0.95687616E-06	0.40460084E-00	0.21644001E 07	0.13159417E 09
0.18749999E-02	0.18749999E-02	0.11040878E-05	0.46684713E-00	0.15275960E 07	0.92876889E 08
0.21250000E-02	0.21250000E-02	0.12512996E-05	0.52909341E 00	0.11175320E 07	0.67945251E 08
0.23750000E-02	0.23750000E-02	0.13985113E-05	0.59133969E 00	0.84065425E 06	0.51111255E 08
0.27500000E-02	0.27500000E-02	0.16193289E-05	0.68470912E 00	0.57112270E 06	0.34723905E 08
0.32500000E-02	0.32500000E-02	0.19137523E-05	0.80920169E 00	0.36104526E 06	0.21951327E 08
0.37499999E-02	0.37499999E-02	0.22081757E-05	0.93369426E 00	0.23944148E 06	0.14557893E 08
0.42500000E-02	0.42500000E-02	0.25025992E-05	0.10581868E 01	0.16459537E 06	0.10007296E 08
0.47499999E-02	0.47499999E-02	0.27970226E-05	0.11826794E 01	0.11634342E 06	0.70736078E 07
0.55000000E-02	0.55000000E-02	0.32386578E-05	0.13694182E 01	0.71995281E 05	0.43772683E 07
0.64999999E-02	0.64999999E-02	0.38275046E-05	0.16184033E 01	0.40185542E 05	0.24432559E 07
0.74999999E-02	0.74999999E-02	0.44163515E-05	0.18673885E 01	0.23531041E 05	0.14306726E 07
0.84999999E-02	0.84999999E-02	0.50051984E-05	0.21163736E 01	0.14282128E 05	0.86834452E 06
0.94999999E-02	0.94999999E-02	0.55940452E-05	0.23653588E 01	0.89135505E 04	0.54193832E 06
0.11250000E-01	0.11250000E-01	0.66245273E-05	0.28010827E 01	0.41111218E 04	0.24995364E 06
0.13750000E-01	0.13750000E-01	0.80966444E-05	0.34235456E 01	0.14769209E 04	0.89789793E 05
0.16249999E-01	0.16249999E-01	0.95687615E-05	0.40460084E 01	0.56740654E 03	0.34497964E 05
0.18749999E-01	0.18749999E-01	0.11040878E-04	0.46684712E 01	0.22870009E 03	0.13904823E 05
0.21250000E-01	0.21250000E-01	0.12512996E-04	0.52909341E 01	0.95547388E 02	0.58092216E 04
0.23750000E-01	0.23750000E-01	0.13985113E-04	0.59133969E 01	0.41046609E 02	0.24956083E 04
0.26250000E-01	0.26250000E-01	0.15457230E-04	0.65358598E 01	0.18030746E 02	0.10962582E 04
0.28749999E-01	0.28749999E-01	0.16929347E-04	0.71583226E 01	0.80661162E 01	0.49041484E 03
0.31250000E-01	0.31250000E-01	0.18401464E-04	0.77807856E 01	0.36635987E 01	0.22274452E 03
0.33750000E-01	0.33750000E-01	0.19873582E-04	0.84032483E 01	0.16854980E 01	0.10247722E 03
0.36250000E-01	0.36250000E-01	0.21345699E-04	0.90257111E 01	0.78402082E 00	0.47667977E 02
0.38750000E-01	0.38750000E-01	0.22817816E-04	0.96481740E 01	0.36818663E-00	0.22385518E 02
0.41249999E-01	0.41249999E-01	0.24289933E-04	0.10270637E 02	0.17435379E-00	0.10600601E 02
0.43749999E-01	0.43749999E-01	0.25762051E-04	0.10893099E 02	0.83174650E-01	0.50569669E 01
0.46249999E-01	0.46249999E-01	0.27234168E-04	0.11515562E 02	0.39938471E-01	0.24282341E 01
0.48749999E-01	0.48749999E-01	0.28706285E-04	0.12138025E 02	0.19290058E-01	0.11728235E 01
0.51250000E-01	0.51250000E-01	0.30178402E-04	0.12760488E 02	0.93661876E-02	0.56945837E 00
0.53749999E-01	0.53749999E-01	0.31650519E-04	0.13382950E 02	0.45694233E-02	0.27781809E-00
0.56249999E-01	0.56249999E-01	0.33122636E-04	0.14005414E 02	0.22389332E-02	0.13612574E-00
0.58750000E-01	0.58750000E-01	0.34594753E-04	0.14627876E 02	0.11013827E-02	0.66963384E-01

NOTES FOR TABLE 12

This table gives the results for K and K_{sc} from the auxillary code for a 14 Mev source on the density interface. The notation is as follows:

Radius -------- Same as Table 11 (see notes for Table 11).

Slant Range --- Same as Table 11 (see notes for Table 11).

Adjusted mu r - The number of source energy mean free paths from the z axis to the midpoint of a radial bin along a line on the observation plane.

Direct Beam --- First collision dosage from the unscattered flux at the midpoint of radial bin.

Scattered ----- Total scattered dosage (not including direct beam) at the midpoint of a radial bin as obtained from the main code.

B ------------ Dose build-up factor for an infinite homogeneous medium (obtained with main code).

K ------------ $K = \frac{D_{db} + D_{sc}}{BD_{db}}$

where D_{db} = unscattered dosage

D_{sc} = scattered dosage

B = dose build-up factor as above

K_{sc} ---------- $K_{sc} = \frac{D_{sc}}{(B-1)D_{db}}$

Table 12

PROBLEM 206 OBSERVATION LEVEL = 0. NEW RADS

RADIUS	SLANT RANGE	ADJUSTED MU R	DIRECT BEAM	SCATTERED	H	K	KSC
0.49999999E-06	0.49999999E-06	0.12449256E-03	0.20828848E 16	0.16419999E 15	0.10001577E 01	0.10786628E 01	0.49994244E 03
0.15000000E-05	0.15000000E-05	0.37347770E-03	0.23137403E 15	0.43449999E 14	0.10004731E 01	0.11872295E 01	0.39696512E 03
0.24999999E-05	0.24999999E-05	0.62246282E-03	0.83273915E 14	0.17240000E 14	0.10007884E 01	0.12063767E 01	0.26257536E 03
0.34999999E-05	0.34999999E-05	0.87144797E-03	0.42476113E 14	0.10720000E 14	0.10011038E 01	0.12509962E 01	0.22863699E 03
0.45000000E-05	0.45000000E-05	0.11204331E-02	0.25689030E 14	0.51520000E 13	0.10014192E 01	0.11988511E 01	0.14131363E 03
0.55000000E-05	0.55000000E-05	0.13694182E-02	0.17192507E 14	0.33989999E 13	0.10017346E 01	0.11956284E 01	0.11397680E 03
0.64999999E-05	0.64999999E-05	0.16184033E-02	0.12306363E 14	0.21430000E 13	0.10020500E 01	0.11717355E 01	0.84966483E 02
0.74999999E-05	0.74999993E-05	0.18673885E-02	0.92411434E 13	0.13240000E 13	0.10023654E 01	0.11405744E 01	0.60571262E 02
0.84999999E-05	0.84999999E-05	0.21163736E-02	0.71928723E 13	0.88539999E 12	0.10026807E 01	0.11200914E 01	0.45919053E 02
0.95000000E-05	0.95000000E-05	0.23653588E-02	0.57568492E 13	0.56509999E 12	0.10029961E 01	0.10914171E 01	0.31603310E 02
0.10999999E-04	0.10999999E-04	0.27388364E-02	0.42922451E 13	0.27220000E 12	0.10034692E 01	0.10597402E 01	0.18280002E 02
0.13000000E-04	0.13000000E-04	0.32368067E-02	0.30716158E 13	0.15690000E 12	0.10040999E 01	0.10467888E 01	0.12458836E 02
0.14999999E-04	0.14999999E-04	0.37347770E-02	0.23059762E 13	0.99549999E 11	0.10047307E 01	0.10382587E 01	0.91255598E 01
0.16999999E-04	0.16999999E-04	0.42327472E-02	0.17944164E 13	0.60420000E 11	0.10053615E 01	0.10170723E 01	0.62013550E 01
0.19000000E-04	0.19000000E-04	0.47307175E-02	0.14358120E 13	0.20130000E 11	0.10059922E 01	0.10079799E 01	0.23396851E 01
0.22499999E-04	0.22499999E-04	0.56021655E-02	0.10229662E 13	0.34700000E 10	0.10070960E 01	0.99632211E 00	0.47802483E-00
0.27499999E-04	0.27499999E-04	0.68470911E-02	0.68394360E 12	0.71980000E 10	0.10086729E 01	0.10018353E 01	0.12134553E 01
0.32500000E-04	0.32500000E-04	0.80920167E-02	0.48907819E 12	0.28169999E 10	0.10102499E 01	0.99555548L 00	0.56193960E 00
0.37499999E-04	0.37499999E-04	0.93369423E-02	0.36689502E 12	0.32820000E 10	0.10118268E 01	0.99715222E 00	0.75636271E 00
0.42499999E-04	0.42499999E-04	0.10581867E-01	0.28528953E 12	0.33950000E 08	0.10134037E 01	0.98689101E 00	0.48782891E-02
0.47499999E-04	0.47499999E-04	0.11826793E-01	0.22810552E 12	0.96520000E 09	0.10149806E 01	0.98940942E 00	0.28245699E-00
0.54999999E-04	0.54999999E-04	0.13694182E-01	0.16981914E 12	0.69690000E 09	0.10173459E 01	0.98575206E 00	0.22300496E-00
0.64999999E-04	0.64999999E-04	0.16184033E-01	0.12128413E 12	0.91050000E 09	0.10204998E 01	0.98726839E 00	0.36620734E-00
0.74999999E-04	0.74999999E-04	0.18673884E-01	0.90871322E 11	0.12710000E 10	0.10236535E 01	0.99055658E 00	0.59131894E 00
0.84999999E-04	0.84999999E-04	0.21163736E-01	0.70571637E 11	0.61719999E 09	0.10268076E 01	0.98240986E 00	0.32624289E-00
0.94999999E-04	0.94999999E-04	0.23653587E-01	0.56355914E 11	0.32749999E 10	0.10299612E 01	0.10273326E 01	0.19396020E 01
0.12499999E-03	0.12499994E-03	0.31173141E-01	0.32708939E 11	0.90920000E 09	0.10394226E 01	0.98914607E 00	0.71382394E 00
0.17500000E-03	0.17500000E-03	0.43572398E-01	0.16280209E 11	0.59750000E 09	0.10551917E 01	0.98247645E 00	0.66497325E 00
0.24999999E-03	0.24999999E-03	0.62246282E-01	0.78297177E 10	0.38860000E 09	0.10788453E 01	0.97292117E 00	0.62947864E 00
0.34999999E-03	0.34999999E-03	0.87144797E-01	0.38965184E 10	0.28349999E 09	0.11103833E 01	0.96611426E 00	0.65913219E 00
0.45000000E-03	0.45000000E-03	0.11204331E-00	0.22991881E 10	0.21540000E 09	0.11419215E 01	0.95775867L 00	0.66012007E 00
0.55000000E-03	0.55000000E-03	0.13694182E-00	0.15012771E 10	0.20339999E 09	0.11734596E 01	0.96763843E 00	0.78137303E 00
0.64999999E-03	0.64999999E-03	0.16184033E-00	0.10484464E 10	0.78520000E 08	0.12053924E 01	0.89173593E 00	0.36462763E-00
0.74999999E-03	0.74999999E-03	0.18673885E-00	0.7681343CE 09	0.14700000E 09	0.12377605E 01	0.96252286E 00	0.80489729E 00
0.84999999E-03	0.84999999E-03	0.21163736E-00	0.58332224E 09	0.11929999E 09	0.12701286E 01	0.94834350E 00	0.75711419E 00
0.94999999E-03	0.94999999E-03	0.23653588E-00	0.45549739E 09	0.84159999E 08	0.13024966E 01	0.90961083E 00	0.61080036E 00
0.11250000E-02	0.11250000E-02	0.28010827E-00	0.31096020E 09	0.79409999E 08	0.13621516E 01	0.92160836E 00	0.70514755E 00
0.13750000E-02	0.13750000E-02	0.34235456E-00	0.19560107E 09	0.10010000E 09	0.14492963E 01	0.10430964E 01	0.11390162E 01
0.16249999E-02	0.16249999E-02	0.40460084E-00	0.13159417E 09	0.70739999E 08	0.15369012E 01	0.10004298E 01	0.10312302E 01
0.18749999E-02	0.18749999E-02	0.46684712E-00	0.92876869E 08	0.52920000E 08	0.16302706E 01	0.96289931E 00	0.90433464E 00
0.21250000E-02	0.21250000E-02	0.52909341E 00	0.67945251E 08	0.59800000E 08	0.17265494E 01	0.10889467E 01	0.12113702E 01
0.23750000E-02	0.23750000E-02	0.59133964E 00	0.51111255E 08	0.40759999E 08	0.18261435E 01	0.98430162E 00	0.96529961E 00
0.27500000E-02	0.27500000E-02	0.68470912E 00	0.34723905E 08	0.80390000E 08	0.19840055E 01	0.16709226E 01	0.23527508E 01
0.32500000E-02	0.32500000E-02	0.80920168E 00	0.21951327E 08	0.17930000E 08	0.22284033E 01	0.81529544E 00	0.66493395E 00
0.37499999E-02	0.37499999E-02	0.93369425E 00	0.14557893E 08	0.13689999E 08	0.24907579E 01	0.77903328E 00	0.63080887E 00
0.42500000E-02	0.42500000E-02	0.10581868E 01	0.10007296E 08	0.16040000E 08	0.27971044E 01	0.93054461E 00	0.89189613E 00
0.47499999E-02	0.47499999E-02	0.11826793E 01	0.70736078E 07	0.10670000E 08	0.31563061E 01	0.79473408E 00	0.69954076E 00
0.55000000E-02	0.55000000E-02	0.13694182E 01	0.43772683E 07	0.11319999E 08	0.37499057F 01	0.95631411E 00	0.94042780E 00
0.64999999E-02	0.64999999E-02	0.16184033E 01	0.24432559E 07	0.68440000E 07	0.46504538E 01	0.81737832E 00	0.76735120E 00
0.74999999E-02	0.74999999E-02	0.18673885E 01	0.14306726E 07	0.52860000E 07	0.57383566E 01	0.81813763E 00	0.77975674E 00
0.84999999E-02	0.84999999E-02	0.21163736E 01	0.86834452E 06	0.26000000E 07	0.69341100E 01	0.57602244E 00	0.50457495E 00
0.94999999E-02	0.94999999E-02	0.23653587E 01	0.54193832E 06	0.21160000E 07	0.83067602E 01	0.59042312E 00	0.53436861E 00
0.11250000E-01	0.11250000E-01	0.28010827E 01	0.24995364E 06	0.12220000E 07	0.11459745E 02	0.51387760E 00	0.46740206E-00
0.13750000E-01	0.13750000E-01	0.34235455E 01	0.89789793E 05	0.66590000E 06	0.17482547E 02	0.48146642E-00	0.44994322E-00
0.16249999E-01	0.16249999E-01	0.40460083E 01	0.34497964E 05	0.45370000E 06	0.26059138E 02	0.54305328E 00	0.52481855E 00
0.18749999E-01	0.18749999E-01	0.46684712E 01	0.13904823E 05	0.20970000E 06	0.38006368E 02	0.42311587E-00	0.40752710E-00
0.21250000E-01	0.21250000E-01	0.52909341E 01	0.59092216E 04	0.13840000E 06	0.54528025E 02	0.45525561E-00	0.44507881E-00
0.23750000E-01	0.23750000E-01	0.59133968E 01	0.24956083E 04	0.59350000E 05	0.77562671E 02	0.31950649E-00	0.31061843E-00
0.26250000E-01	0.26250000E-01	0.65358597E 01	0.10962582E 04	0.34700000E 05	0.10888264E 03	0.29983287E-00	0.29340134E-00
0.28749999E-01	0.28749999E-01	0.71583226E 01	0.49041484E 03	0.30060000E 05	0.14687420E 03	0.42413879E-00	0.42019113E-00
0.31250000E-01	0.31250000E-01	0.77807856E 01	0.22274452E 03	0.23159999E 05	0.19727070E 03	0.53213993E 00	0.52975617E 00
0.33750000E-01	0.33750000E-01	0.84032482E 01	0.10247722E 03	0.10100000E 05	0.26387355E 03	0.37729615E-00	0.37492732E-00
0.36250000E-01	0.36250000E-01	0.90257110E 01	0.47667977E 02	0.58350000E 04	0.35167807E 03	0.35091531E-00	0.34906637E-00
0.38750000E-01	0.38750000E-01	0.96481737E 01	0.22385518E 02	0.20919999E 04	0.46785744E 03	0.20188473E-00	0.20017519E-00
0.41249999E-01	0.41249999E-01	0.10270637E 02	0.10600601E 02	0.84039999E 03	0.62583786E 03	0.12827367E-00	0.12687854E-00
0.43749999E-01	0.43749999E-01	0.10993099E 02	0.50569669E 01	0.37530000E 03	0.82991238E 03	0.90629385E-01	0.89532314E-01
0.46249999E-01	0.46249999E-01	0.11715562E 02	0.24282341E 01	0.31999999E 03	0.11115810E 04	0.11945418E-00	0.11866131E-00
0.48749999E-01	0.48749999E-01	0.12438025E 02	0.11728235E 01	0.21699999E 03	0.14885189E 04	0.12497225E-00	0.12438400E-00
0.51250000E-01	0.51250000E-01	0.13160488E 02	0.56945837E 00	0.19430000E 03	0.19744393E 04	0.17331573E-00	0.17289682E-00
0.53749999E-01	0.53749999E-01	0.13882950E 02	0.27781809E-00	0.51100000E 03	0.26395413E 04	0.69721696E 00	0.69710220E 00
0.56249999E-01	0.56249999E-01	0.14605414E 02	0.13612574E-00	0.33920000E 02	0.34981208E 04	0.71308786E-01	0.71043227E-01
0.58750000E-01	0.58750000E-01	0.15327876E 02	0.66963384E-01	0.14760000E 03	0.46285413E 04	0.47643295E-00	0.47631980E-00

NOTES FOR TABLE 13

Radius -- Same as Tables 11 and 12

List ---- K factor as taken from Table 12.

Av 1 ---- Moving average of K three radial bins at a time as defined on page 17.

Av 2 ---- Moving average of Av 1 column three radial bins at a time.

Av 3 through 10 -- Moving average of previous Av column three bins at a time.

Table 13

AVERAGED K FACTOR FOR PROBLEM 206 OBSERVATION LEVEL = 0. NEW RADS

RADIUS	LIST	AV1	AV2	AV3	AV4	AV5	AV6	AV7	AV8	AV9	AV10
0.5000E-06	0.1079E 01	0.	0.	0.	0.	0.	0.	0.	0.	0.	0.
0.1500E-05	0.1187E 01	0.1157E 01	0.	0.	0.	0.	0.	0.	0.	0.	0.
0.2500E-05	0.1206E 01	0.1215E 01	0.1197E 01	0.	0.	0.	0.	0.	0.	0.	0.
0.3500E-05	0.1251E 01	0.1219E 01	0.1216E 01	0.1207E 01	0.	0.	0.	0.	0.	0.	0.
0.4500E-05	0.1199E 01	0.1215E 01	0.1208E 01	0.1205E 01	0.1200E 01	0.	0.	0.	0.	0.	0.
0.5500E-05	0.1196E 01	0.1189E 01	0.1191E 01	0.1189E 01	0.1187E 01	0.1184E 01	0.	0.	0.	0.	0.
0.6500E-05	0.1172E 01	0.1169E 01	0.1167E 01	0.1167E 01	0.1166E 01	0.1165E 01	0.1164E 01	0.	0.	0.	0.
0.7500E-05	0.1141E 01	0.1144E 01	0.1144E 01	0.1143E 01	0.1143E 01	0.1142E 01	0.1142E 01	0.1141E 01	0.	0.	0.
0.8500E-05	0.1120E 01	0.1117E 01	0.1117E 01	0.1117E 01	0.1117E 01	0.1118E 01	0.1118E 01	0.1118E 01	0.1119E 01	0.	0.
0.9500E-05	0.1091E 01	0.1090E 01	0.1091E 01	0.1092E 01	0.1093E 01	0.1094E 01	0.1094E 01	0.1095E 01	0.1096E 01	0.1096E 01	0.
0.1100E-04	0.1060E 01	0.1066E 01	0.1069E 01	0.1070E 01	0.1071E 01	0.1072E 01	0.1073E 01	0.1074E 01	0.1375E 01	0.1075E 01	0.1076E 01
0.1300E-04	0.1047E 01	0.1048E 01	0.1049E 01	0.1051E 01	0.1052E 01	0.1053E 01	0.1054E 01	0.1055E 01	0.1356E 01	0.1057E 01	0.1057E 01
0.1500E-04	0.1038E 01	0.1034E 01	0.1034E 01	0.1035E 01	0.1036E 01	0.1037E 01	0.1038E 01	0.1039E 01	0.1040E 01	0.1041E 01	0.1041E 01
0.1700E-04	0.1017E 01	0.1021E 01	0.1021E 01	0.1022E 01	0.1023E 01	0.1024E 01	0.1024E 01	0.1025E 01	0.1026E 01	0.1027E 01	0.1028E 01
0.1900E-04	0.1004E 01	0.1007E 01	0.1010E 01	0.1011E 01	0.1012E 01	0.1013E 01	0.1014E 01	0.1015E 01	0.1016E 01	0.1017E 01	0.1018E 01
0.2250E-04	0.9963E 00	0.1002E 01	0.1002E 01	0.1004E 01	0.1005E 01	0.1006E 01	0.1006E 01	0.1007E 01	0.1008E 01	0.1009E 01	0.1009E 01
0.2750E-04	0.1002E 01	0.9979E 00	0.9994E 00	0.9994E 00	1.0000E 00	0.1000E 01	0.1001E 01	0.1002E 01	0.1002E 01	0.1003E 01	0.1003E 01
0.3250E-04	0.9956E 00	0.9982E 00	0.9964E 00	0.9967E 00	0.9966E 00	0.9968E 00	0.9971E 00	0.9974E 00	0.9978E 00	0.9981E 00	0.9985E 00
0.3750E-04	0.9972E 00	0.9972E 00	0.9942E 00	0.9938E 00	0.9939E 00	0.9940E 00	0.9941E 00	0.9943E 00	0.9946E 00	0.9949E 00	0.9952E 00
0.4250E-04	0.9869E 00	0.9912E 00	0.9907E 00	0.9912E 00	0.9914E 00	0.9916E 00	0.9918E 00	0.9921E 00	0.9923E 00	0.9926E 00	0.9929E 00
0.4750E-04	0.9894E 00	0.9877E 00	0.9889E 00	0.9892E 00	0.9895E 00	0.9899E 00	0.9903E 00	0.9906E 00	0.9910E 00	0.9913E 00	0.9916E 00
0.5500E-04	0.9868E 00	0.9878E 00	0.9879E 00	0.9881E 00	0.9884E 00	0.9893E 00	0.9898E 00	0.9902E 00	0.9905E 00	0.9908E 00	0.9910E 00
0.6500E-04	0.9873E 00	0.9882E 00	0.9876E 00	0.9891E 00	0.9896E 00	0.9902E 00	0.9905E 00	0.9908E 00	0.9909E 00	0.9911E 00	0.9911E 00
0.7500E-04	0.9906E 00	0.9867E 00	0.9917E 00	0.9916E 00	0.9921E 00	0.9921E 00	0.9920E 00	0.9919E 00	0.9917E 00	0.9916E 00	0.9914E 00
0.8500E-04	0.9824E 00	0.1000E 01	0.9955E 00	0.9957E 00	0.9945E 00	0.9938E 00	0.9931E 00	0.9925E 00	0.9920E 00	0.9915E 00	0.9910E 00
0.9500E-04	0.1027E 01	0.9996E 00	0.9998E 00	0.9963E 00	0.9947E 00	0.9935E 00	0.9925E 00	0.9915E 00	0.9907E 00	0.9900E 00	0.9893E 00
0.1250E-03	0.9891E 00	0.9997E 00	0.9936E 00	0.9928E 00	0.9911E 00	0.9900E 00	0.9890E 00	0.9881E 00	0.9873E 00	0.9866E 00	0.9859F 00
0.1750E-03	0.9825E 00	0.9815E 00	0.9850E 00	0.9841E 00	0.9841E 00	0.9834E 00	0.9829E 00	0.9822E 00	0.9817E 00	0.9811E 00	0.9806E 00
0.2500E-03	0.9729E 00	0.9738E 00	0.9736E 00	0.9755E 00	0.9751E 00	0.9751E 00	0.9749E 00	0.9746E 00	0.9743E 00	0.9741E 00	0.9738E 00
0.3500E-03	0.9661E 00	0.9656E 00	0.9678E 00	0.9659E 00	0.9662F 00	0.9660E 00	0.9661E 00	0.9662E 00	0.9662F 00	0.9662E 00	0.9663E 00
0.4500F-03	0.9578E 00	0.9638E 00	0.9562E 00	0.9573E 00	0.9568E 00	0.9572E 00	0.9574E 00	0.9578E 00	0.9581E 00	0.9585E 00	0.9588E 00
0.5500E-03	0.9676E 00	0.9390E 00	0.9478E 00	0.9473E 00	0.9486E 00	0.9491E 00	0.9498F 00	0.9504E 00	0.9511E 00	0.9518E 00	0.9526E 00
0.6500E-03	0.8917E 00	0.9406E 00	0.9380E 00	0.9414E 00	0.9418E 00	0.9430E 00	0.9440E 00	0.9452E 00	0.9463E 00	0.9474E 00	0.9484E 00
0.7500E-03	0.9625E 00	0.9342F 00	0.9383E 00	0.9366E 00	0.9386E 00	0.9400E 00	0.9417E 00	0.9432E 00	0.9447F 00	0.9461E 00	0.9476E 00
0.8500E-03	0.9483E 00	0.9402E 00	0.9334E 00	0.9379E 00	0.9396E 00	0.9419E 00	0.9439E 00	0.9457E 00	0.9475E 00	0.9492E 00	0.9509E 00
0.9500E-03	0.9C96E 00	0.9265E 00	0.9416E 00	0.9443E 00	0.9476E 00	0.9497E 00	0.9517E 00	0.9536E 00	0.9555E 00	0.9574E 00	0.9592E 00
0.1125E-02	0.9216E 00	0.9581E 00	0.9577E 00	0.9607E 00	0.9620E 00	0.9633E 00	0.9651E 00	0.9671E 00	0.9591E 00	0.9711E 00	0.9730E 00
0.1375E-02	0.1043E 01	0.9894E 00	0.9829E 00	0.9811E 00	0.9802E 00	0.9824E 00	0.9845E 00	0.9868E 00	0.9888F 00	0.9904F 00	0.9918E 00
0.1625E-02	0.1000E 01	0.1002E 01	0.1003E 01	0.9987E 00	0.1005E 01	0.1008E 01	0.1011E 01	0.1012E 01	0.1013F 01	0.1014E 01	0.1014F 01
0.1875E-02	0.9629E 00	0.1017E 01	0.1011E 01	0.1035E 01	0.1038E 01	0.1042E 01	0.1042E 01	0.1041F 01	0.1040E 01	0.1038E 01	0.1035E 01
0.2125E-02	0.1089E 01	0.1012E 01	0.1093E 01	0.1081E 01	0.1083E 01	0.1076E 01	0.1071E 01	0.1065E 01	0.1060E 01	0.1055E 01	0.1050E 01
0.2375E-02	0.9843E 00	0.1248E 01	0.1139E 01	0.1132E 01	0.1108E 01	0.1095E 01	0.1083E 01	0.1073F 01	0.1065E 01	0.1057E 01	0.1051E 01
0.2750E-02	0.1671E 01	0.1157E 01	0.1164E 01	0.1111E 01	0.1094E 01	0.1077E 01	0.1065E 01	0.1056E 01	0.1049E 01	0.1041E 01	0.1036E 01
0.3250E-02	0.3153E 00	0.1088E 01	0.1029E 01	0.1038E 01	0.1028E 01	0.1024E 01	0.1020E 01	0.1015E 01	0.1012E 01	0.1008E 01	0.1004E 01
0.3750E-02	0.7790E 00	0.8416E 00	0.9216E 00	0.9358E 00	0.9514E 00	0.9576E 00	0.9617E 00	0.9634E 00	0.9640E 00	0.9638E 00	0.9629E 00
0.4250E-02	0.9305E 00	0.8348E 00	0.8568E 00	0.8800E 00	0.8930E 00	0.9030E 00	0.9091F 00	0.9132E 00	0.9157F 00	0.9170E 00	0.9175E 00
0.4750E-02	0.7747E 00	0.8939E 00	0.9614E 00	0.8632E 00	0.8646E 00	0.8668E 00	0.8688E 00	0.8703F 00	0.8713E 00	0.8718E 00	0.8720E 00
0.5500E-02	0.9561E 00	0.8561E 00	0.8713E 00	0.8507E 00	0.8429E 00	0.8367E 00	0.8329E 00	0.8304E 00	0.8286E 00	0.8273E 00	0.8263E 00
0.6500E-02	0.8174E 00	0.8639E 00	0.8191E 00	0.8149E 00	0.8025E 00	0.7952E 00	0.7893E 00	0.7851E 00	0.7820E 00	0.7797E 00	0.7780E 00
0.7500E-02	0.8131E 00	0.7372E 00	0.7542E 00	0.7421E 00	0.7402E 00	0.7360E 00	0.7330E 00	0.7305E 00	0.7285E 00	0.7271E 00	0.7259E 00
0.8500E-02	0.5760E 00	0.6615E 00	0.6529E 00	0.6635E 00	0.6652E 00	0.6679E 00	0.6692E 00	0.6701E 00	0.6706E 00	0.6710E 00	0.6713E 00
0.9500E-02	0.5904E 00	0.5601E 00	0.5834E 00	0.5901E 00	0.5984E 00	0.6037E 00	0.6081F 00	0.6113E 00	0.6134E 00	0.6150E 00	0.6175F 00
0.1125E-01	0.5137E 00	0.5296E 00	0.5338E 00	0.5417E 00	0.5474E 00	0.5526E 00	0.5566E 00	0.5601E 00	0.5630E 00	0.5659E 00	0.5678E 00
0.1375E-01	0.4814E-00	0.5128E 00	0.5080E 00	0.5105E 00	0.5118E 00	0.5136F 00	0.5155F 00	0.5176F 00	0.5194E 00	0.5220E 00	0.5243E 00
0.1625E-01	0.5431E 00	0.4825E-00	0.4897E-00	0.4832E-00	0.4814E-00	0.4804E-00	0.4907E-00	0.4818E-00	0.4833E-00	0.4852E-00	0.4872E-00
0.1875E-01	0.4231E-00	0.4738E-00	0.4519E-00	0.4507E-00	0.4480E-00	0.4482E-00	0.4491E-00	0.4506E-00	0.4524E-00	0.4544E-00	0.4565E-00
0.2125E-01	0.4553F-00	0.3993E-00	0.4104E-00	0.4103E-00	0.4152E-00	0.4185E-00	0.4220E-00	0.4249E-00	0.4275E-00	0.4298E-00	0.4319E-00
0.2375E-01	0.3195E-00	0.3582E-00	0.3685E-00	0.3846E-00	0.3926E-00	0.3991E-00	0.4036E-00	0.4070E-00	0.4096E-00	0.4116E-00	0.4131E-00
0.2625E-01	0.2999E-00	0.3478E-00	0.3749E-00	0.3824E-00	0.3897E-00	0.3932E-00	0.3956E-00	0.3969E-00	0.3976E-00	0.3979E-00	0.3979E-00
0.2875E-01	0.4241E-00	0.4187E-00	0.4037E-00	0.4021E-00	0.3974E-00	0.3945E-00	0.3915E-00	0.3899E-00	0.3864E-00	0.3842E-00	0.3822E-00
0.3125E-01	0.5321E 00	0.4445E-00	0.4278E-00	0.4077E-00	0.3964E-00	0.3867E-00	0.3795E-00	0.3735E-00	0.3686E-00	0.3645E-00	0.3611E-00
0.3375E-01	0.3773F-00	0.4201E-00	0.3916F-00	0.3795E-00	0.3664E-00	0.3572E-00	0.3496E-00	0.3435E-00	0.3386E-00	0.3347E-00	0.3316E-00
0.3625E-01	0.3509E-00	0.3100E-00	0.3191E-00	0.3121E-00	0.3088E-00	0.3047E-00	0.3014E-00	0.2988E-00	0.2969E-00	0.2955E-00	0.
0.3875E-01	0.2019E-00	0.2770E-00	0.2258E-00	0.2350E-00	0.2387E-00	0.2423E-00	0.2454E-00	0.2483E-00	0.2509E-00	0.	0.
0.4125E-01	0.1283E-00	0.1403E-00	0.1600E-00	0.1691F-00	0.1795E-00	0.1893E-00	0.1979E-00	0.2057E-00	0.	0.	0.
0.4375E-01	0.9063E-01	0.1128E-00	0.1216E-00	0.1343E-00	0.1497E-00	0.1622E-00	0.1738E-00	0.	0.	0.	0.
0.4625E-01	0.1195E-00	0.1117E-00	0.1212E-00	0.1457E-00	0.1575E-00	0.1699E-00	0.	0.	0.	0.	0.
0.4875E-01	0.1250E-00	0.1392E-00	0.1943E-00	0.1924E-00	0.2026E-00	0.	0.	0.	0.	0.	0.
0.5125E-01	0.1731E-00	0.3318E-00	0.2617E-00	0.2698E-00	0.	0.	0.	0.	0.	0.	0.
0.5375E-01	0.5972F 00	0.3139E-00	0.3536E-00	0.	0.	0.	0.	0.	0.	0.	0.
0.5625E-01	0.7131E-01	0.4190E-00	0.	0.	0.	0.	0.	0.	0.	0.	0.
0.5875E-01	0.4764E-00	0.	0.	0.	0.	0.	0.	0.	0.	0.	0.

NOTATION FOR TABLE 14

This table is the same as Table 13 for the K factor in every way except that it is for the K_{sc} factor.

Table 14

AVERAGED K SCATTERED FACTOR FOR PROBLEM 206 OBSERVATION LEVEL = 0. NEW RADS

RADIUS	LIST	AV1	AV2	AV3	AV4	AV5	AV6	AV7	AV8	AV9	AV10
0.5000E-C6	0.4999E 03	0.	0.	0.	0.	0.	0.	0.	0.	0.	0.
0.1500E-C5	0.3970E 03	0.3865E 03	0.	0.	0.	0.	0.	0.	0.	0.	0.
0.2500E-05	0.2626E 03	0.2961E 03	0.2978E 03	0.	0.	0.	0.	0.	0.	0.	0.
0.3500E-C5	0.2286E 03	0.2108E 03	0.2227E 03	0.2275E 03	0.	0.	0.	0.	0.	0.	0.
0.4500E-C5	0.1413E 03	0.1613E 03	0.1619E 03	0.1683E 03	0.1731E 03	0.	0.	0.	0.	0.	0.
0.5500E-C5	0.1140E 03	0.1134E 03	0.1204E 03	0.1234E 03	0.1277E 03	0.1315E 03	0.	0.	0.	0.	0.
0.6500E-C5	0.8495E 02	0.8650E 02	0.8791E 02	0.9125E 02	0.9384E 02	0.9680E 02	0.9972E 02	0.	0.	0.	0.
0.7500E-C5	0.6C57E 02	0.6381E 02	0.6545E 02	0.6687E 02	0.6880E 02	0.7085E 02	0.7299E 02	0.7518E 02	0.	0.	0.
0.8500E-C5	0.4592E 02	0.4603E 02	0.4726E 02	0.4856E 02	0.4982E 02	0.5131E 02	0.5284E 02	0.5447E 02	0.5616E 02	0.	0.
0.9500E-05	0.3160E 02	0.3193E 02	0.3292E 02	0.3406E 02	0.3521E 02	0.3637E 02	0.3758E 02	0.3882E 02	0.4011E 02	0.4144E 02	0.
0.1100E-C4	0.1828E 02	0.2078E 02	0.2200E 02	0.2305E 02	0.2406E 02	0.2506E 02	0.2604E 02	0.2704E 02	0.2805E 02	0.2909E 02	0.3016E 02
0.1300E-C4	0.1246E 02	0.1329E 02	0.1422E 02	0.1509E 02	0.1589E 02	0.1670E 02	0.1750E 02	0.1830E 02	0.1911E 02	0.1993E 02	0.2077E 02
0.1500E-C4	0.9126E 01	0.8595E 01	0.9035E 01	0.9547E 01	0.1014E 02	0.1075E 02	0.1137E 02	0.1200E 02	0.1263E 02	0.1328E 02	0.1393E 02
0.1700E-C4	0.4201E 01	0.5222E 01	0.5386E 01	0.5796E 01	0.6207E 01	0.6659E 01	0.7127E 01	0.7598E 01	0.8082E 01	0.8574E 01	0.9074E 01
0.1900E-C4	0.2340E 01	0.2340E 01	0.2969E 01	0.3277E 01	0.3624E 01	0.3960E 01	0.4303E 01	0.4651E 01	0.5007E 01	0.5370E 01	0.5741E 01
0.2250E-C4	0.4780E-00	0.1344E 01	0.1478E 01	0.1809E 01	0.2044E 01	0.2289E 01	0.2528E 01	0.2772E 01	0.3022E 01	0.3278E 01	0.3542E 01
0.2750E-C4	0.1213E 01	0.7511E 00	0.9796E 00	0.1046E 01	0.1196F 01	0.1335E 01	0.1486E 01	0.1642E 01	0.1806E 01	0.1976E 01	0.2153E 01
0.3250E-C4	0.5619E 00	0.8439E 00	0.6792E 00	0.7346E 00	0.7651E 00	0.8348E 00	0.9126E 00	0.1002E 01	0.1100E 01	0.1206E 01	0.1319E 01
0.3750E-C4	0.7564E 00	0.4424E-00	0.5452E 00	0.5151E 00	0.5429E 00	0.5678E 00	0.6081E 00	0.6561E 00	0.7124E 00	0.7756E 00	0.8451E 00
0.4250E-C4	0.8878E-02	0.3492E-00	0.3210E-00	0.3789E-00	0.3954E-00	0.4216E-00	0.4477E-00	0.4789E-00	0.5141E 00	0.5536E 00	0.5971E 00
0.4750E-C4	0.7825E-00	0.1714E-00	0.2704E-00	0.2922E-00	0.3266E-00	0.3536E-00	0.3808E-00	0.4072E-00	0.4342E-00	0.4620E-00	0.4913E-00
0.5500E-C4	0.2230E-00	0.2906E-00	0.2852E-00	0.3087E-00	0.3387E-00	0.3673E-00	0.3931E-00	0.4164E-00	0.4379E-00	0.4583E-00	0.4782E-00
0.6500E-C4	0.3662E-00	0.3935E-00	0.3707E-00	0.4157E-00	0.4363E-00	0.4584E-00	0.4753E-00	0.4901E-00	0.5028E 00	0.5143E 00	0.5250E 00
0.7500E-C4	0.5913E 00	0.4279E-00	0.5913E 00	0.5844E 00	0.6000E 00	0.6004E 00	0.6019E 00	0.6019E 00	0.6021E 00	0.6024E 00	0.6030E 00
0.8500E-C4	0.3267E-00	0.9524E 00	0.7912E 00	0.7999E 00	0.7649E 00	0.7468E 00	0.7285E 00	0.7143E 00	0.7023E 00	0.6924E 00	0.6841E 00
0.9500E-C4	0.1940E 01	0.9932E 00	0.1017E 01	0.9105E 00	0.8756E 00	0.8383E 00	0.8126E 00	0.7906E 00	0.7727E 00	0.7575E 00	0.7446E 00
0.1250E-C3	0.7138E 00	0.1106E 01	0.9229E 00	0.9164E 00	0.8743E 00	0.8526E 00	0.8307E 00	0.8132E 00	0.7976E 00	0.7840E 00	0.7719E 00
0.1750E-C3	0.6650E 00	0.6694E 00	0.8087E 00	0.7962E 00	0.8078E 00	0.8013E 00	0.7962E 00	0.7889E 00	0.7816E 00	0.7743E 00	0.7671E 00
0.2500E-C3	0.6295E 00	0.6512E 00	0.6567E 00	0.7109E 00	0.7217E 00	0.7348E 00	0.7398E 00	0.7428E 00	0.7436E 00	0.7432E 00	0.7420E 00
0.3500E-C3	0.6591E 00	0.6496E 00	0.6670E 00	0.6581E 00	0.6750E 00	0.6832E 00	0.6925E 00	0.6991E 00	0.7044E 00	0.7084E 00	0.7115E 00
0.4500E-C3	0.6601E 00	0.7001E 00	0.6505E 00	0.6561E 00	0.6524E 00	0.6595E 00	0.6649E 00	0.6714E 00	0.6773E 00	0.6828E 00	0.6877E 00
0.5500E-C3	0.7811E 00	0.6019E 00	0.6507E 00	0.6442E 00	0.6506E 00	0.6521E 00	0.6567E 00	0.6613E 00	0.6666E 00	0.6720E 00	0.6773E 00
0.6500E-C3	0.3646E-00	0.6502E 00	0.6315E 00	0.6515E 00	0.6530E 00	0.6585E 00	0.6624E 00	0.6672E 00	0.6720E 00	0.6772E 00	0.6824E 00
0.7500E-C3	0.8049E 00	0.6422E 00	0.6722E 00	0.6632E 00	0.6718E 00	0.6765E 00	0.6824E 00	0.6876E 00	0.6928E 00	0.6979E 00	0.7030E 00
0.8500E-C3	0.7571E 00	0.7243E 00	0.6458E 00	0.7009E 00	0.7046E 00	0.7123E 00	0.7181E 00	0.7238E 00	0.7289E 00	0.7338E 00	0.7386E 00
0.9500E-C3	0.6108E 00	0.6910E 00	0.7445E 00	0.7499E 00	0.7604E 00	0.7657E 00	0.7707E 00	0.7753E 00	0.7797E 00	0.7840E 00	0.7881E 00
0.1125E-C2	0.7051E 00	0.8183E 00	0.8193E 00	0.8303E 00	0.8320E 00	0.8342E 00	0.8370E 00	0.8401E 00	0.8434E 00	0.8465E 00	0.8495E 00
0.1375E-C2	0.1139E 01	0.9485E 00	0.9272E 00	0.9157E 00	0.9103E 00	0.9112E 00	0.9126E 00	0.9147E 00	0.9169E 00	0.9181E 00	0.9192E 00
0.1625E-C2	0.1001E 01	0.1015E 01	0.1001E 01	0.9849E 00	0.9913E 00	0.9924E 00	0.9945E 00	0.9948E 00	0.9943E 00	0.9929E 00	0.9909E 00
0.1875E-C2	0.9040E 00	0.1039E 01	0.1027E 01	0.1073E 01	0.1076E 01	0.1080E 01	0.1077E 01	0.1073E 01	0.1068E 01	0.1062E 01	0.1056E 01
0.2125E-C2	0.1211E 01	0.1027E 01	0.1192E 01	0.1169E 01	0.1173E 01	0.1160E 01	0.1148E 01	0.1135E 01	0.1123E 01	0.1112E 01	0.1101E 01
0.2375E-C2	0.9653E 00	0.1510E 01	0.1288E 01	0.1277E 01	0.1230E 01	0.1205E 01	0.1181E 01	0.1161E 01	0.1145E 01	0.1130E 01	0.1117E 01
0.2750E-C2	0.2353E 01	0.1328E 01	0.1351E 01	0.1243E 01	0.1211E 01	0.1178E 01	0.1156E 01	0.1137E 01	0.1122E 01	0.1109E 01	0.1097E 01
0.3250E-C2	0.6647E 00	0.1216E 01	0.1091E 01	0.1113E 01	0.1092E 01	0.1095E 01	0.1075E 01	0.1067E 01	0.1060E 01	0.1053E 01	0.1047E 01
0.3750E-C2	0.6308E 00	0.7292E 00	0.8956E 00	0.9192E 00	0.9509E 00	0.9628E 00	0.9715E 00	0.9758E 00	0.9781E 00	0.9787E 00	0.9783E 00
0.4250E-C2	0.8919E 00	0.7407E 00	0.7713E 00	0.8208E 00	0.8458E 00	0.8673E 00	0.8810E 00	0.8911E 00	0.8980E 00	0.9028E 00	0.9061E 00
0.4750E-C2	0.6995E 00	0.8440E 00	0.7957E 00	0.7974E 00	0.8053E 00	0.8129E 00	0.8207E 00	0.8270E 00	0.8324E 00	0.8367E 00	0.8401E 00
0.5500E-C2	0.9404E 00	0.8024E 00	0.8252E 00	0.7976E 00	0.7976E 00	0.7818E 00	0.7794E 00	0.7790E 00	0.7796E 00	0.7809E 00	0.7823E 00
0.6500E-C2	0.7574E 00	0.8292E 00	0.7718E 00	0.7678E 00	0.7524E 00	0.7435E 00	0.7370E 00	0.7329E 00	0.7306E 00	0.7294E 00	0.7291E 00
0.7500E-C2	0.7794E 00	0.6839E 00	0.7764E 00	0.6919E 00	0.6904E 00	0.6857E 00	0.6824E 00	0.6798E 00	0.6780E 00	0.6770E 00	0.6765E 00
0.8500E-C2	0.5046E 00	0.6062E 00	0.5974E 00	0.6115E 00	0.6142E 00	0.6181E 00	0.6200E 00	0.6214E 00	0.6223E 00	0.6231E 00	0.6239E 00
0.9500E-02	0.5344E 00	0.5021E 00	0.5308E 00	0.5390E 00	0.5496E 00	0.5562E 00	0.5617E 00	0.5658E 00	0.5690E 00	0.5715E 00	0.5736E 00
0.1125E-C1	0.4674E-00	0.4839E-00	0.4089E-00	0.4983E-00	0.5048E 00	0.5108E 00	0.5156E 00	0.5198E 00	0.5232E 00	0.5262E 00	0.5289E 00
0.1375E-C1	0.4499E-00	0.4807E-00	0.4751E-00	0.4770E-00	0.4782E-00	0.4799E-00	0.4819E-00	0.4842E-00	0.4865E-00	0.4889E-00	0.4913E-00
0.1625E-C1	0.5248E 00	0.4608E-00	0.4669E-00	0.4593E-00	0.4567E-00	0.4551E-00	0.4550E-00	0.4557E-00	0.4570E-00	0.4587E-00	0.4606E-00
0.1875E-C1	0.4075E-00	0.4591E-00	0.4359E-00	0.4339E-00	0.4304E-00	0.4299E-00	0.4301E-00	0.4311E-00	0.4325E-00	0.4341E-00	0.4359E-00
0.2125E-C1	0.4451E-00	0.3877E-00	0.3989E-00	0.3981E-00	0.4026E-00	0.4054E-00	0.4083E-00	0.4107E-00	0.4129E-00	0.4148E-00	0.4165E-00
0.2375E-C1	0.3106E-00	0.3497E-00	0.3596E-00	0.3757E-00	0.3832E-00	0.3896E-00	0.3937E-00	0.3968E-00	0.3990E-00	0.4006E-00	0.4018E-00
0.2625E-C1	0.2934E-00	0.3414E-00	0.3685E-00	0.3758E-00	0.3830E-00	0.3862E-00	0.3884E-00	0.3895E-00	0.3897E-00	0.3899E-00	0.3896E-00
0.2875E-C1	0.4202E-00	0.4145E-00	0.3992E-00	0.3974E-00	0.3925E-00	0.3875E-00	0.3861E-00	0.3835E-00	0.3804E-00	0.3784E-00	0.3762E-00
0.3125E-C1	0.5298E 00	0.4416E-00	0.4747E-00	0.4043E-00	0.3929E-00	0.3831E-00	0.3757E-00	0.3696E-00	0.3645E-00	0.3603E-00	0.3566E-00
0.3375E-C1	0.3749E-00	0.4173E-00	0.3892E-00	0.3770E-00	0.3638E-00	0.3545E-00	0.3467E-00	0.3406E-00	0.3356E-00	0.3315E-00	0.3283E-00
0.3625E-C1	0.3491E-00	0.3081E-00	0.3171E-00	0.3101E-00	0.3068E-00	0.3026E-00	0.2992E-00	0.2966E-00	0.2945E-00	0.2931E-00	0.
0.3875E-C1	0.2002E-00	0.2254E-00	0.2241E-00	0.2333E-00	0.2371E-00	0.2406E-00	0.2437E-00	0.2465E-00	0.2491E-00	0.	0.
0.4125E-C1	0.1269E-00	0.1399E-00	0.1586E-00	0.1677E-00	0.1781E-00	0.1879E-00	0.1965E-00	0.2043E-00	0.	0.	0.
0.4375E-01	0.8953E-01	0.1117E-00	0.1205E-00	0.1332E-00	0.1486E-00	0.1611E-00	0.1727E-00	0.	0.	0.	0.
0.4625E-C1	0.1187E-00	0.1109E-00	0.1204E-00	0.1448E-00	0.1566E-00	0.1691E-00	0.	0.	0.	0.	0.
0.4875E-C1	0.1244E-00	0.1386E-00	0.1437E-00	0.1918E-00	0.2020E-00	0.	0.	0.	0.	0.	0.
0.5125E-C1	0.1729E-00	0.3315E-00	0.2613E-00	0.2694E-00	0.	0.	0.	0.	0.	0.	0.
0.5375E-C1	0.6971E 00	0.3137E-00	0.3533E-00	0.	0.	0.	0.	0.	0.	0.	0.
0.5625E-C1	0.7104E-01	0.4148E-00	0.	0.	0.	0.	0.	0.	0.	0.	0.
0.5875E-C1	0.4763E-00	0.	0.	0.	0.	0.	0.	0.	0.	0.	0.

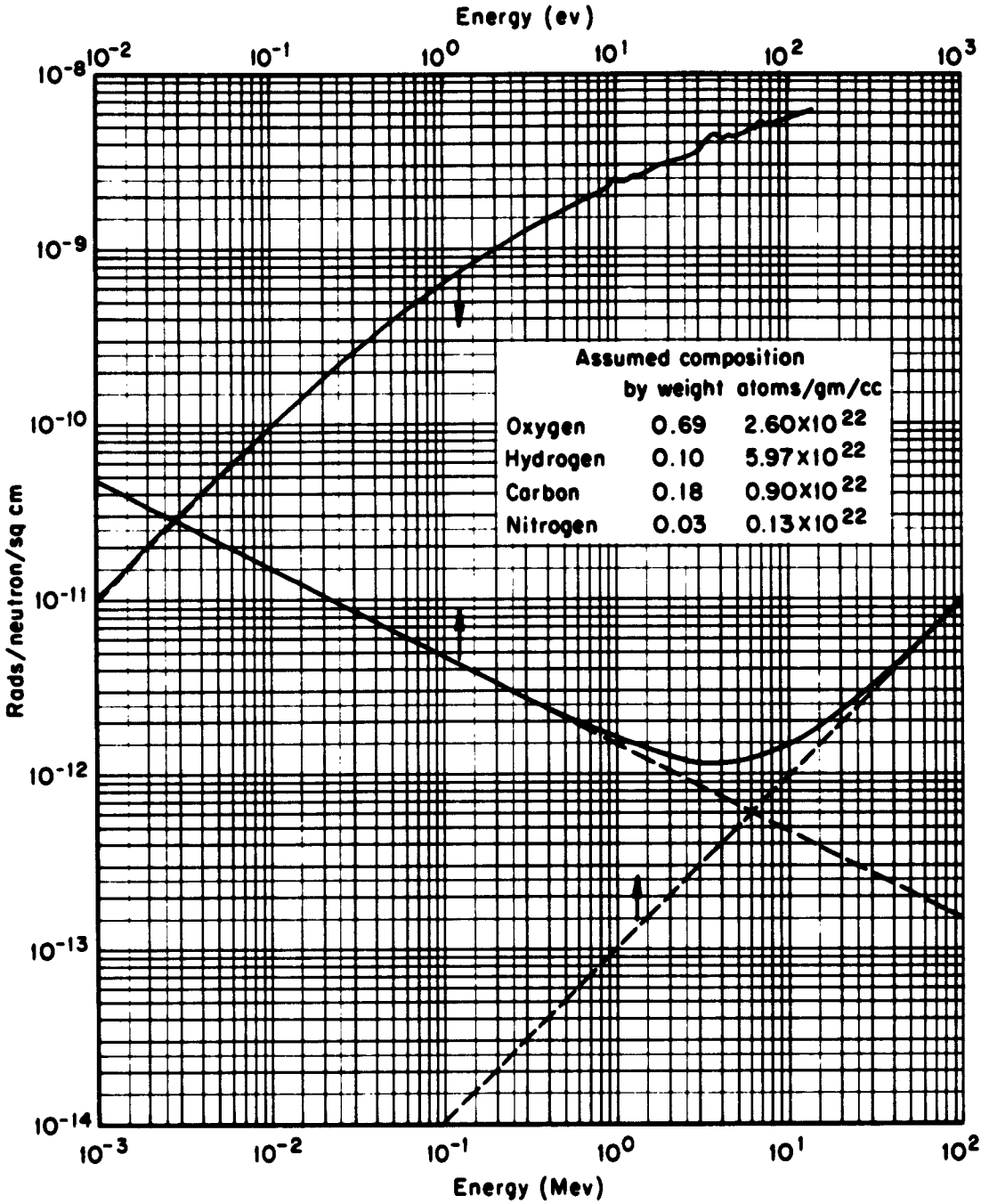

Fig. 1 — First collision tissue dosage as a function of neutron energy

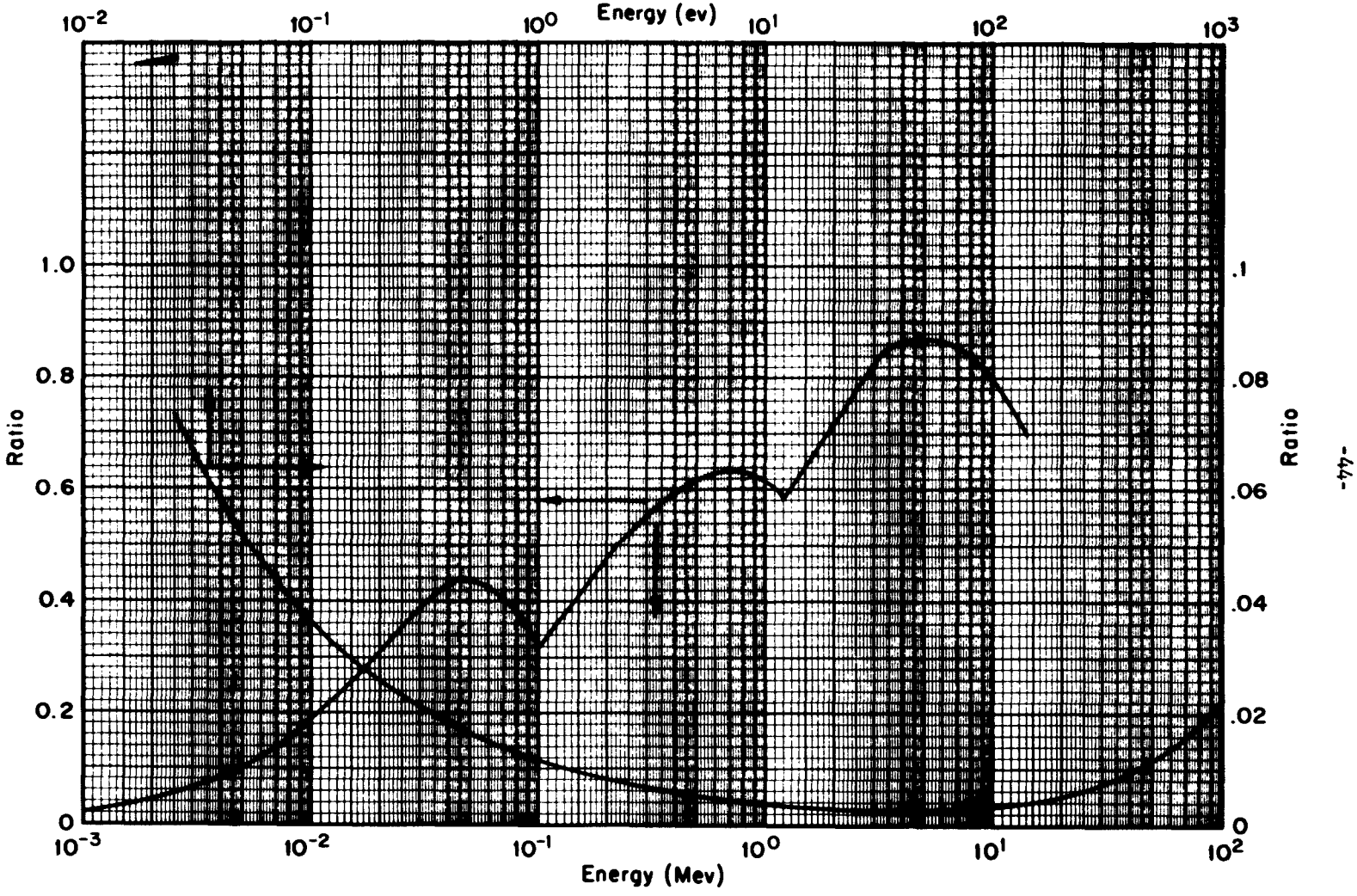

Fig. 2 — Ratio of first collision rads to phantom surface rads

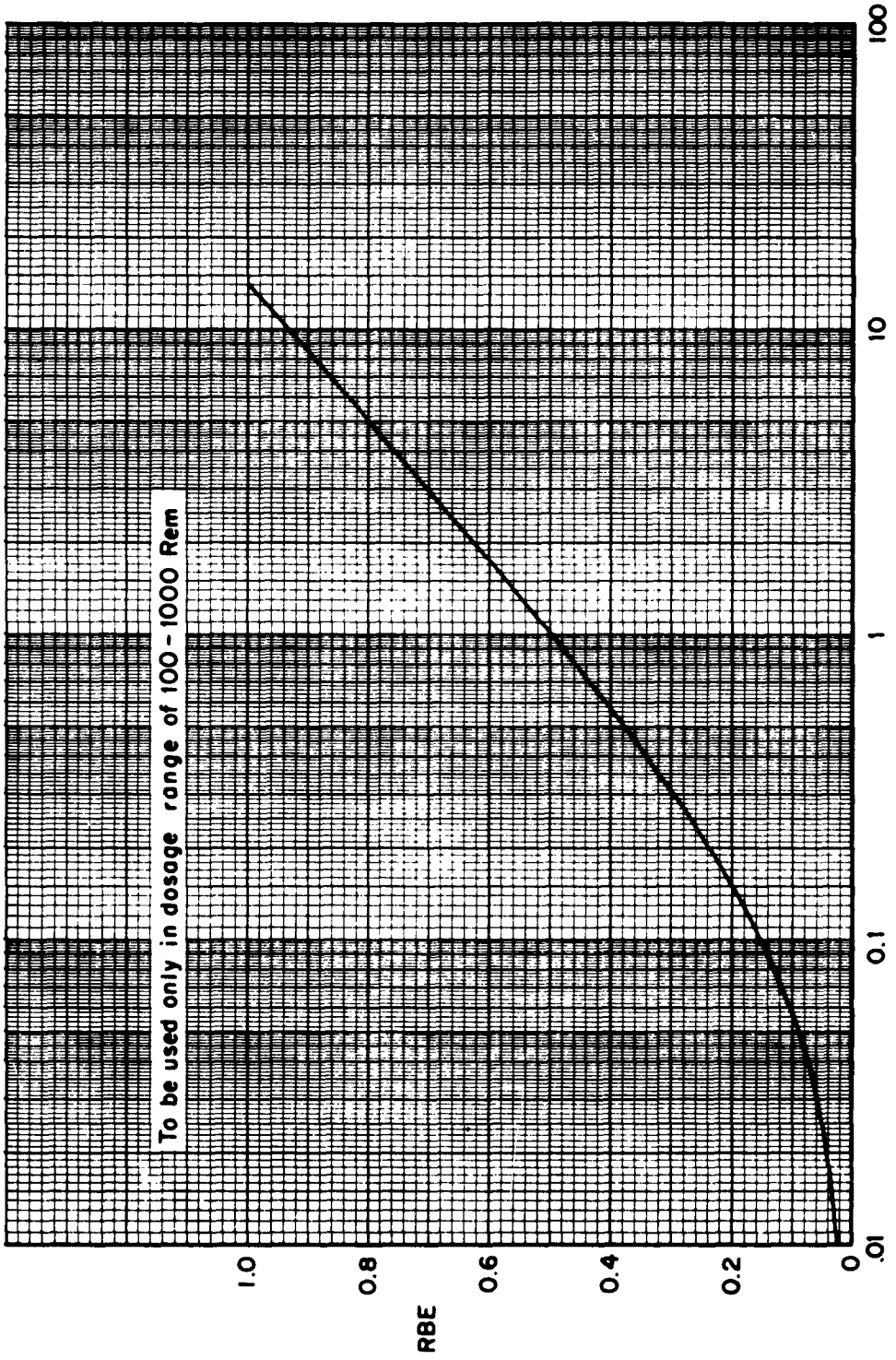

Fig. 3 — RBE dependence on incident neutron energy for quasi-isotropic incidence

INPUT PARAMETERS FOR PROBLEMS OF FIGS. 4 THROUGH 9

Radial bins - 0 (?,000) 14,000 (4,000) 30,000 (5,000) 100,000 (10,000) 250,000 (25,000) 500,000 feet.

Polar angles for starting histories - 48 were aimed at boundaries between radial bins on 60,000 foot level. 10 additional angles as follows: μ = - 1, - 5/6, - 2/3, - 1/2, - 1/3, - 1/6, 0, + 1/5, + 1/2, + 1.0.

Number of histories - 200 histories per angle, or 11,600 total.

Energy subdivisions of arrival dosage*-

14 - 8 Mev
8 - 2 Mev
2 - .05 Mev
.05 - .38 x 10^{-6} Mev

Note: Standard deviations for each radial collection bin are computed by the code. This information is contained in the original printout, but is not shown in this report.

*This information is available in original printout, but is not presented in this report.

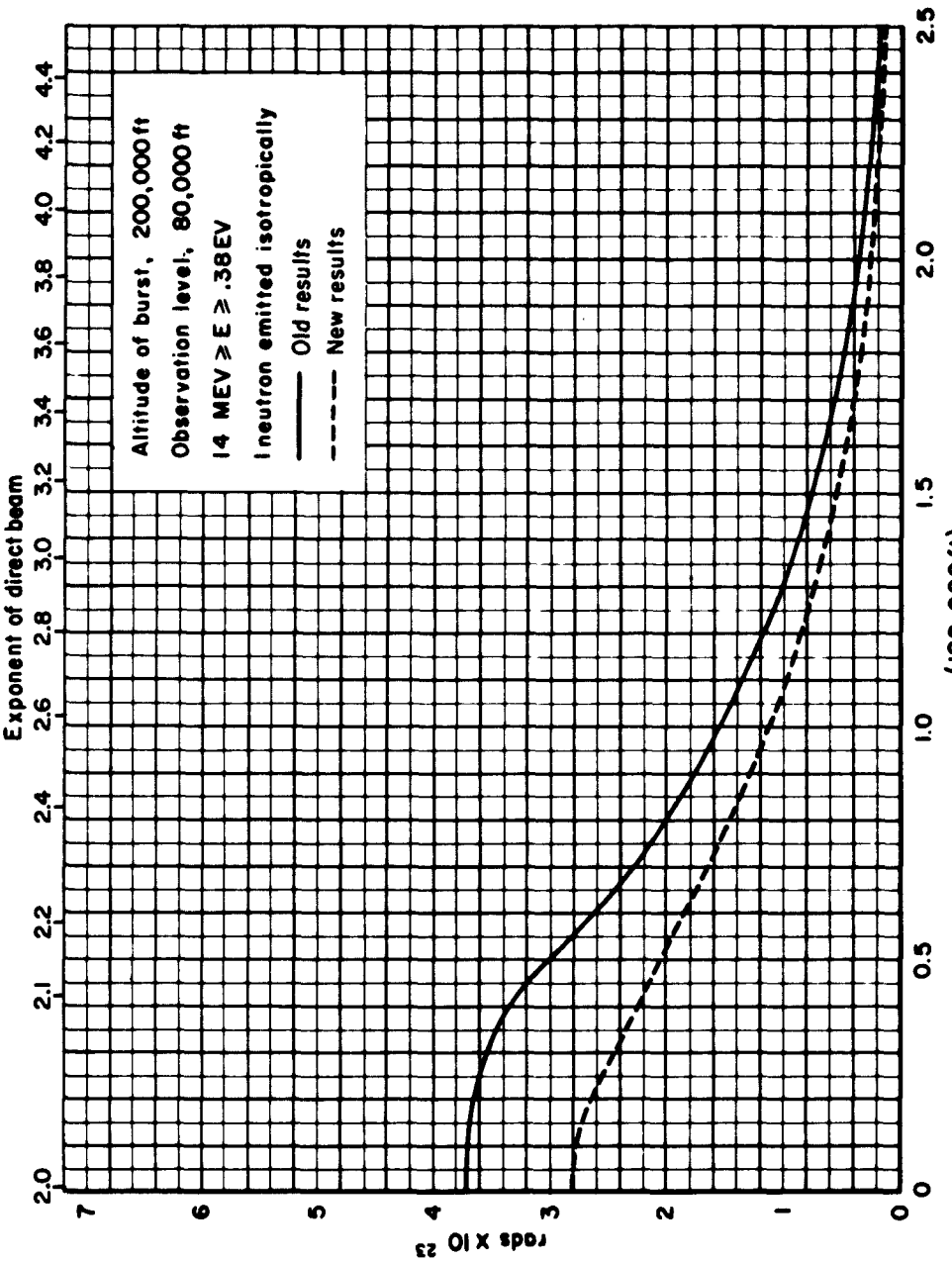
Altitude of burst, 200,000 ft
Observation level, 80,000 ft
14 MEV ≥ E ≥ .38EV
1 neutron emitted isotropically
Old results
New results
rads x 10 23
r (100,000 ft)
Exponent of direct beam
0
1
2
3
4
5
6
7
0
0.5
1.0
1.5
2.0
2.5
2.0
2.1
2.2
2.4
2.6
2.8
3.0
3.2
3.4
3.6
3.8
4.0
4.2
4.4

Fig. 4

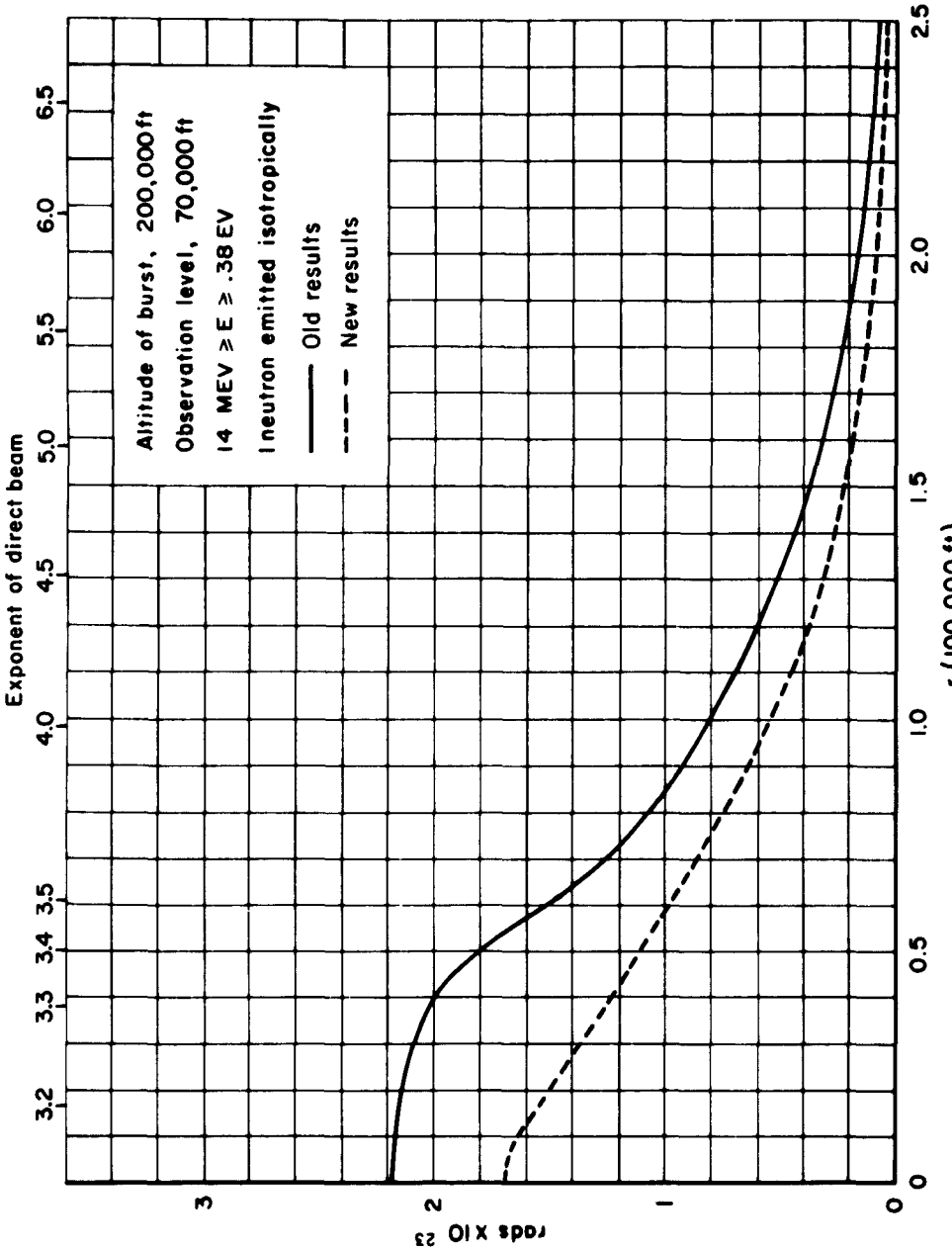
Altitude of burst, 200,000 ft
Observation level, 70,000 ft
14 MEV ≥ E ≥ .38 EV
1 neutron emitted isotropically
Old results
New results
Exponent of direct beam
3.2
3.3
3.4
3.5
4.0
4.5
5.0
5.5
6.0
6.5
rads x 10 23
0
1
2
3
r (100,000 ft)
0
0.5
1.0
1.5
2.0
2.5

Fig. 5

NOTES FOR FIGS. 6, 7, 8 AND 9

The very close-in radial bins subtend a small solid angle. The result is that the statistical fluctuations inherent in the Monte Carlo process become evident in these bins before they are felt in the more distant bins which subtend more solid angle.

In Figs. 6 through 9, the results of the old problem suffer from this effect, with the consequence that the dosages are low at radii from 0 to 25,000 feet or so. In the results shown in Figs. 6 through 9 for the new problem corrections have been made for this effect by means of the build-up factor of Fig. 19. The assumption made was that in the vertically down direction (0 radius on the various planes) the dosage would be only slightly less than that for the scaled results for an infinite homogeneous medium. This assumption is borne out by the results of Figs. 4 and 5 for the 80,000 foot and 70,000 foot cases where the fluctuations are not yet so severe that bias is introduced. There the assumption is easily checked and found to hold.

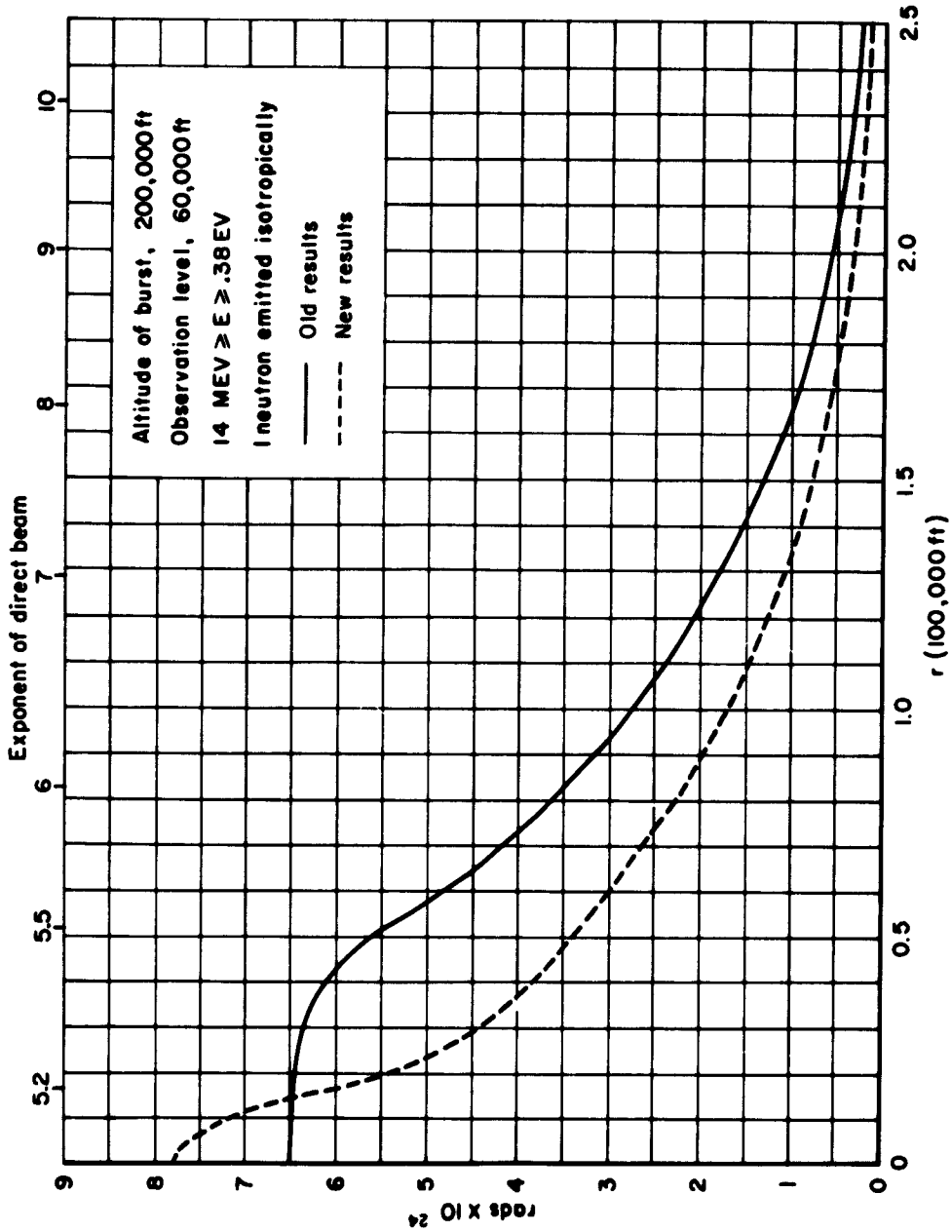
Altitude of burst, 200,000 ft
Observation level, 60,000 ft
14 MEV ≥ E ≥ .38 EV
1 neutron emitted isotropically
Old results
New results
Exponent of direct beam
rads x 10 24
r (100,000 ft)
10
9
8
7
6
5.5
5.2
0
1
2
3
4
5
6
7
8
9
0
0.5
1.0
1.5
2.0
2.5

Fig. 6

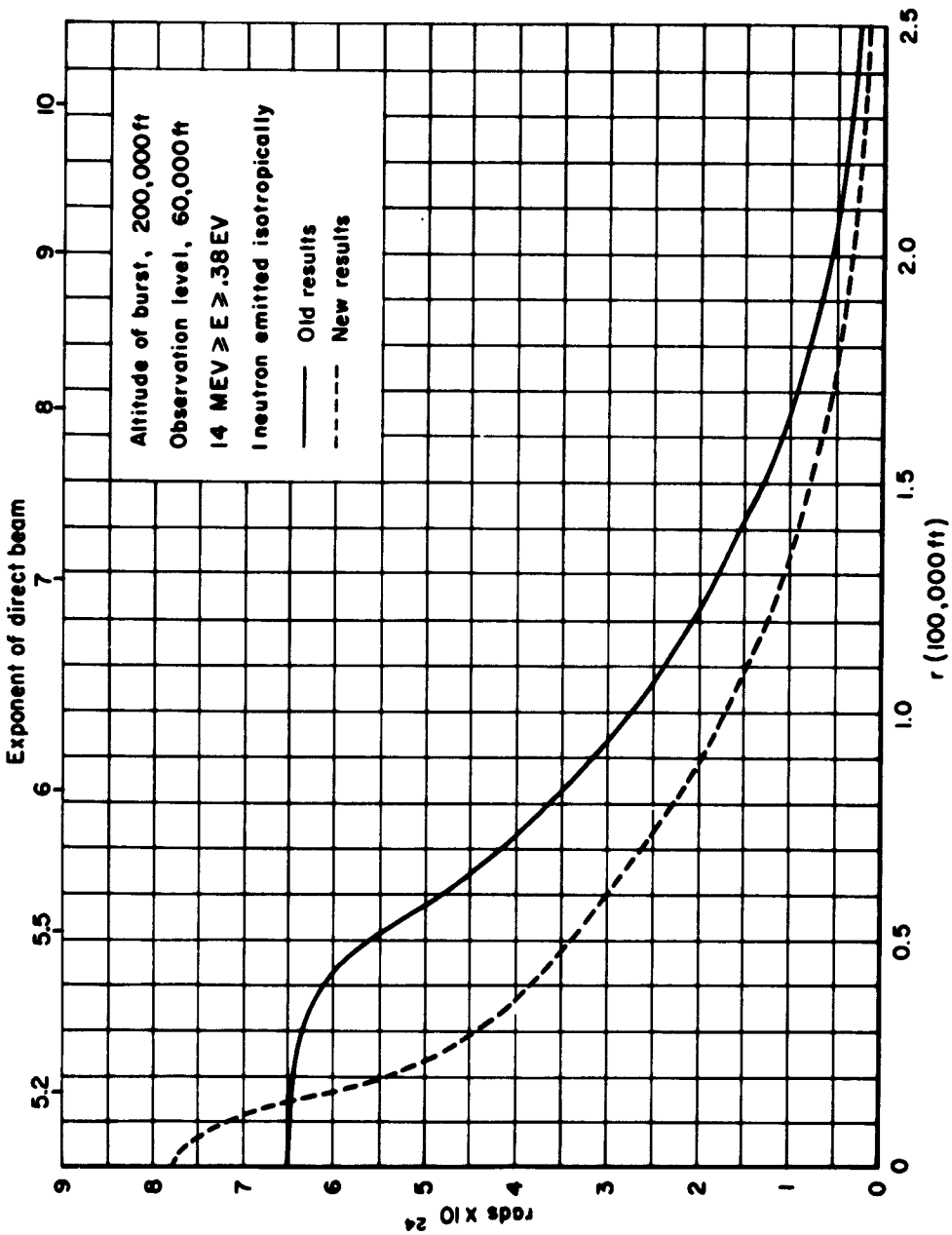
Altitude of burst, 200,000 ft
Observation level, 60,000 ft
14 MEV ≥ E ≥ .38 EV
1 neutron emitted isotropically
Old results
New results
Exponent of direct beam
rads x 10 24
r (100,000 ft)
10
9
8
7
6
5.5
5.2
0
1
2
3
4
5
6
7
8
9
0
0.5
1.0
1.5
2.0
2.5

Fig. 6

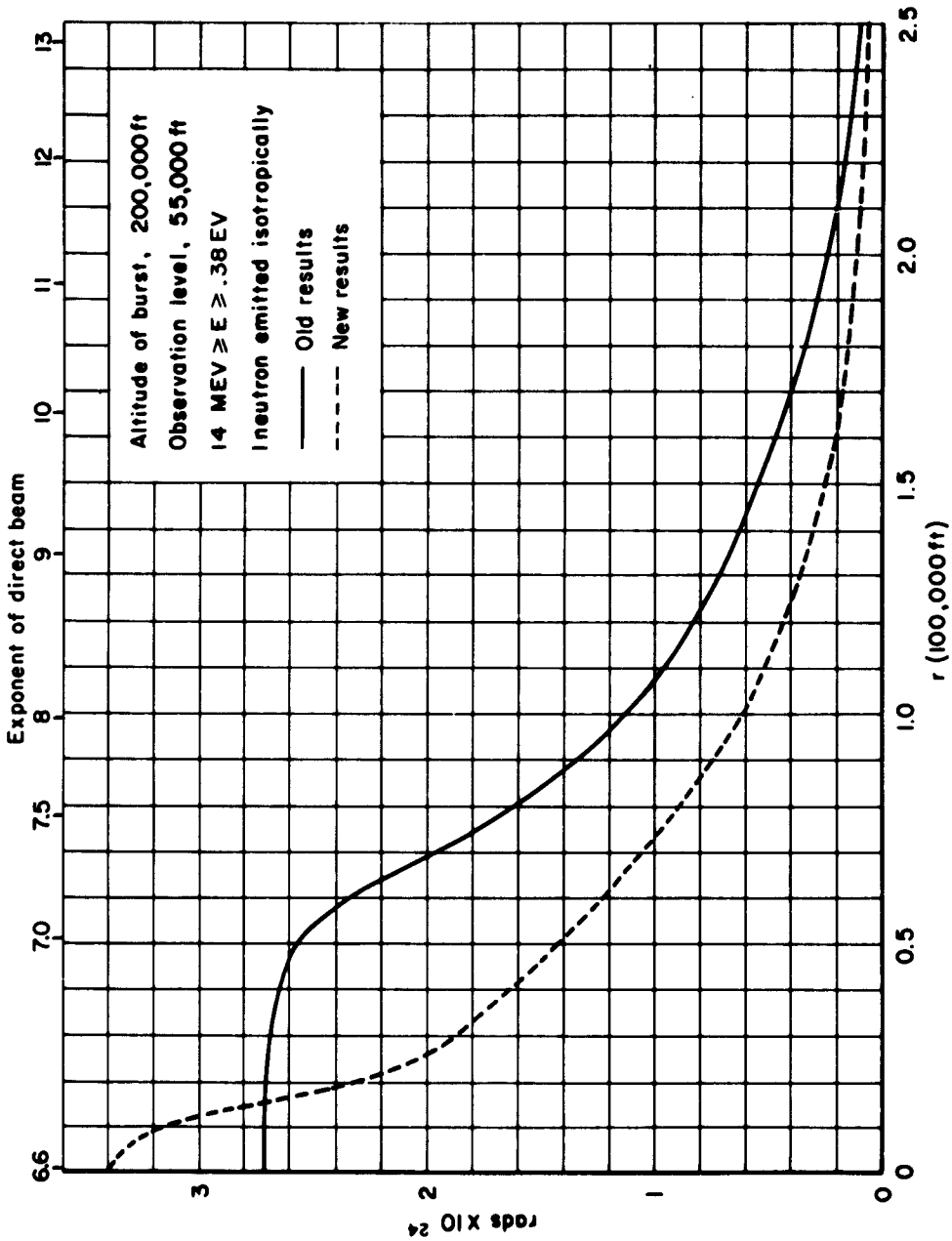
Altitude of burst, 200,000 ft
Observation level, 55,000 ft
14 MEV ≥ E ≥ .38 EV
1 neutron emitted isotropically
Old results
New results
Exponent of direct beam
rads x 10 24
r (100,000 ft)
13
12
11
10
9
8
7.5
7.0
6.6
3
2
1
0
2.5
2.0
1.5
1.0
0.5
0

Fig. 7

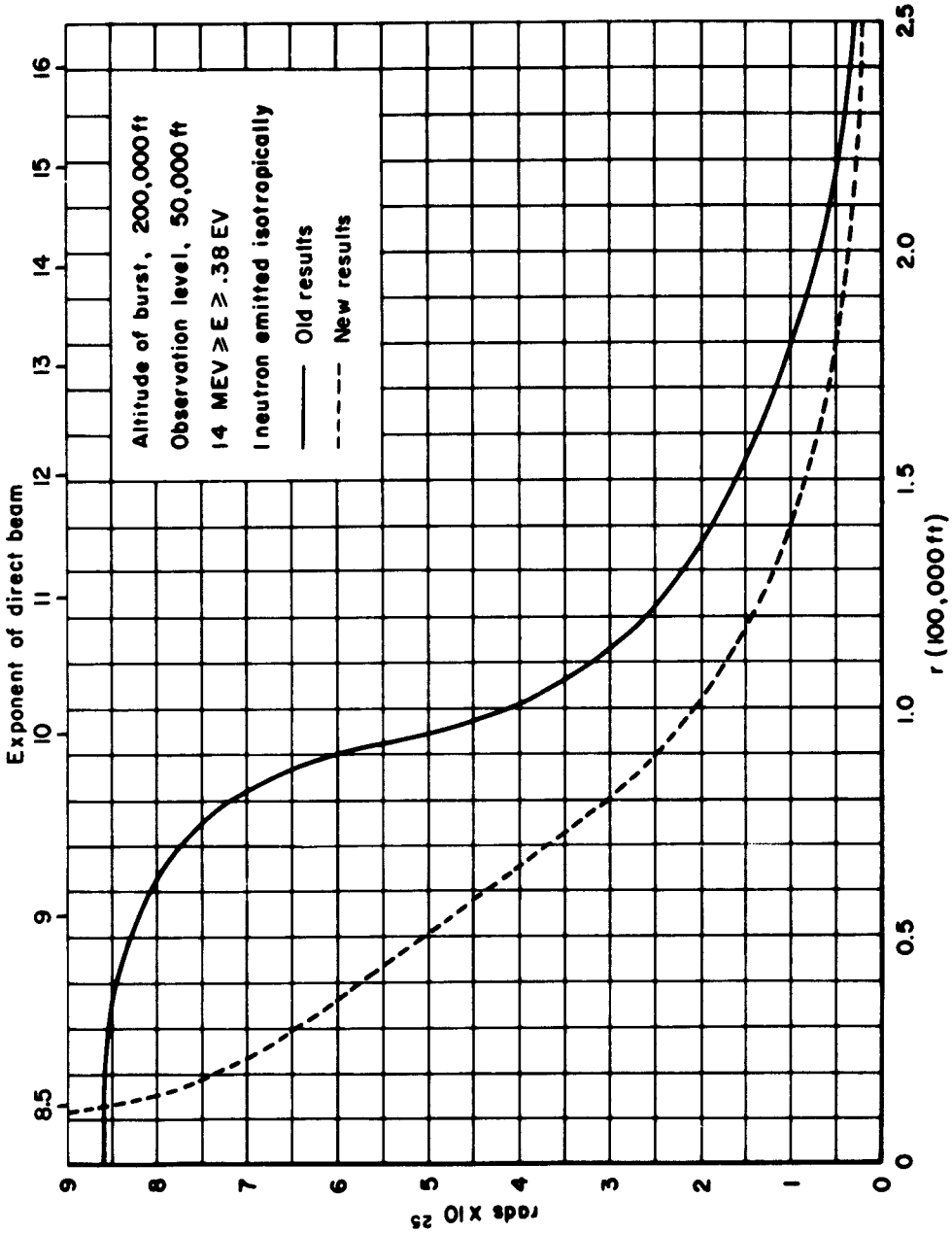
Altitude of burst, 200,000 ft
Observation level, 50,000 ft
14 MEV ≥ E ≥ .38 EV
1 neutron emitted isotropically
Old results
New results
Exponent of direct beam
rads x 10 25
r (100,000 ft)
8.5
9
10
11
12
13
14
15
16
0
1
2
3
4
5
6
7
8
9
0
0.5
1.0
1.5
2.0
2.5

Fig. 8

NOTE FOR FIG. 9

These results on this level are not statistically significant. They are presented only to show the results as given by the code, but should not be used otherwise.

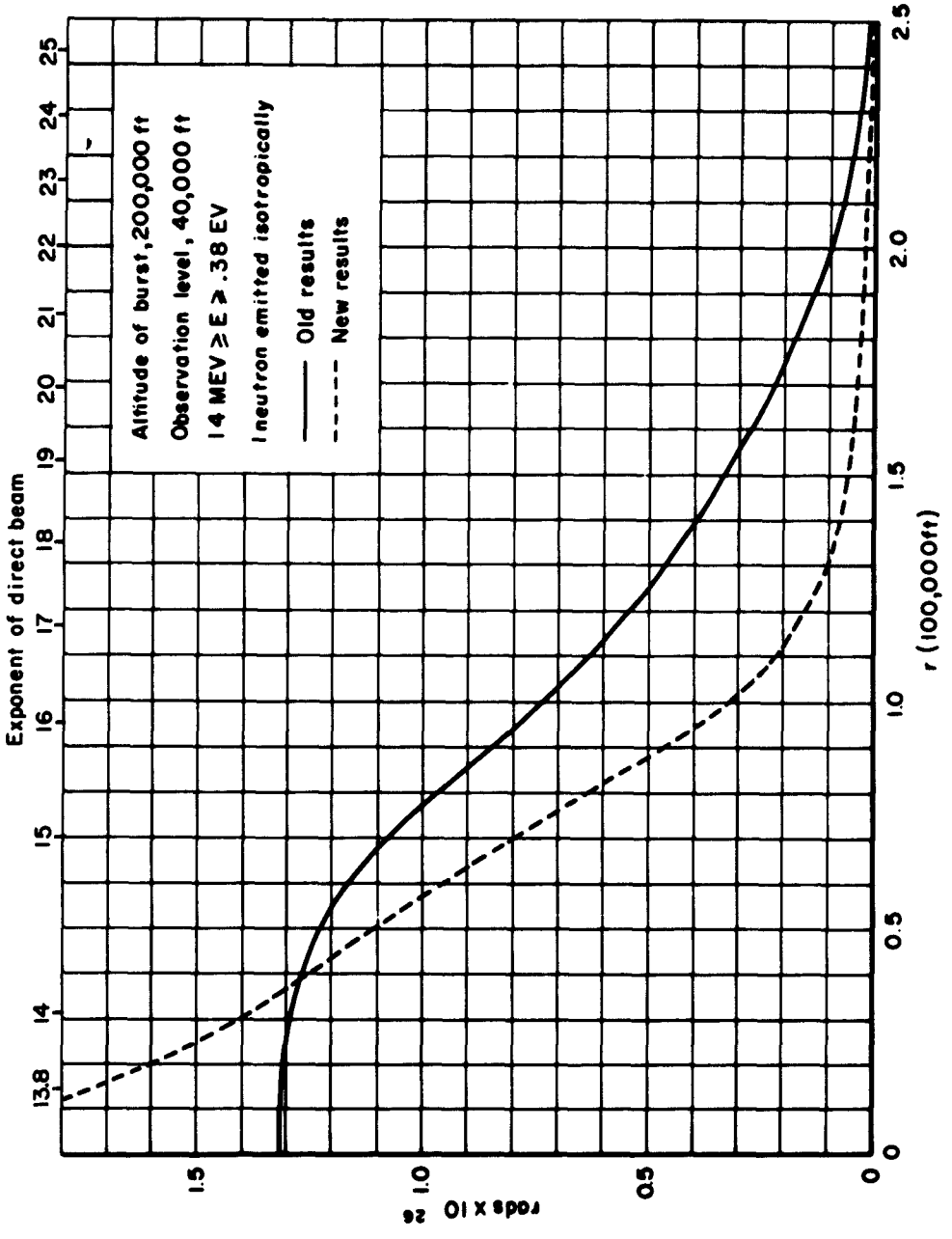
Altitude of burst, 200,000 ft
Observation level, 40,000 ft
14 MEV ≥ E ≥ .38 EV
1 neutron emitted isotropically
Old results
New results
Exponent of direct beam
rads x 10 26
r (100,000ft)
13.8
14
15
16
17
18
19
20
21
22
23
24
25
0
0.5
1.0
1.5
2.0
2.5

Fig. 9

INPUT PARAMETERS FOR PROBLEMS OF FIGS. 10 THROUGH 15

Radial Bins - 0 (4,000) 40,000 (5,000) 200,000 (10,000) 250,000 (25,000) 350,000 (50,000) 400,000 feet.

Polar angles for starting histories - 50 were aimed at midpoints of radial bins on 60,000 foot level plus 5 additional as follows: $\mu = 1, 0, +1/5, +1/2, +1$.

Number of histories - 100 per angle or 5500 total.

Energy subdivision of arrival dosage* -

14 - 8 Mev
8 - 5 Mev
5 - 2 Mev
2 - 1 Mev
1 - .45 Mev
.45 - .05 Mev
.05 - .38 x 10^{-6} Mev

*This information is available in original printout, but is not presented in this report.

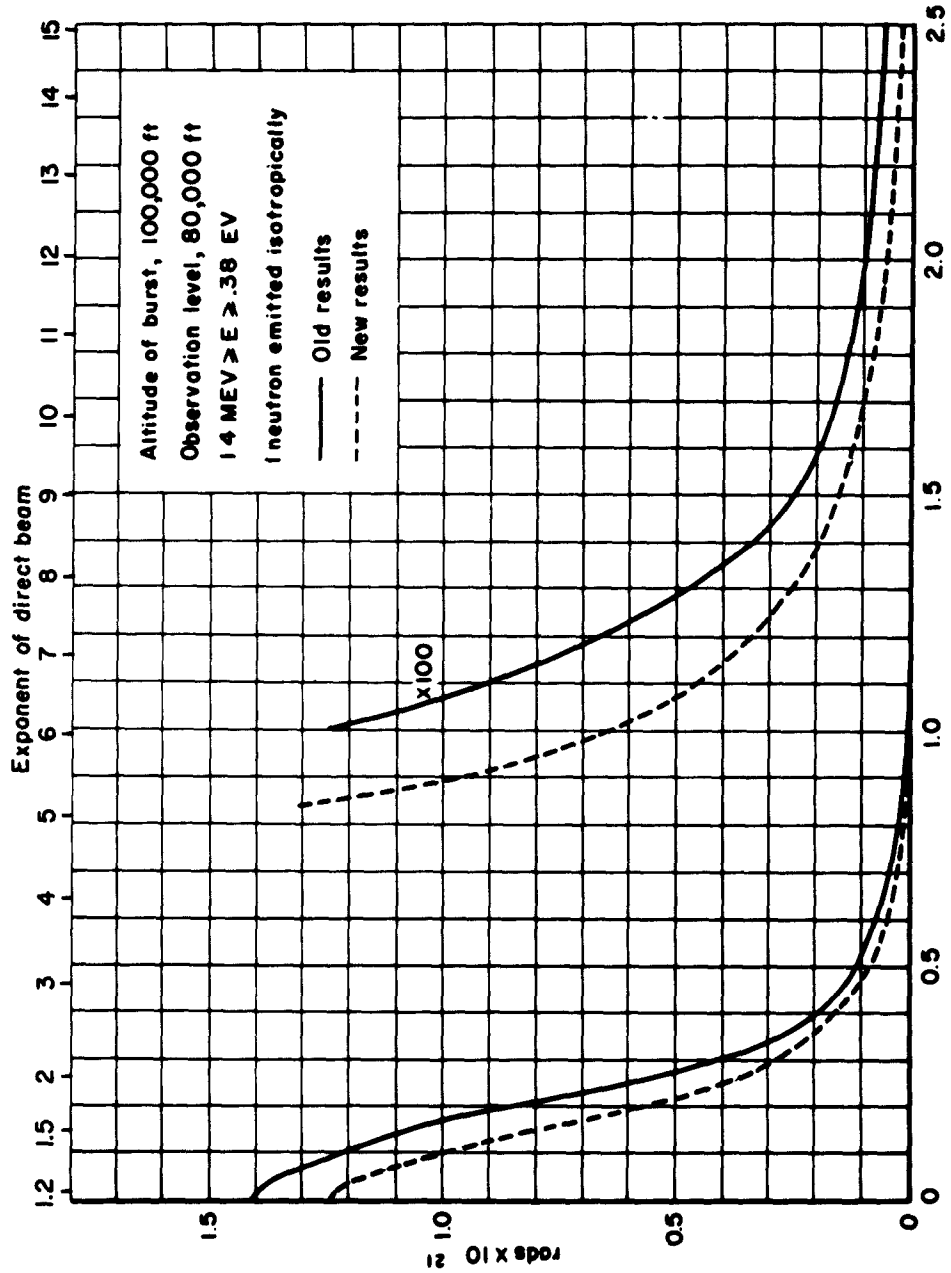
Altitude of burst, 100,000 ft
Observation level, 80,000 ft
1.4 MEV ≥ E ≥ .38 EV
1 neutron emitted isotropically
Old results
New results
x100
Exponent of direct beam
rads x 10 21
r (100,000ft)

Fig. 10

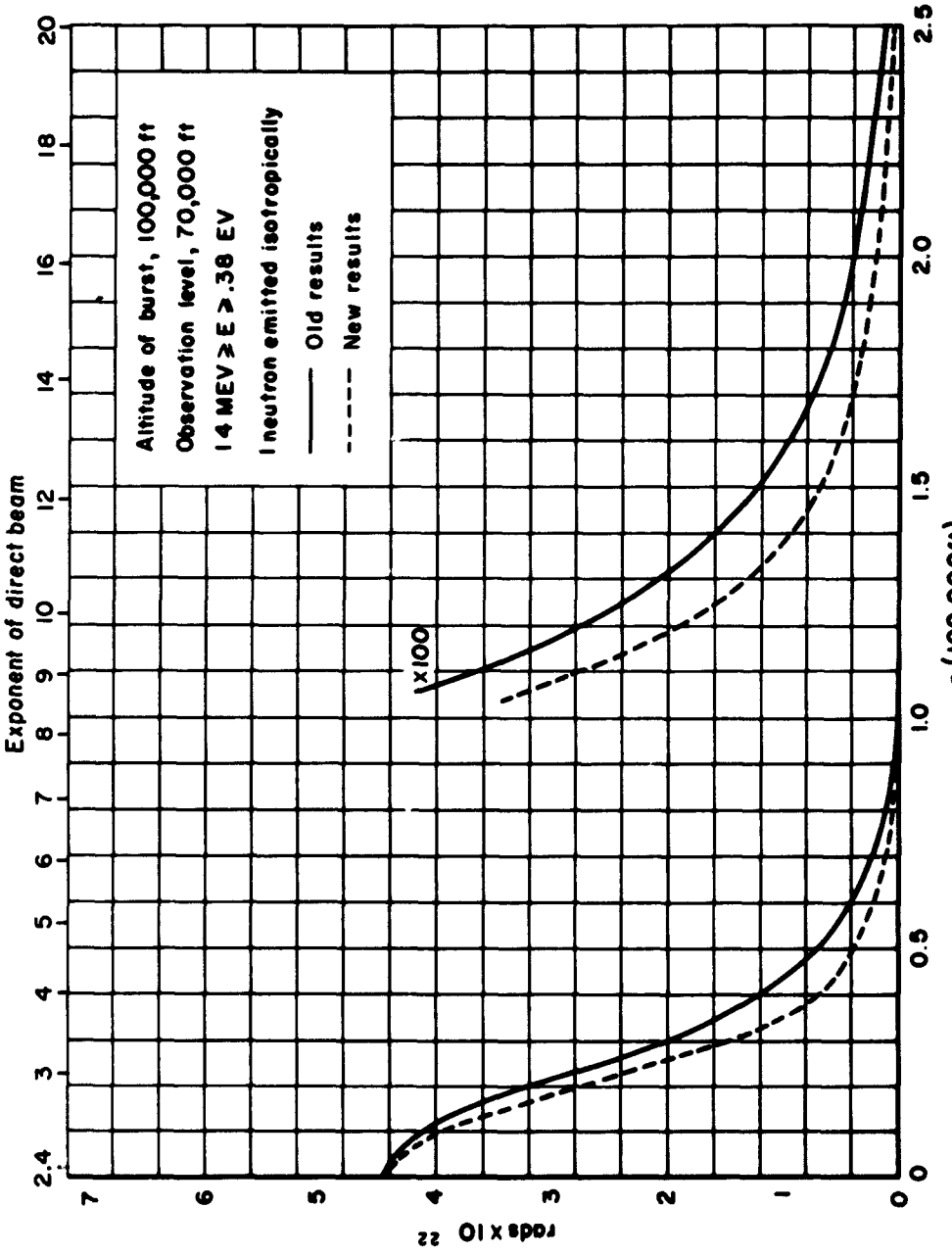
Altitude of burst, 100,000 ft
Observation level, 70,000 ft
14 MEV ≥ E ≥ .38 EV
1 neutron emitted isotropically
Old results
New results
x100
Exponent of direct beam
rads x 10 22
r (100,000ft)

Fig. 11

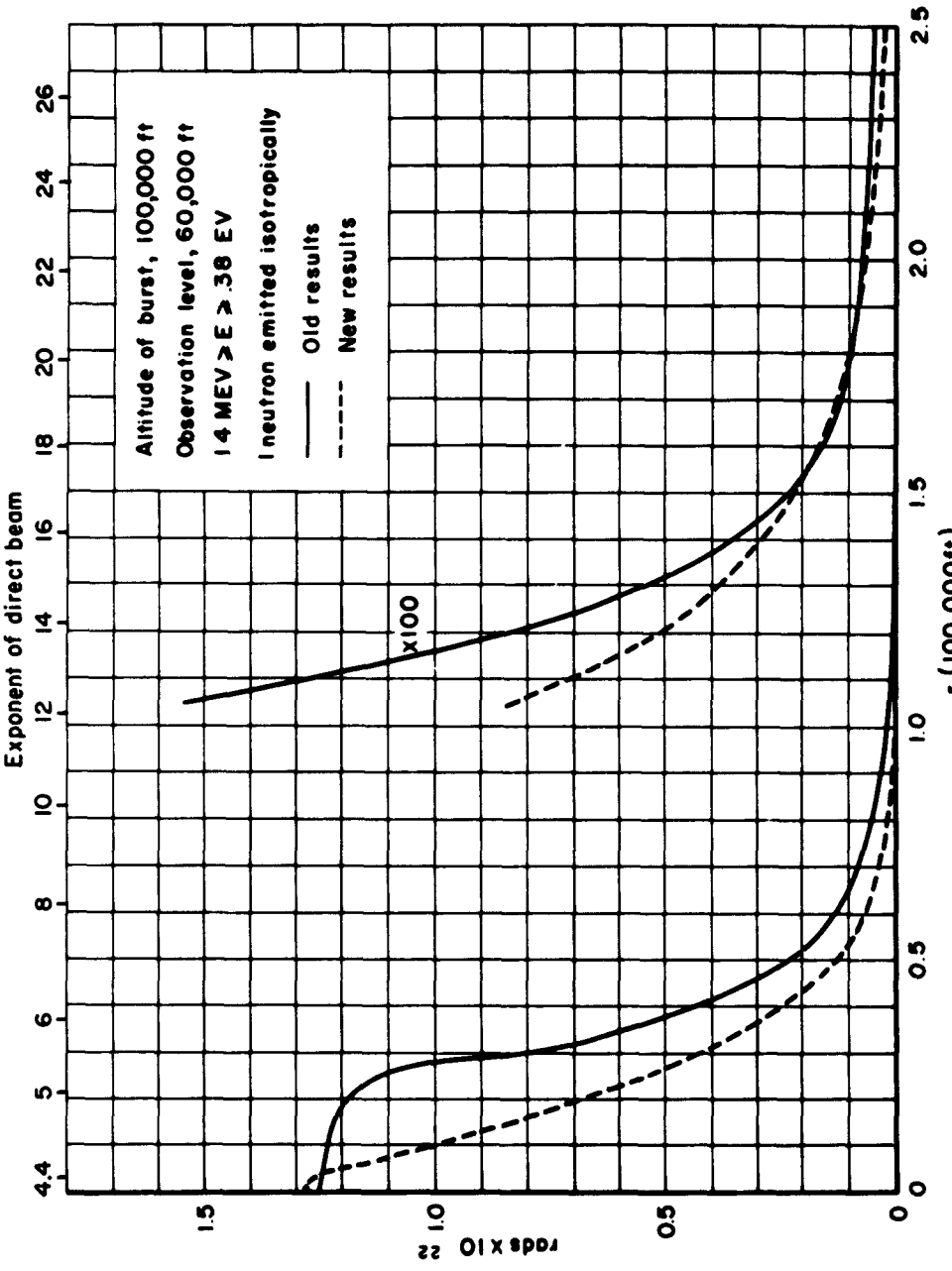
Altitude of burst, 100,000 ft
Observation level, 60,000 ft
1.4 MEV ≥ E ≥ .38 EV
1 neutron emitted isotropically
Old results
New results
x100
Exponent of direct beam
4.4
5
6
8
10
12
14
16
18
20
22
24
26
rads x 10 22
1.5
1.0
0.5
0
r (100,000ft)
2.5
2.0
1.5
1.0
0.5
0

Fig. 12

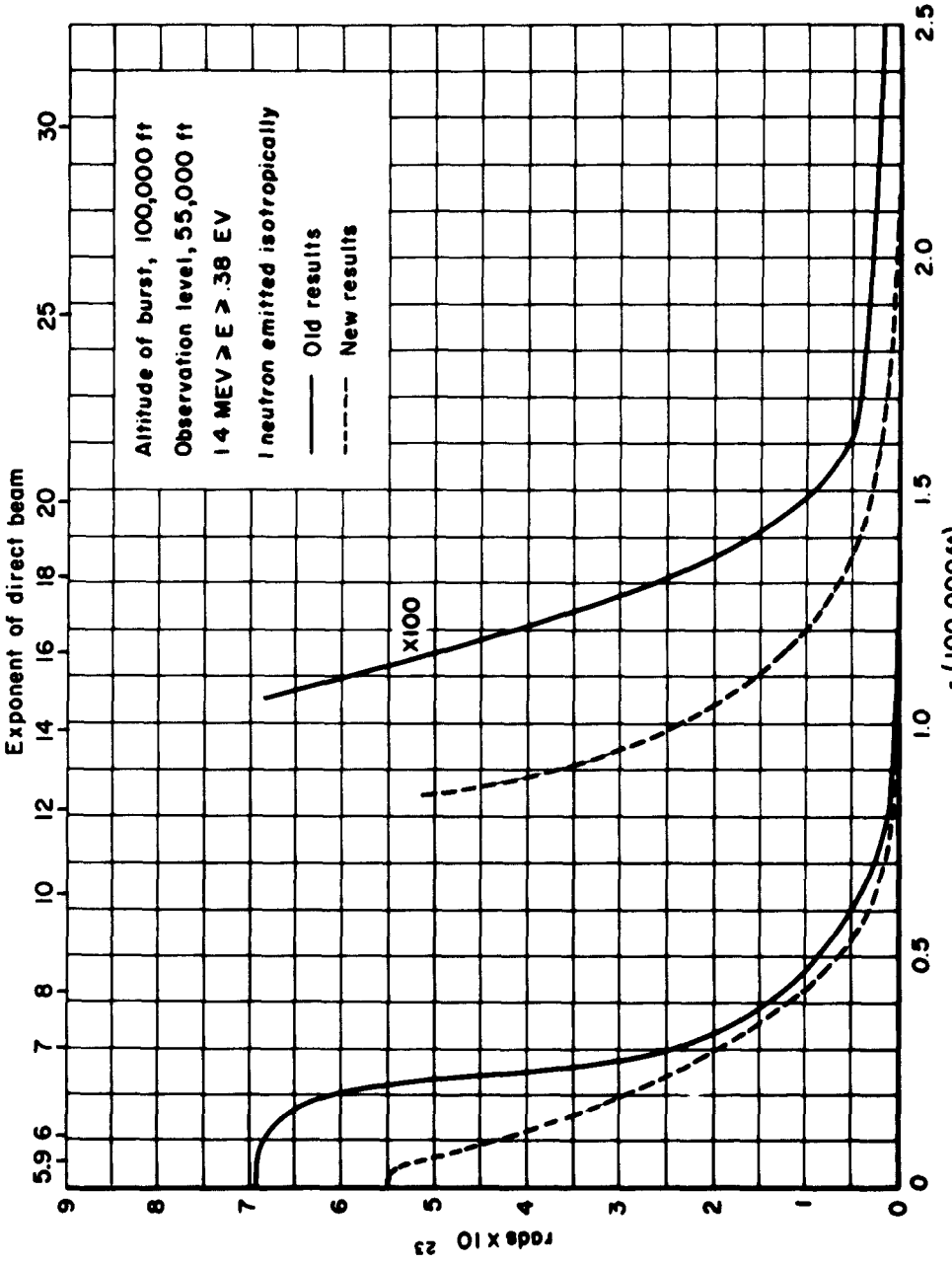
Altitude of burst, 100,000 ft
Observation level, 55,000 ft
14 MEV > E > .38 EV
1 neutron emitted isotropically
Old results
New results
x100
Exponent of direct beam
5.9 6 7 8 10 12 14 16 18 20 25 30
rads x 10 23
0 1 2 3 4 5 6 7 8 9
r (100,000 ft)
0 0.5 1.0 1.5 2.0 2.5

Fig. 13

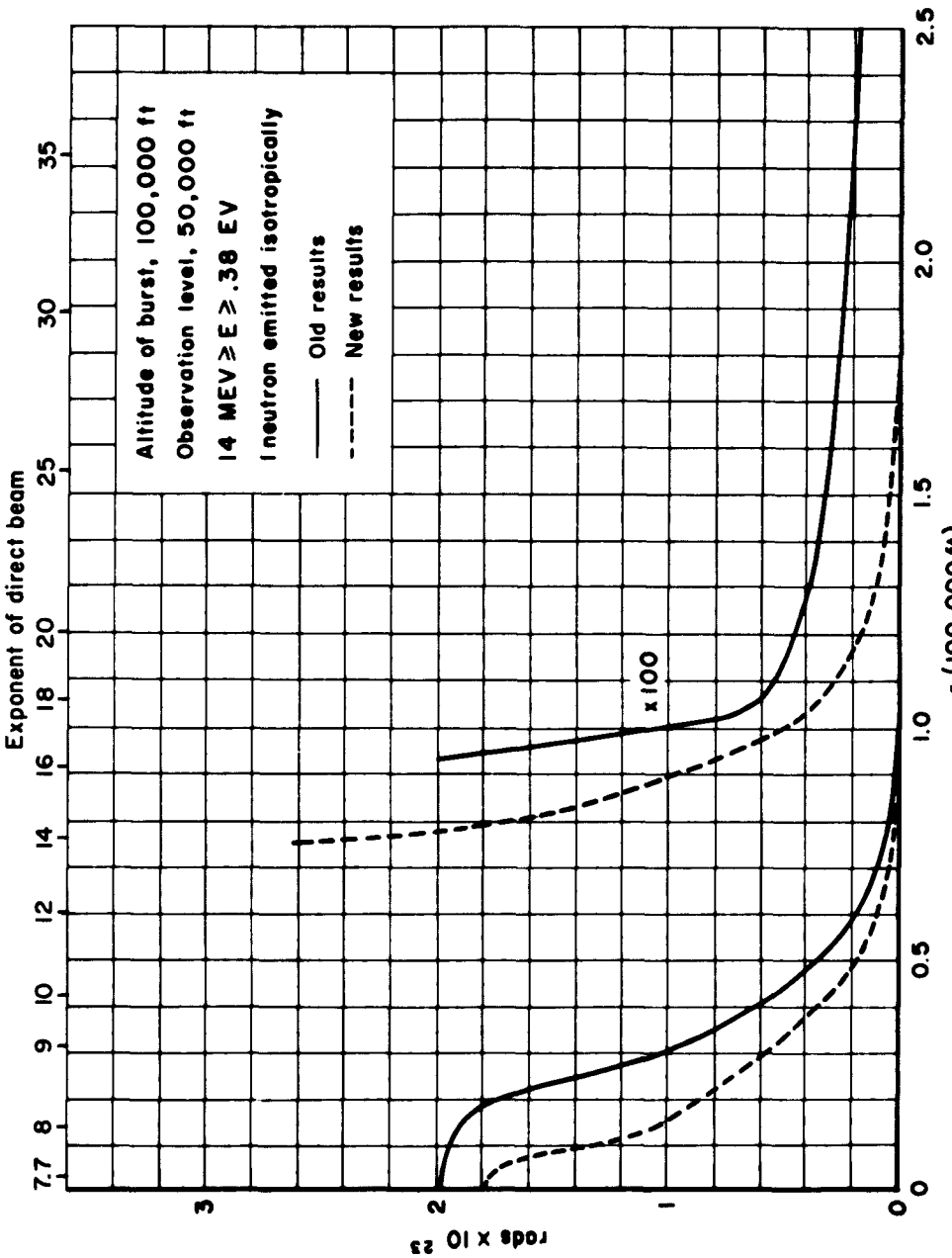
Altitude of burst, 100,000 ft
Observation level, 50,000 ft
14 MEV ≥ E ≥ .38 EV
1 neutron emitted isotropically
Old results
New results
x100
Exponent of direct beam
7.7
8
9
10
12
14
16
18
20
25
30
35
rads x 10 23
0
1
2
3
r (100,000 ft)
0
0.5
1.0
1.5
2.0
2.5

Fig. 14

NOTE FOR FIG. 15

These results on this level are not statistically significant. They are presented only to show the results as given by the code, but should not be used otherwise.

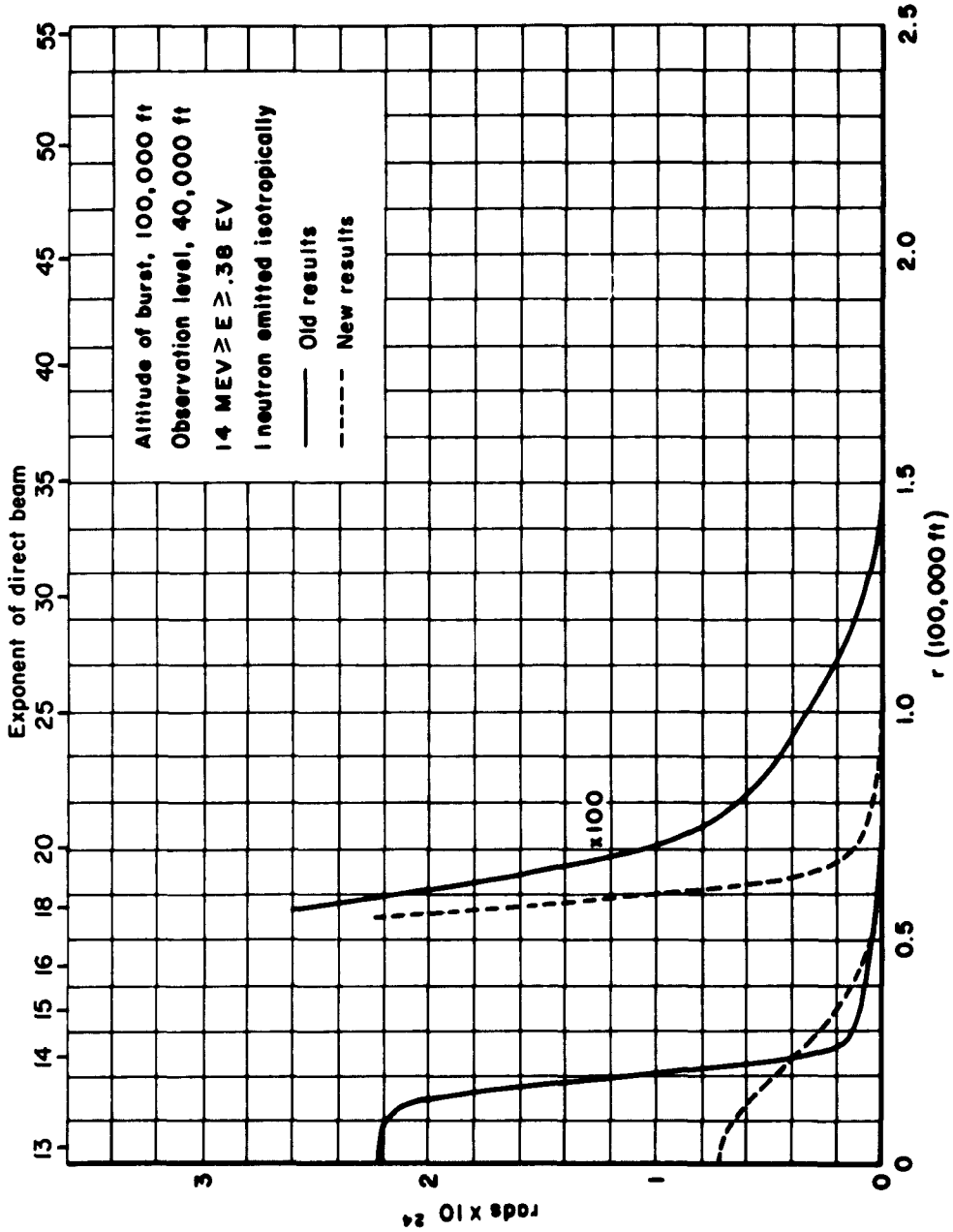
Altitude of burst, 100,000 ft
Observation level, 40,000 ft
14 MEV≥E≥.38 EV
1 neutron emitted isotropically
Old results
New results
x100
Exponent of direct beam
rads x 10 24
r (100,000 ft)

Fig. 15

INPUT PARAMETERS FOR PROBLEMS OF FIGS. 16 THROUGH 18

0 foot, 750 foot and 3000 foot source height problems run with old code.

Radial bins - 0 (200) 2,000 (400) 6,000 (600) 10,200 feet.

Polar angles for starting histories - $\mu = -1\ (.08) + 1.$

Number of histories - 200 histories per angle or 5,200 total.

Energy subdivisions of arriving dosage -

14 - 8 Mev
8 - 3 Mev
3 - 1 Mev
1 - .5 Mev
.5 - .25 Mev
.25 - .05 Mev
.05 - .38 x 10^{-6} Mev

0 foot source height problem run with corrected code.*

Radial bins - 0 (.1) 1 (.2) 2 (.5) 5 (1) 10 (5) 20 (10)
100 (25) 250 (50) 500 (100) 1,000 (250 6,000.

Polar angles for starting histories - $\mu = -1\ (.04) -.04\ (.041)$
.001 (.039) .04 (.04) + 1.**

Number of histories - 200 histories per angle or 10,200 total.

Energy subdivisions of arriving dosage - same as above.

*Also used to obtain new results for 750 foot and 3000 foot source height. See page 14 for details.

**A horizontal angle (μ=0) is always avoided when dosage on the co-altitude plane is obtained. This is necessary in order to avoid a small coding error which will be changed shortly.

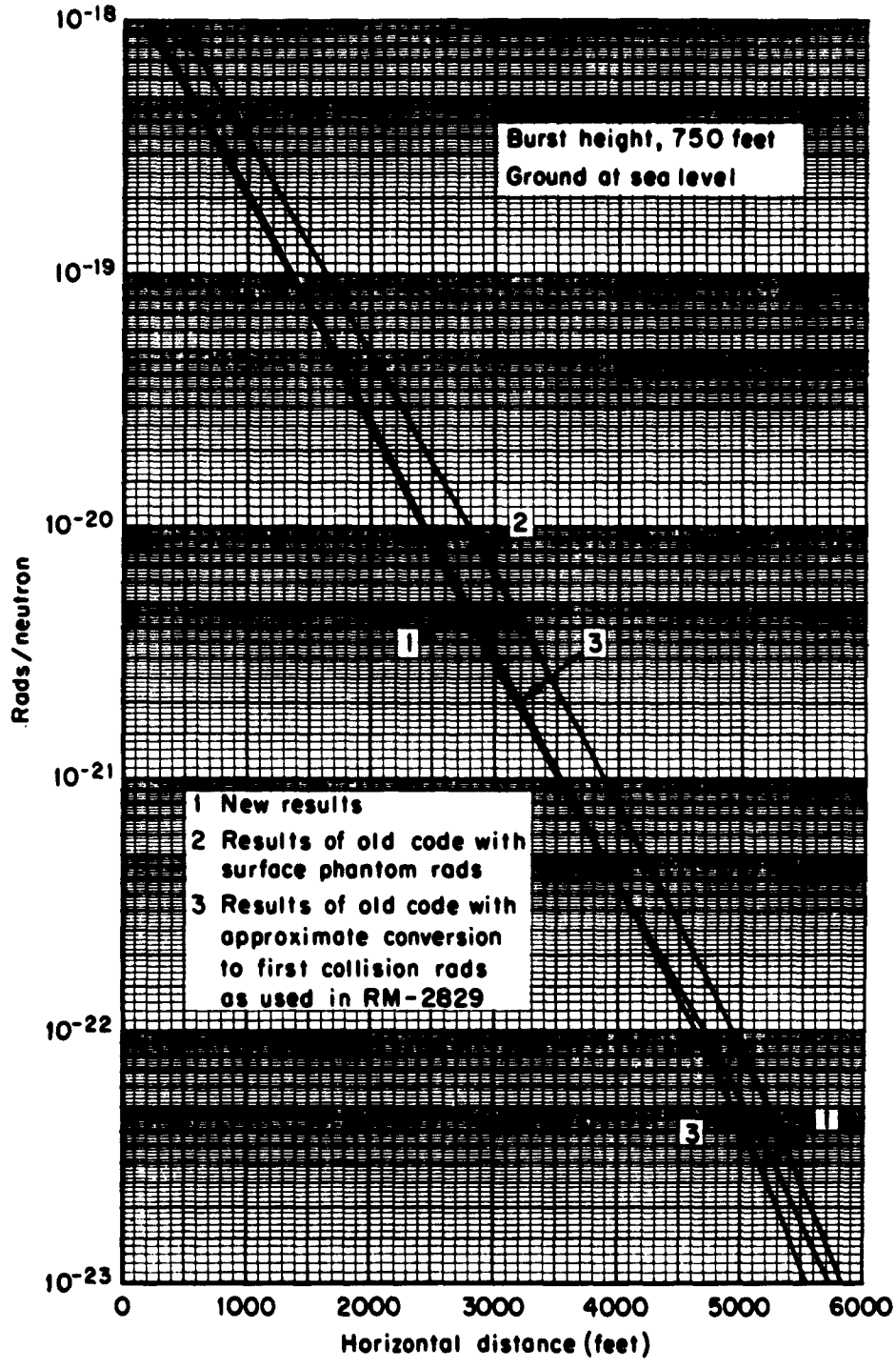
Burst height, 750 feet
Ground at sea level
1 New results
2 Results of old code with surface phantom rads
3 Results of old code with approximate conversion to first collision rads as used in RM-2629
Rads/neutron
10-18
10-19
10-20
10-21
10-22
10-23
0
1000
2000
3000
4000
5000
6000
Horizontal distance (feet)

Fig. 16

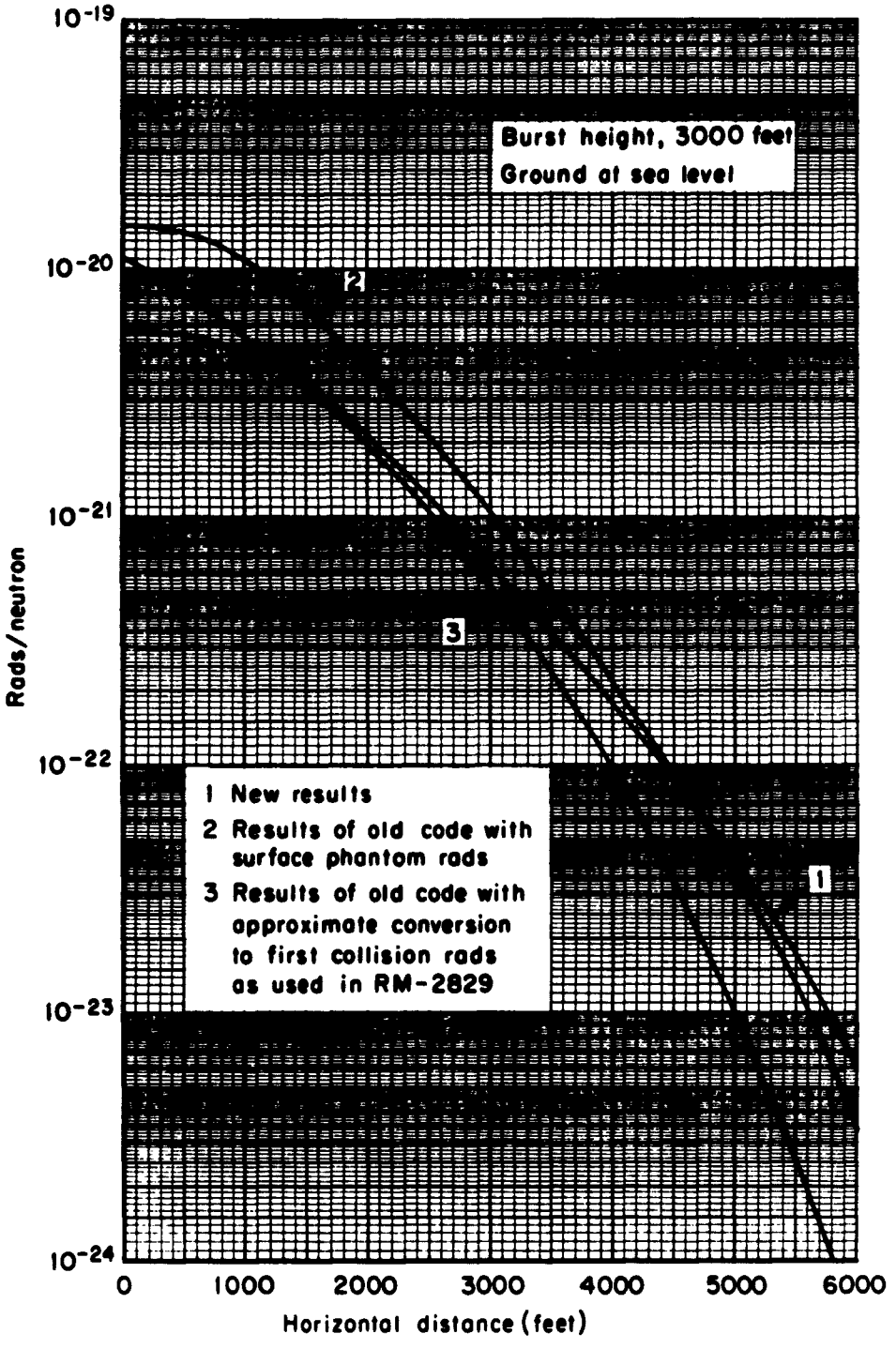
Burst height, 3000 feet
Ground at sea level
1 New results
2 Results of old code with surface phantom rads
3 Results of old code with approximate conversion to first collision rads as used in RM-2829
Rads/neutron
Horizontal distance (feet)
10-19
10-20
10-21
10-22
10-23
10-24
0
1000
2000
3000
4000
5000
6000

Fig. 17

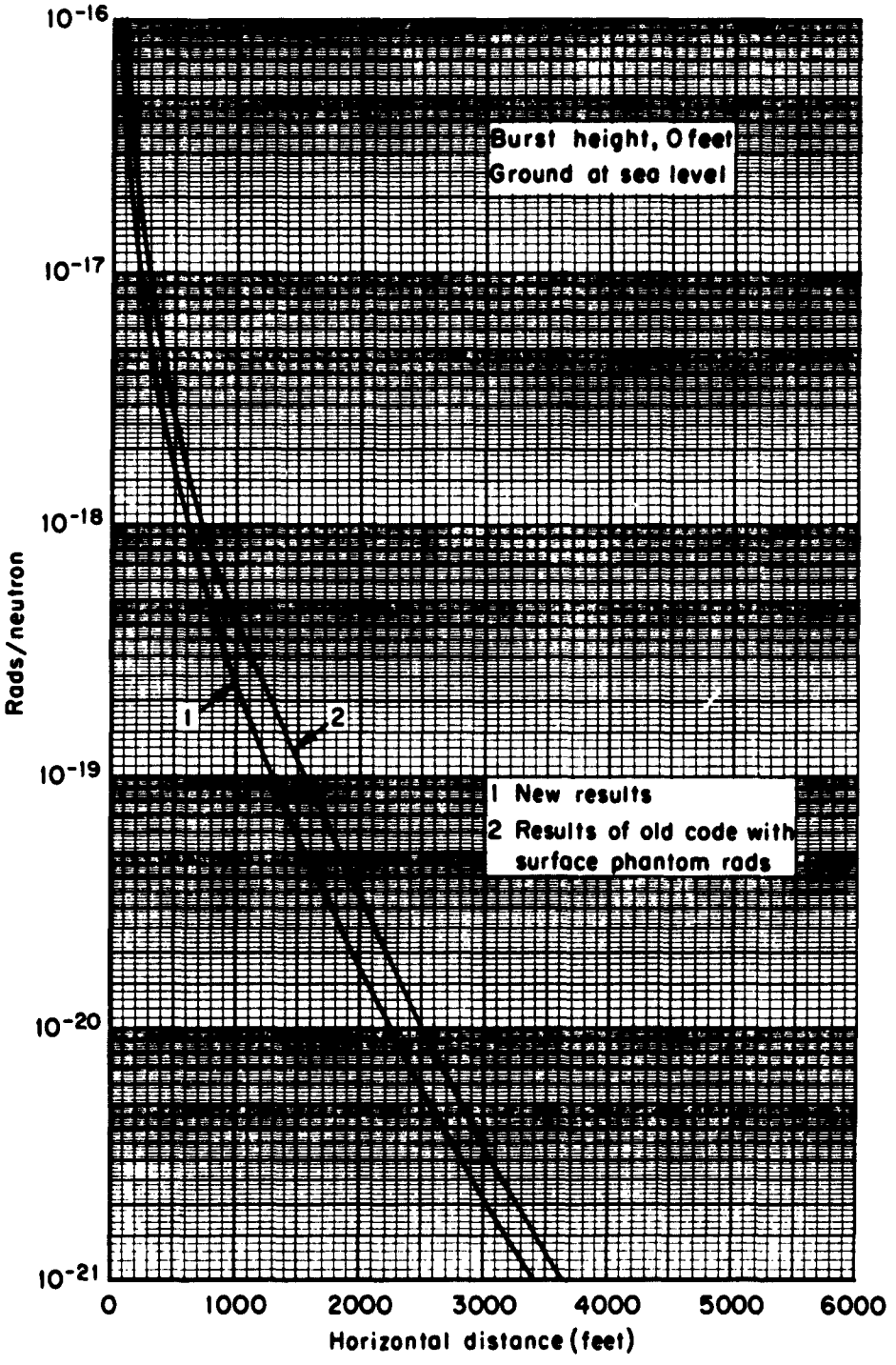
Burst height, 0 feet
Ground at sea level
1 New results
2 Results of old code with surface phantom rads
Rads/neutron
Horizontal distance (feet)
10-16
10-17
10-18
10-19
10-20
10-21
0
1000
2000
3000
4000
5000
6000

Fig. 18

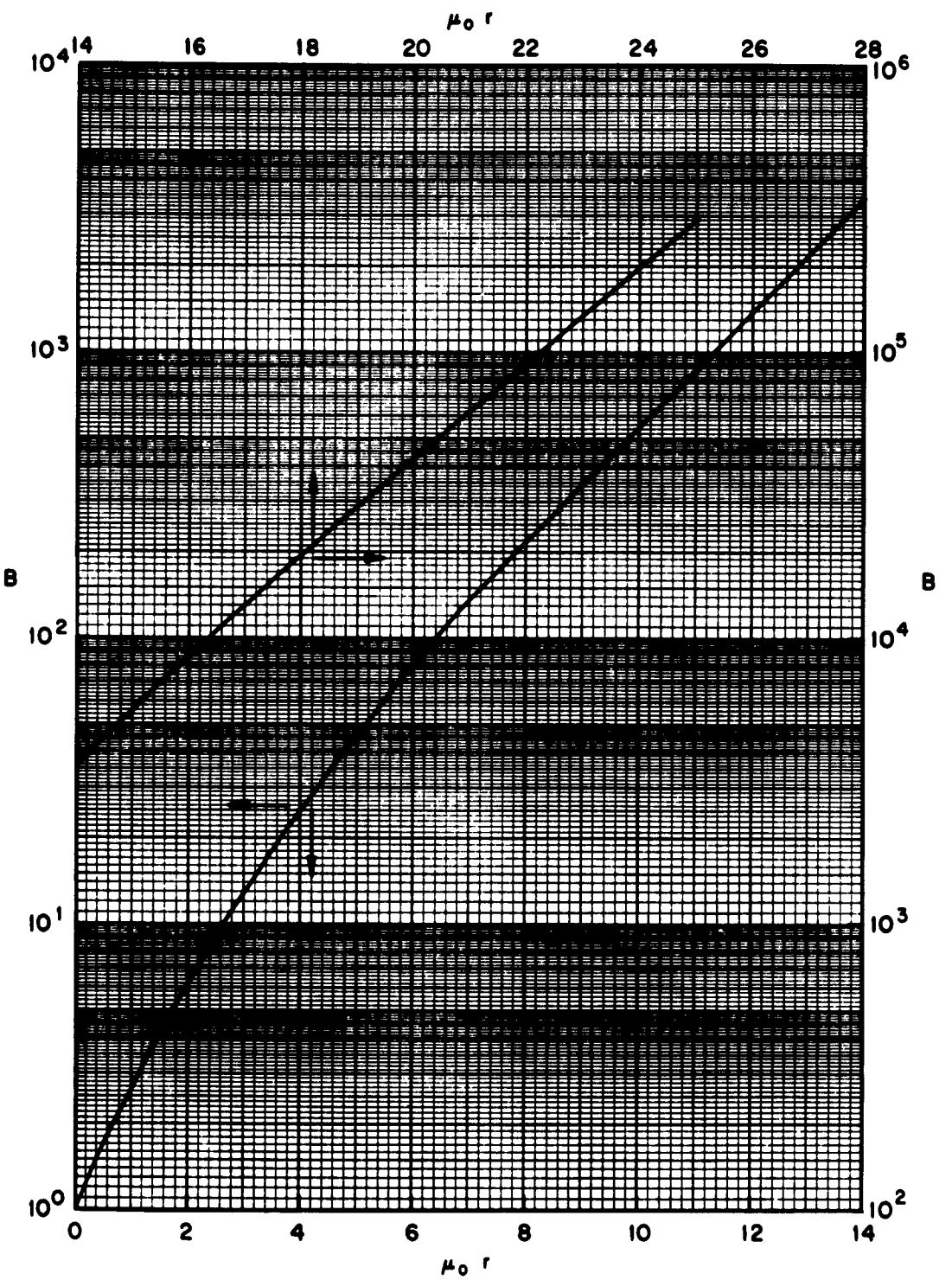

Fig. 19 — Build-up factor for 14.0 Mev neutrons in an infinite homogeneous air medium

PLOTTING ACCURACY IN FIGS. 20 THROUGH 59

The method of graphing shown in Figs. 20 through 59 uses the IBM printer. There are available 50 vertical lines and 100 horizontal lines. In Figs. 20 through 37 the ordinate is K_4 from 0 to 5.0. Since 50 lines are available, the accuracy of K is 5.0/50 or 10 per cent. The horizontal scale goes from 0 to 250,000 feet, and since 100 lines are available, the radial plotting accuracy is 2500 feet.

In Figs. 38 through 59 the K factors are plotted between 0 and 2.5 and the accuracy is therefore 5 per cent. Since the radial scale on these figures is logarithmic, the radial plotting accuracy is a function of the radius.

NOTES FOR FIGS. 20 THROUGH 25

The source altitude, not shown on the figures, is 200,000 feet. The points shown by crosses (x) are averaged four times. The points shown by asterisks (*) are averaged a lesser number of times because of lack of data at the ends. The first radial point is not averaged at all. The second radial point is averaged once, the third one twice, and the fourth one three times. These points are all shown by asterisks. The fifth radial point, which is the first one that can be averaged four times, is shown as a cross. This general scheme is carried out through all of the Figs. 20 through 59.

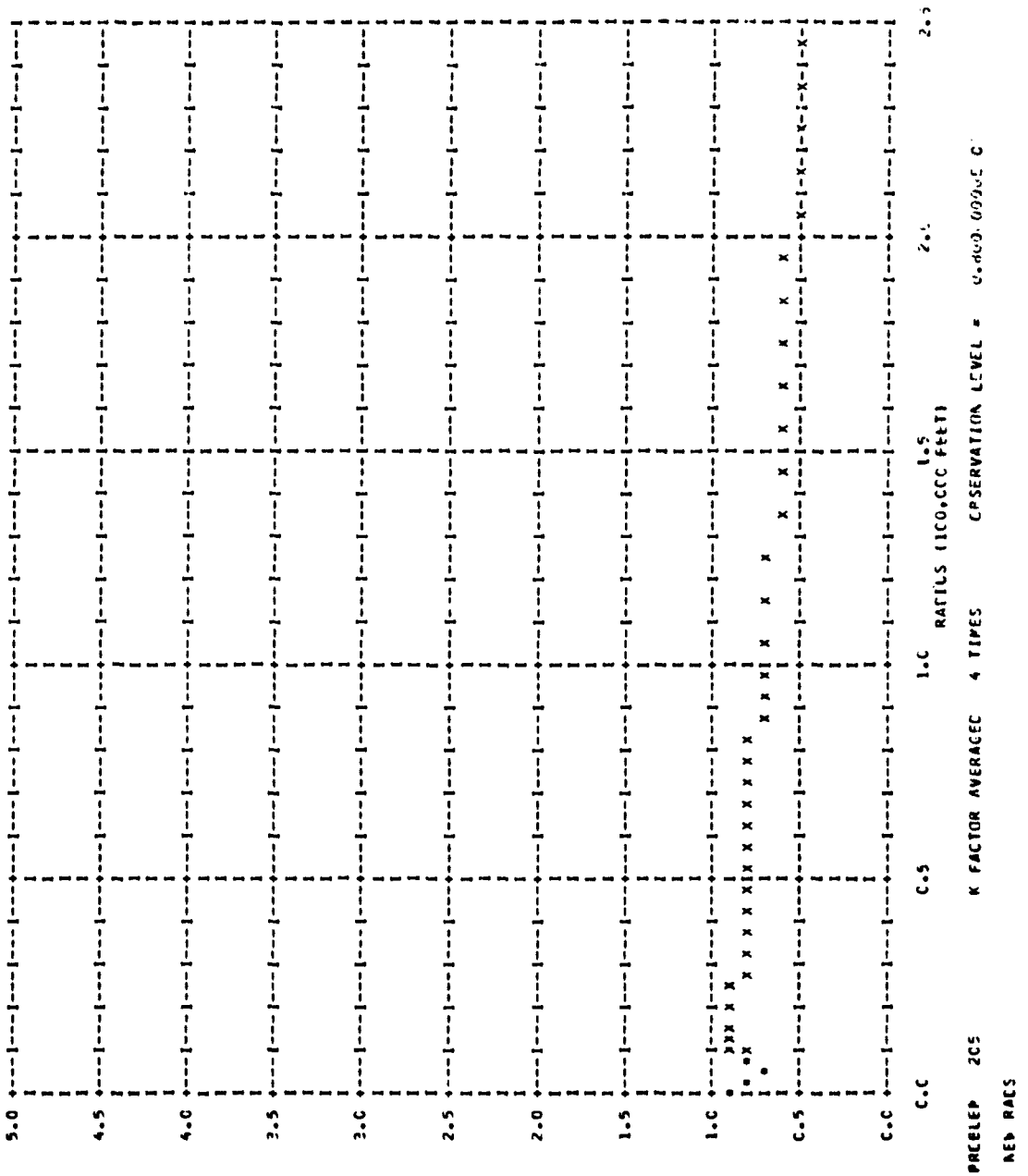
K FACTOR
5.0
4.5
4.0
3.5
3.0
2.5
2.0
1.5
1.0
0.5
0.0
0.0
0.5
1.0
1.5
RATIO (1CO,CCC FEET)
PRECLEP 205
K FACTOR AVERAGED 4 TIMES
OBSERVATION LEVEL =
RED RACS

Fig. 20

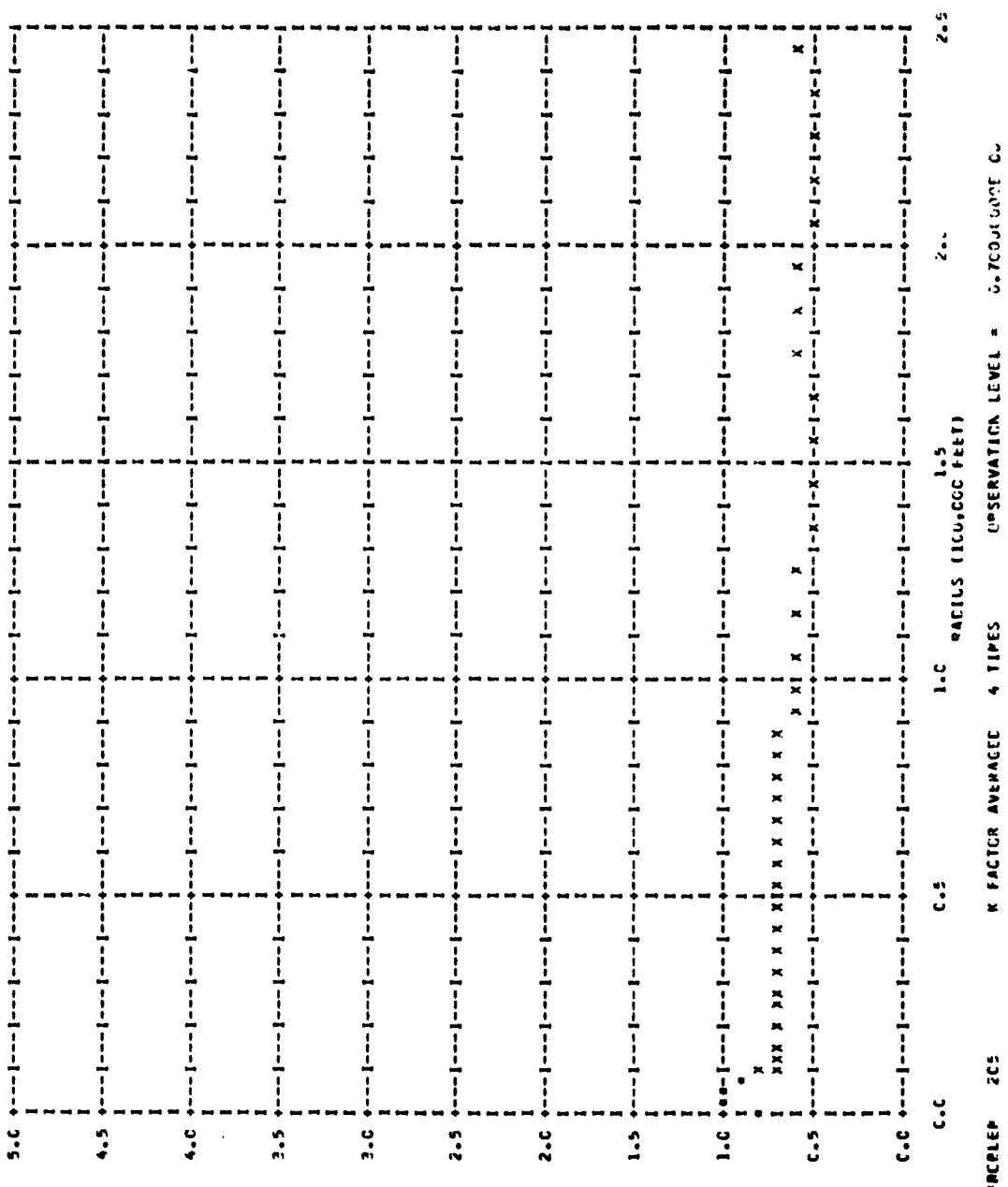
K FACTOR
5.0
4.5
4.0
3.5
3.0
2.5
2.0
1.5
1.0
0.5
0.0
0.0
0.5
1.0
1.5
2.0
2.5
RADIUS (100,000 FEET)
K FACTOR AVERAGED 4 TIMES
OBSERVATION LEVEL =
PROFILE 205
ASR RACS

Fig. 21

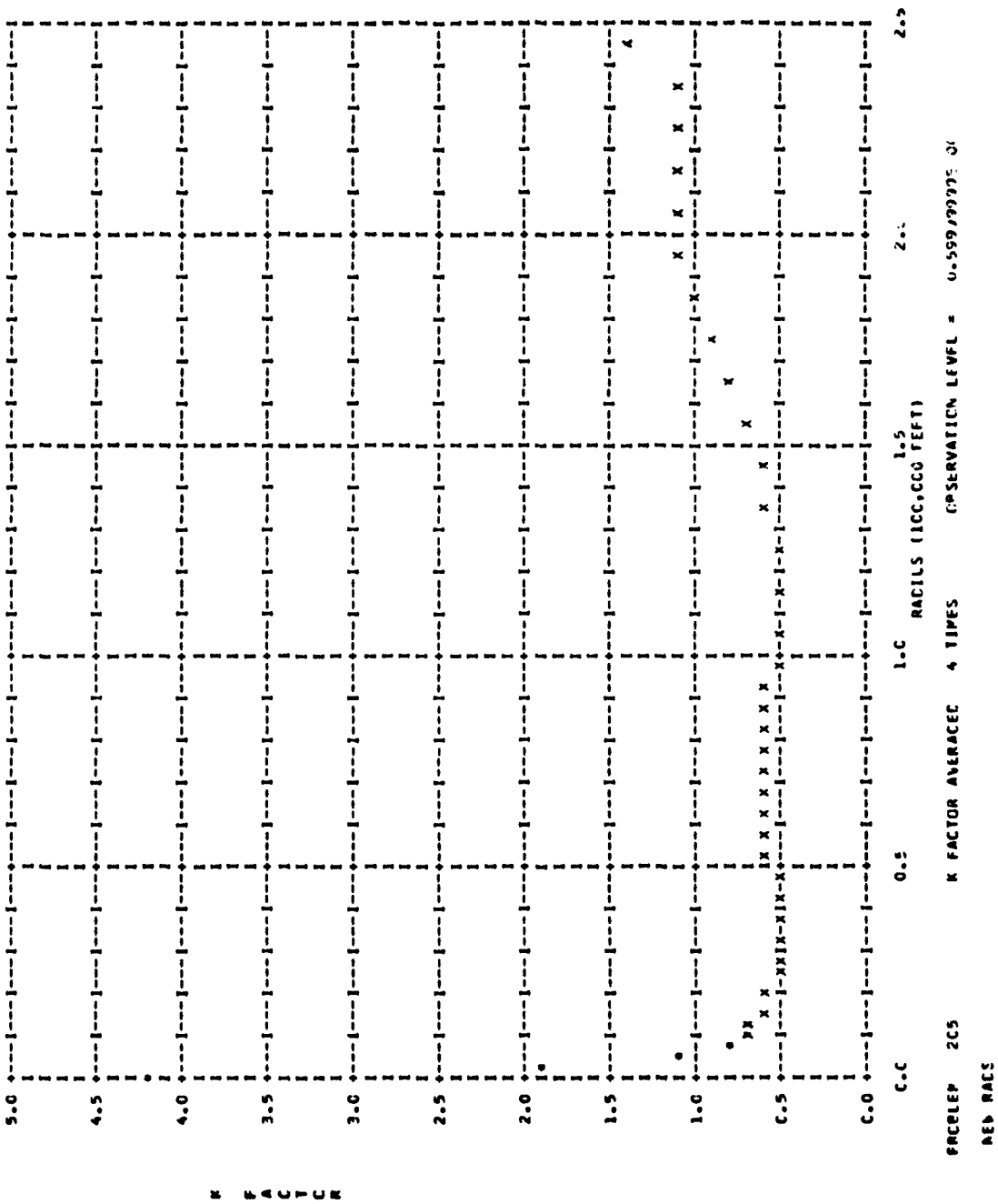
K FACTOR
5.0
4.5
4.0
3.5
3.0
2.5
2.0
1.5
1.0
0.5
0.0
0.0
1.0
1.5
2.0
RADIUS (1000,000 FEET)
K FACTOR AVERAGED 4 TIMES
OBSERVATION LEVEL =
FREELEP 205
RED RACE

Fig. 22

NOTES FOR FIG. 23

At this observation altitude of 55,000 feet the statistical inaccuracy discussed on page 50 shows up. The points near r = 0 should start at about K = .9 and decrease to .5 at about r = 15,000 feet. At this level it is seen that K, after going through a minimum, rises monotonically and gets very large at great distances. This is because the majority of the neutrons which arrive at large distances from the origin travel along paths which are mainly above the optical path. Thus the total number of grams of air along the actual path becomes less and less compared to the same quantity along the optical path.

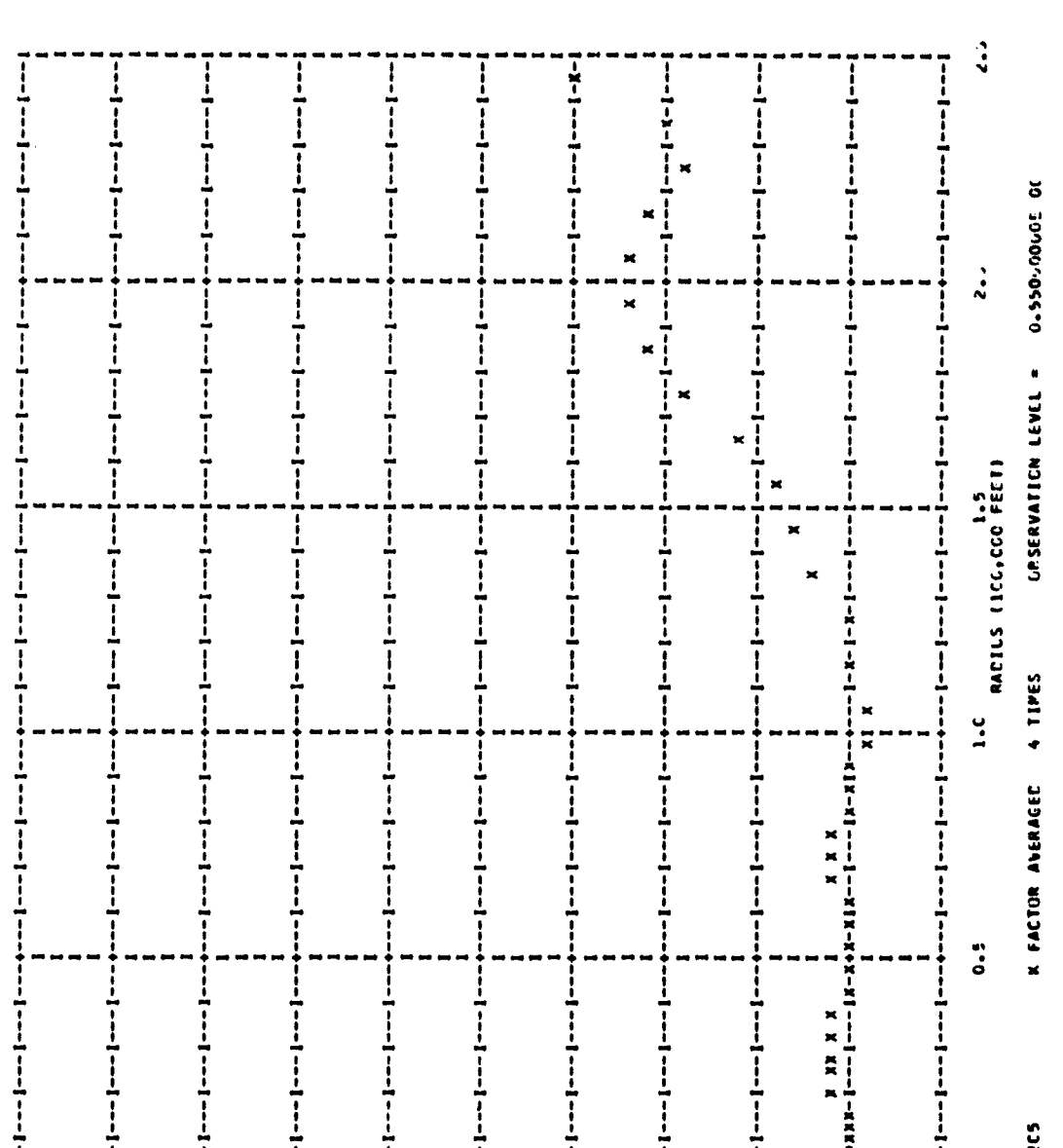
K FACTOR
5.0
4.5
4.0
3.5
3.0
2.5
2.0
1.5
1.0
0.5
0.0
0.0
0.5
1.0
1.5
2.0
RADIUS (100,000 FEET)
K FACTOR AVERAGED 4 TIMES
OBSERVATION LEVEL = 0.550-.00005 OC
PROFILE 205
NEB RADS

Fig. 23

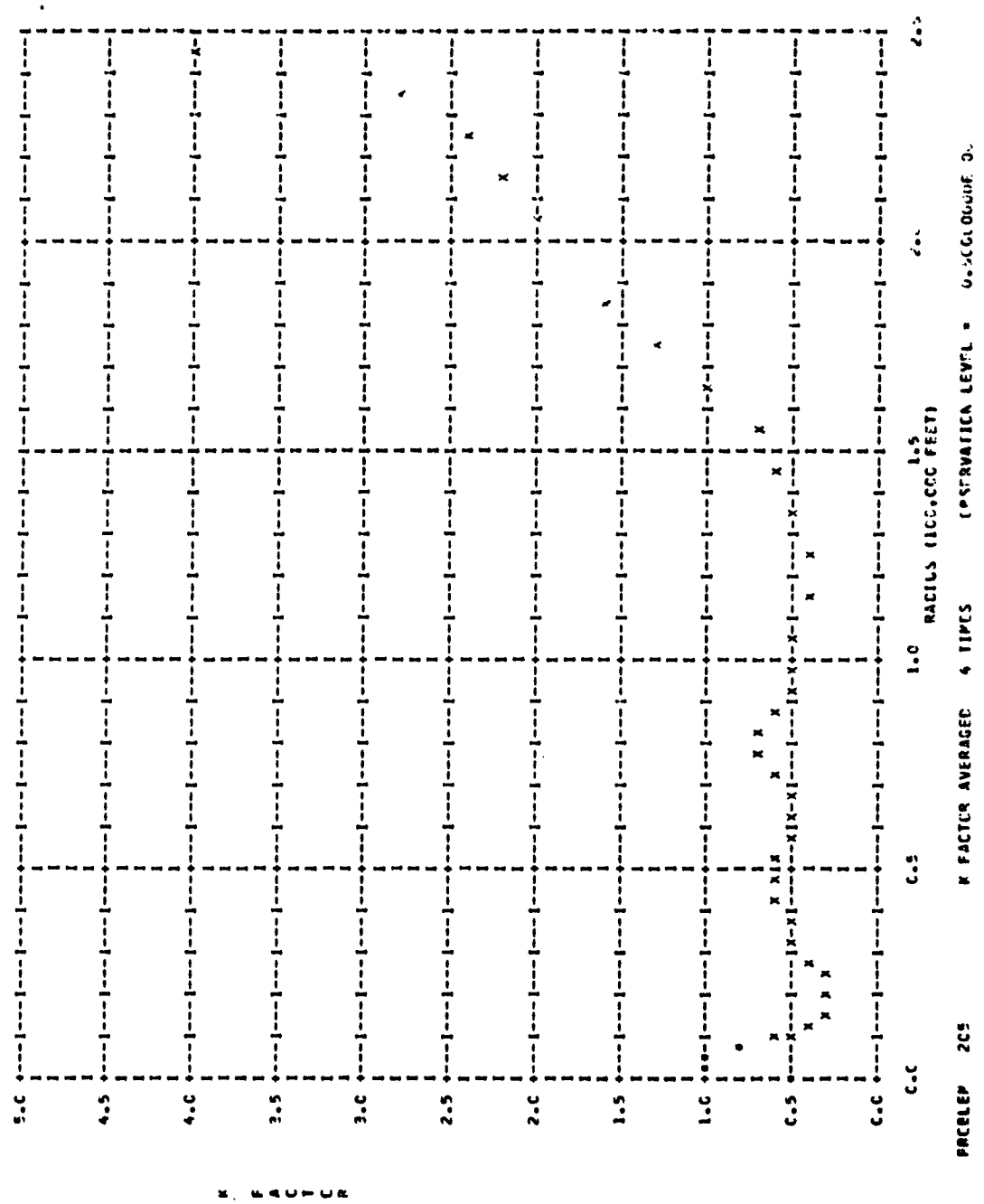
5.0
4.5
4.0
3.5
3.0
2.5
2.0
1.5
1.0
0.5
0.0
0.0
0.5
1.0
1.5
RADIUS (1000.000 FEET)
K FACTOR AVERAGED 4 TIMES
K FACTOR

Fig. 24

NOTES FOR FIG. 25

The statistical inaccuracy for this level is so large that the results are not meaningful. This fact is apparent from an examination of the standard deviations in the original printout. One can surmise this also by noting that the minimum in K is very close to 0.5 for every observation level from 80,000 feet to 50,000 feet. At 40,000 feet (the observation level of this figure) the minimum of K suddenly dips to 0.2.

This difficulty with statistical accuracy could be remedied by running a vastly greater number of histories, or using some of the Monte Carlo tricks for increasing statistical accuracy for deep penetration.

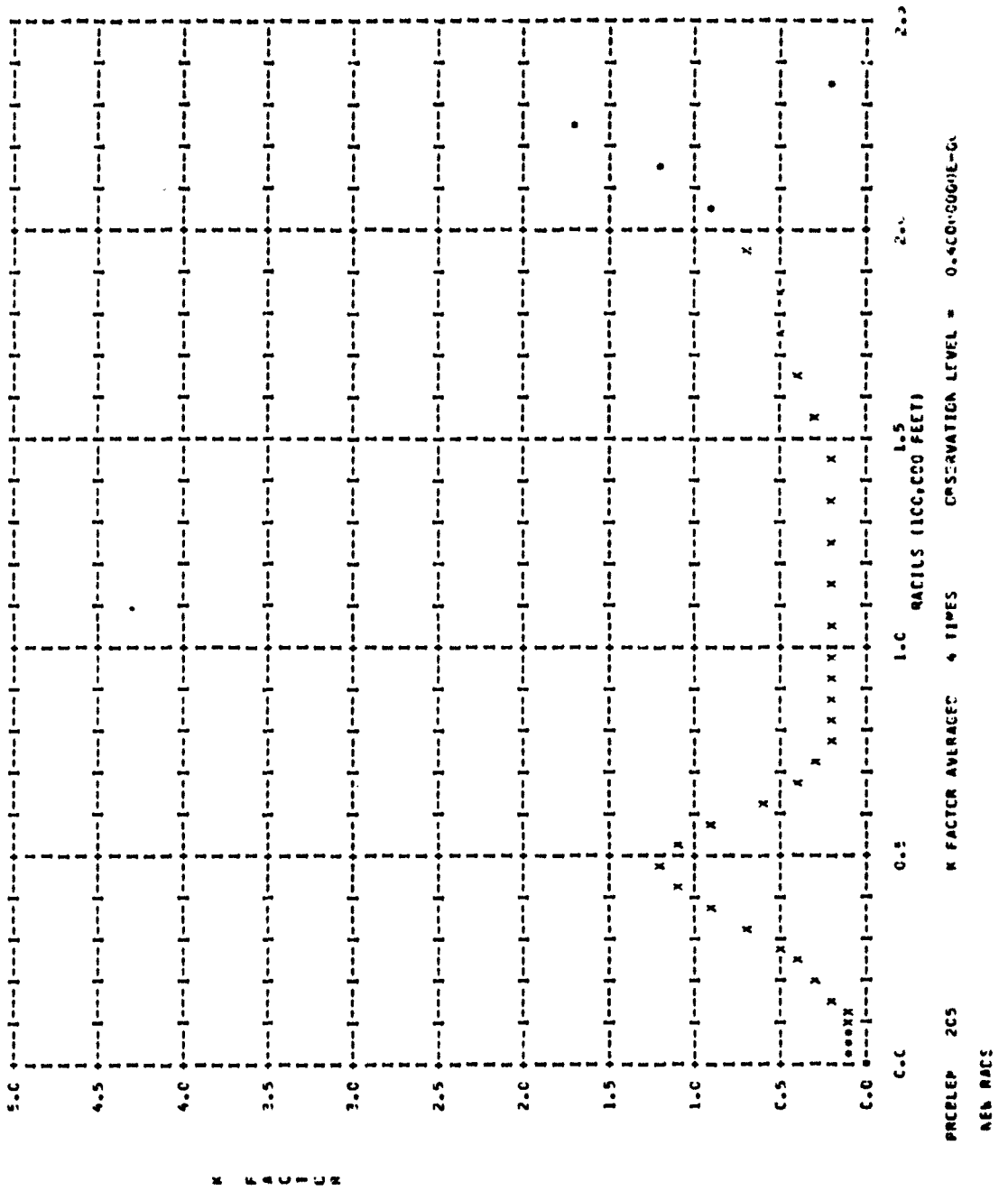
5.0
4.5
4.0
3.5
3.0
2.5
2.0
1.5
1.0
0.5
0.0
0.0
1.0
1.5
2.0
RADIUS (100,000 FEET)
PRCELEP 205
M FACTOR AVERAGED 4 TIMES
OBSERVATION LEVEL =
AEA RACS

Fig. 25

NOTES FOR FIGS. 26 THROUGH 31

The source height for the results shown in these figures is 100,000 feet. The input parameters for this problem are given on page 56. Figures 10 through 15 show the graphs of the dosage for this problem. Those graphs were obtained by the original method of drawing smooth curves through histograms, rather than using the K averaging code so that the old results and new results would be compared on the same basis.

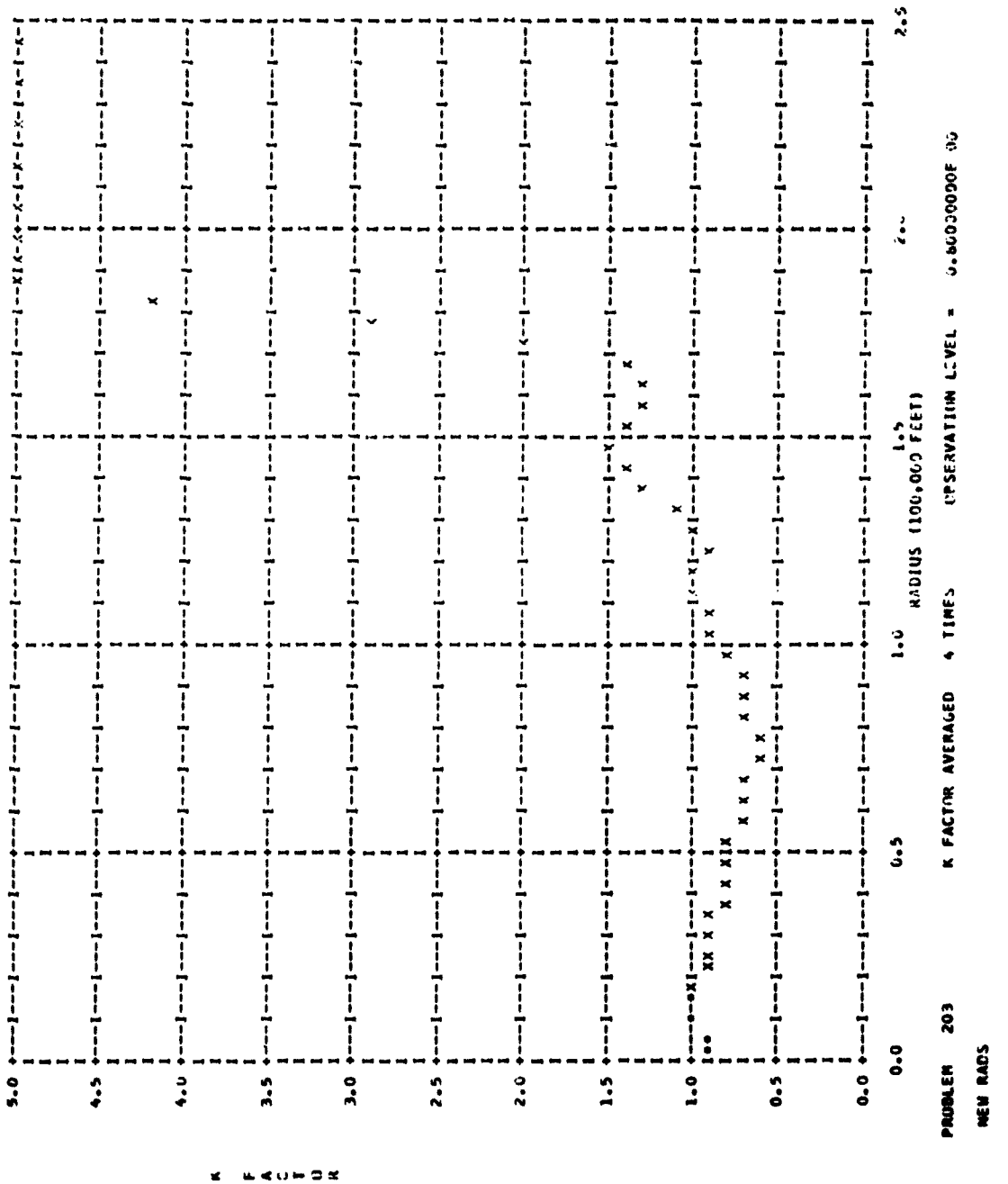
K FACTOR
5.0
4.5
4.0
3.5
3.0
2.5
2.0
1.5
1.0
0.5
0.0
0.0
0.5
1.0
1.5
2.5
RADIUS (100,000 FEET)
PROBLEM 203
K FACTOR AVERAGED 4 TIMES
OBSERVATION LEVEL =
NEW RADS

Fig. 26

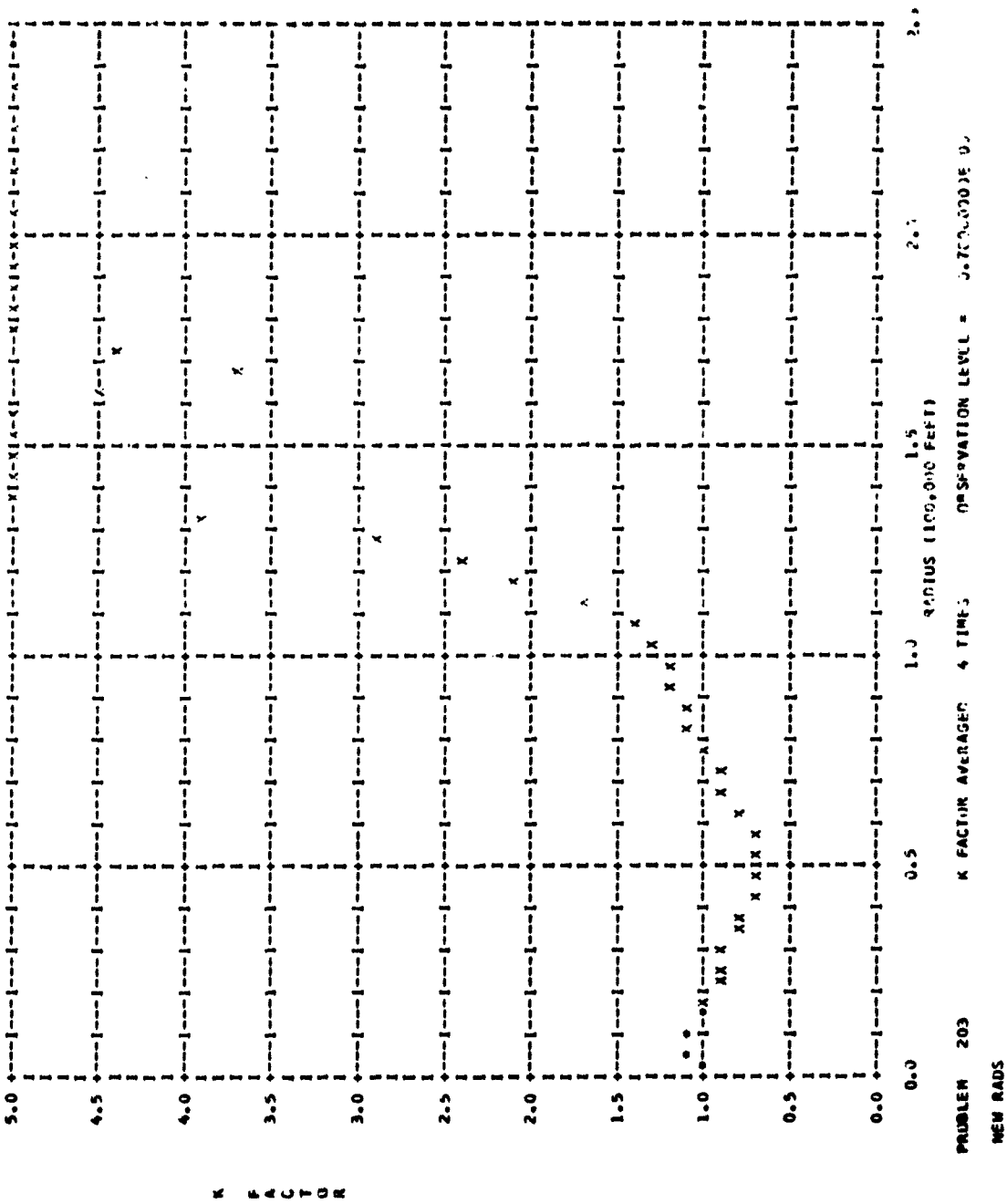
K FACTOR
5.0
4.5
4.0
3.5
3.0
2.5
2.0
1.5
1.0
0.5
0.0
0.0
0.5
1.0
1.5
RADIUS (100,000 FEET)
PROBLEM 203
K FACTOR AVERAGED 4 TIMES
OBSERVATION LEVEL =
NEW RADS

Fig. 27

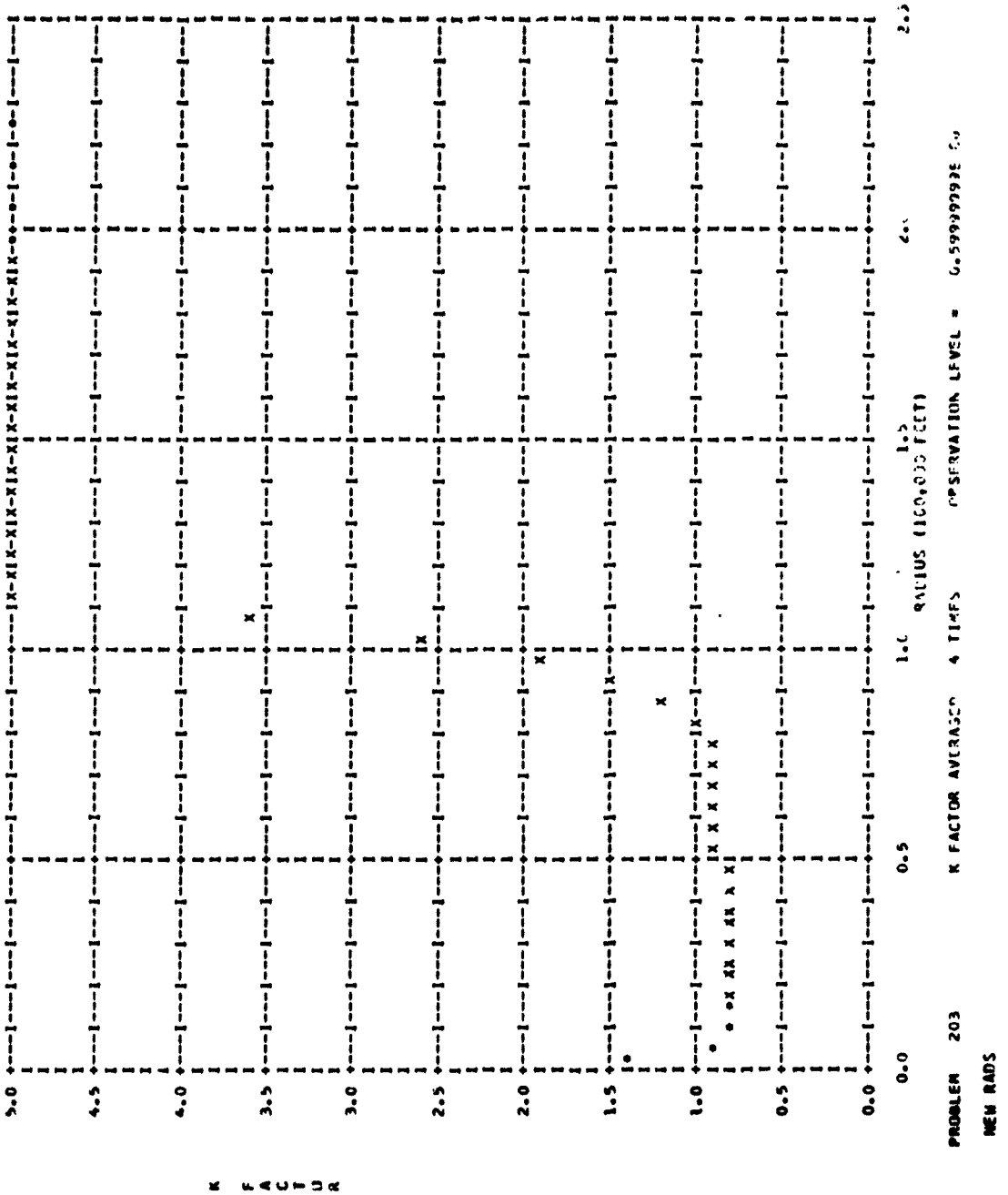
K FACTOR
5.0
4.5
4.0
3.5
3.0
2.5
2.0
1.5
1.0
0.5
0.0
0.0
0.5
RADIUS (1000.000 FEET)
PROBLEM 203
K FACTOR AVERAGED 4 TIMES
PRESERVATION LEVEL =
NEW RADS

Fig. 28

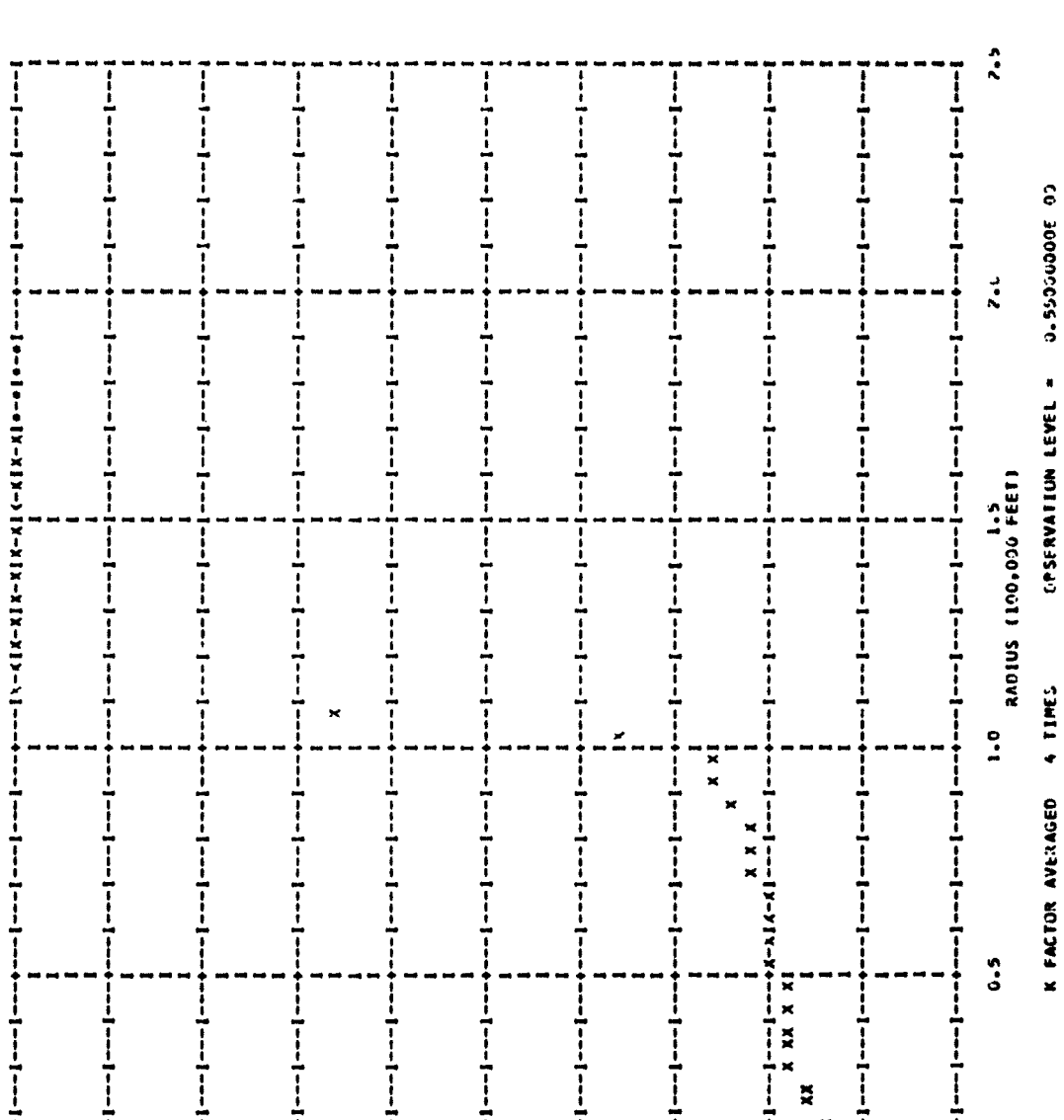
K FACTOR
5.0
4.5
4.0
3.5
3.0
2.5
2.0
1.5
1.0
0.5
0.0
0.0
0.5
1.0
1.5
2.0
2.5
RADIUS (100,000 FEET)
PROBLEM 203
K FACTOR AVERAGED 4 TIMES
OBSERVATION LEVEL =
NEW RAOS

Fig. 29

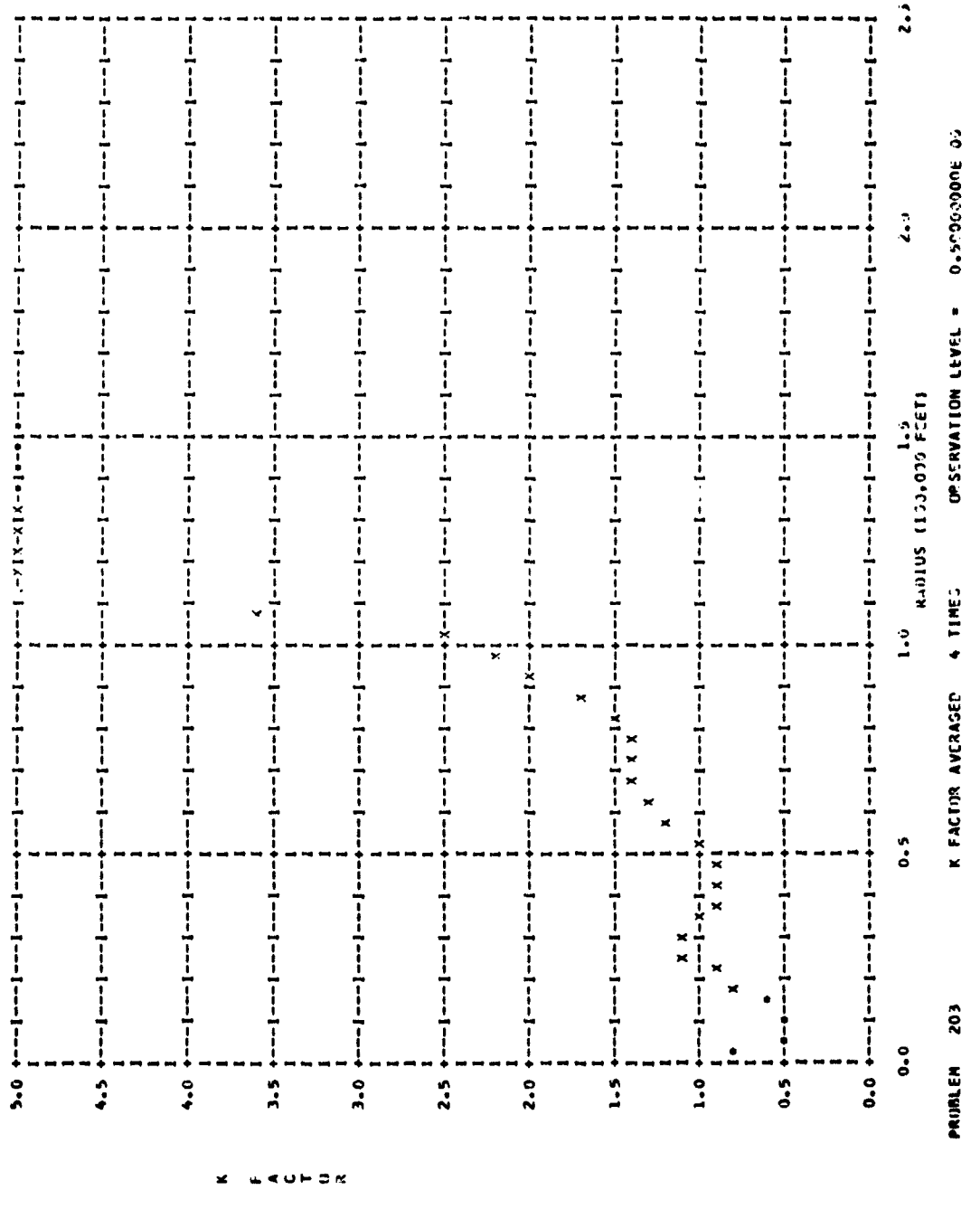
K FACTOR
5.0
4.5
4.0
3.5
3.0
2.5
2.0
1.5
1.0
0.5
0.0
0.0
0.5
1.0
RADIUS (1000 FEET)
PROBLEM 203 K FACTOR AVERAGED 4 TIMES OBSERVATION LEVEL =
NEW RADS

Fig. 30

NOTE FOR FIG. 31

The same note as given on page 54 for the 200,000 foot source height applies to the 40,000 foot observation level here.

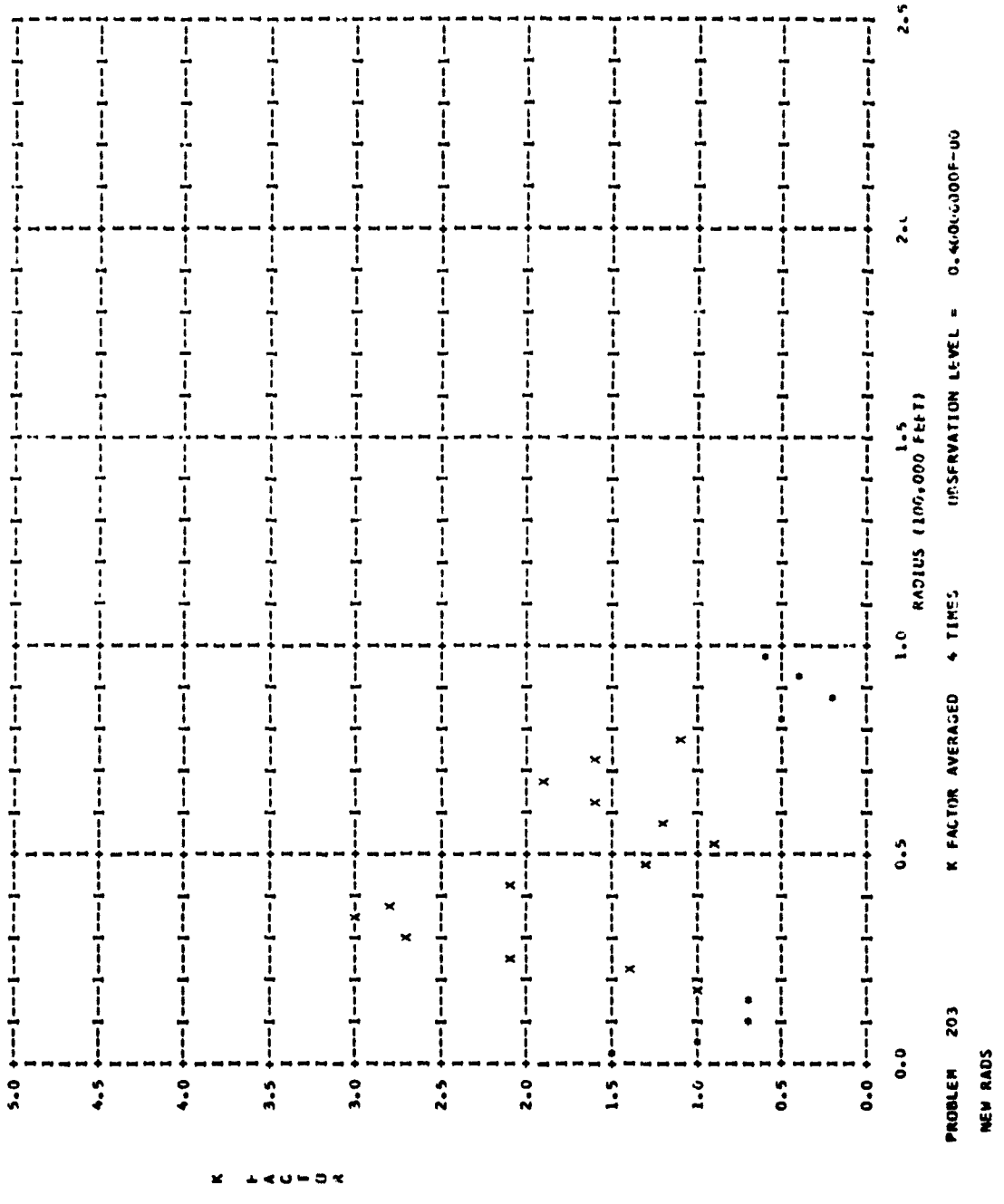
K FACTOR
5.0
4.5
4.0
3.5
3.0
2.5
2.0
1.5
1.0
0.5
0.0
0.0
0.5
1.0
1.5
2.0
2.5
RADIUS (100,000 FEET)
PROBLEM 203
K FACTOR AVERAGED 4 TIMES
OBSERVATION LEVEL = 0.4000000E-00
NEW RADS

Fig. 31

NOTES FOR FIGS. 32 THROUGH 37

The problem results shown in these figures are for a source height of 100,000 feet. The input parameters are the same in every respect as the previous problem shown in Figs. 26 through 31 except for the polar starting angles. Instead of aiming at the bins on the 60,000 foot level, the angles are uniform on cos θ; $\mu = -1(.04) + 1$.* This was done precisely in order to see what differences would show up with the two quite dissimilar angular distributions. (Both distributions of course represent an isotropic source. The integration coefficients are changed in accordance with the angular distribution to insure this.) For the higher levels where the fluctuations are small, the differences in the two cases are also small. For the lower levels where the fluctuations become larger, the differences become much greater as one would expect.

*There were 51 angles with 100 histories per angle or 5100 histories total.

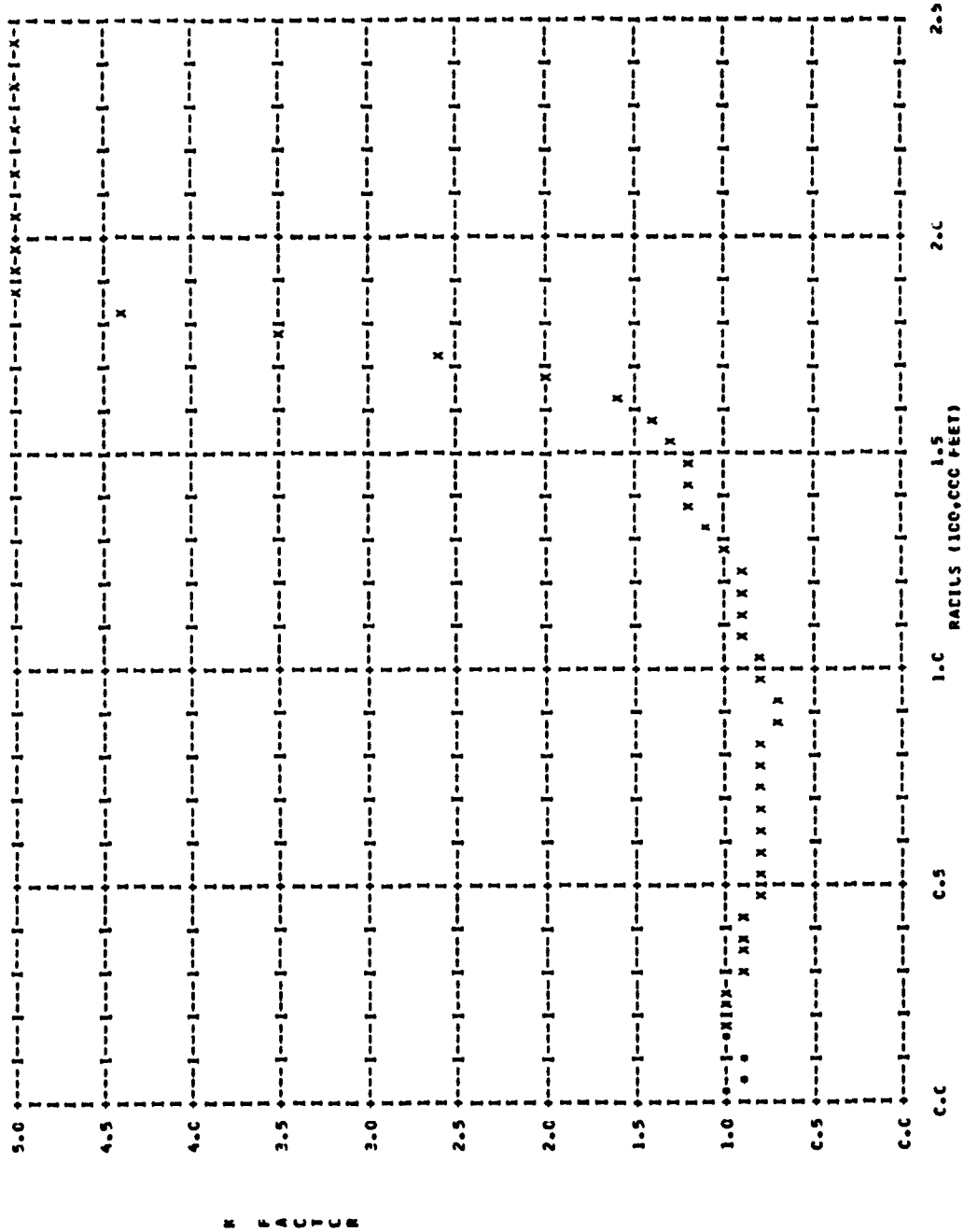
K FACTOR
5.0
4.5
4.0
3.5
3.0
2.5
2.0
1.5
1.0
0.5
0.0
0.0
0.5
1.0
1.5
2.0
2.5
RADIUS (100,000 FEET)
PRECLEP 207
K FACTOR AVERAGED 4 TYPES
OBSERVATION LEVEL = 0.8000000E 04
AEP RACS

Fig. 32

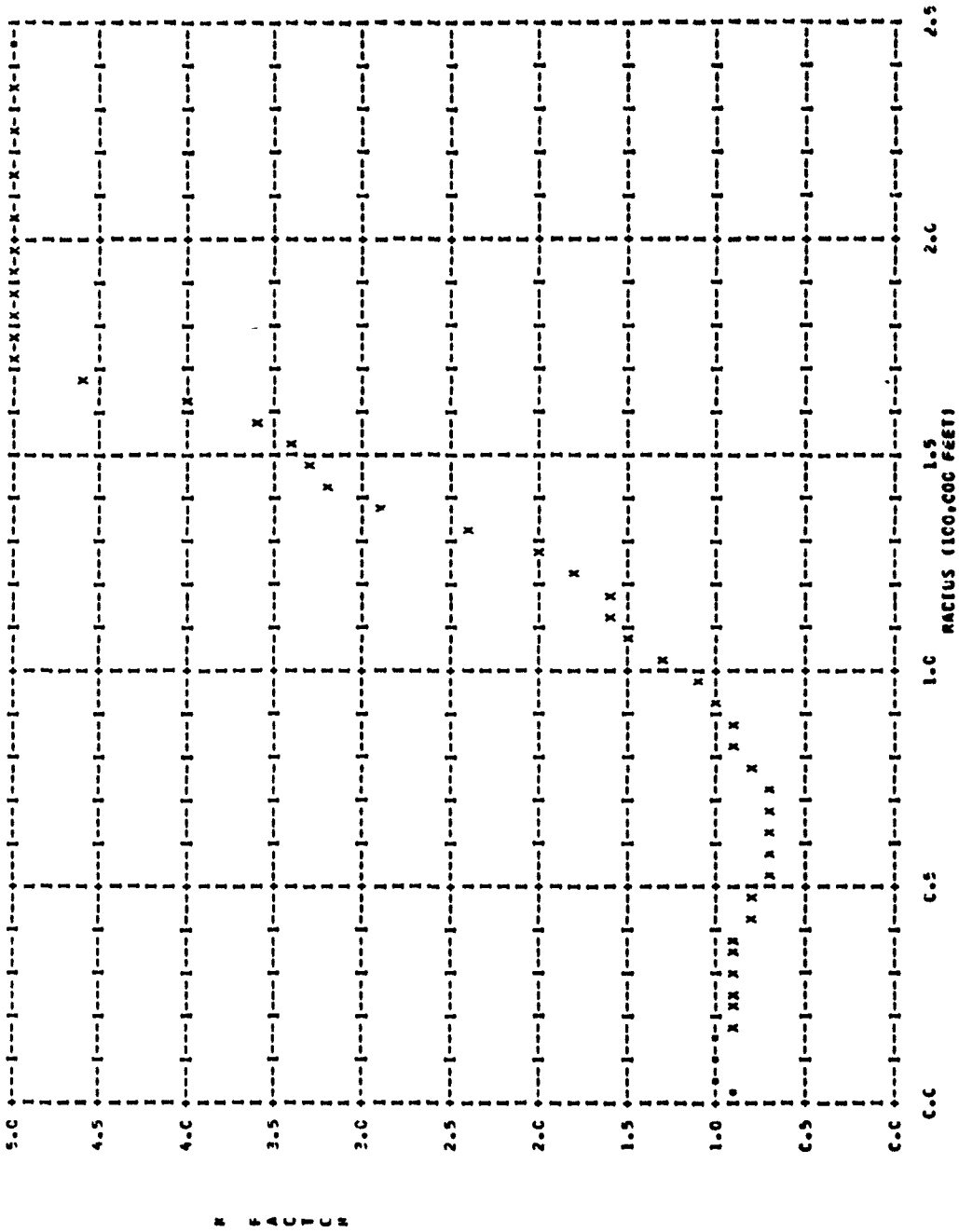
K FACTOR
5.0
4.5
4.0
3.5
3.0
2.5
2.0
1.5
1.0
0.5
0.0
0.0
0.5
1.0
1.5
2.0
2.5
RADIUS (100,000 FEET)
PRCELEP 207
K FACTOR AVERAGED 4 TIMES
CONSERVATION LEVEL = 3.700000000E 00
RED RACE

Fig. 33

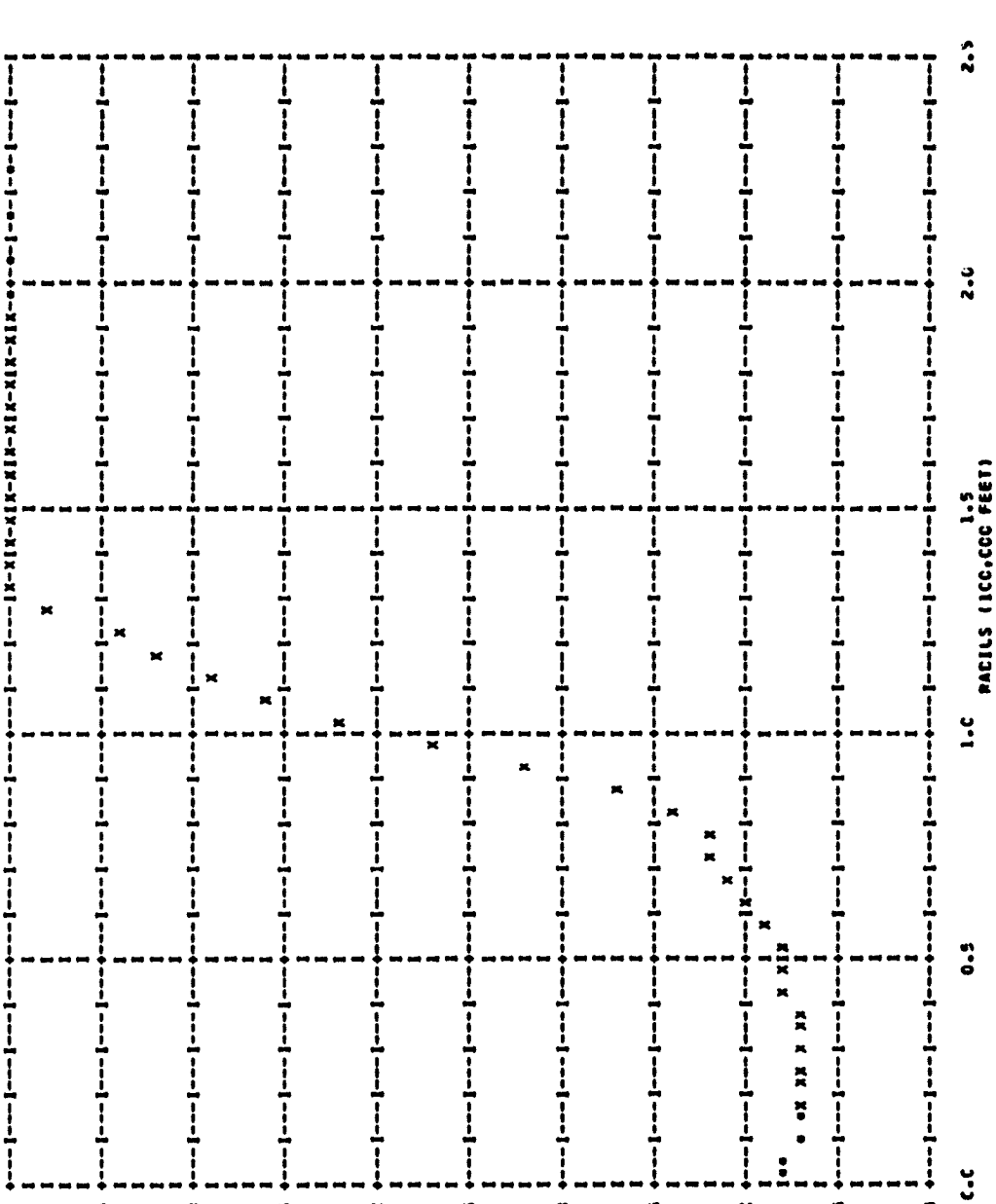
K FACTOR
5.0
4.5
4.0
3.5
3.0
2.5
2.0
1.5
1.0
0.5
0.0
0.0
0.5
1.0
1.5
2.0
2.5
PACILS (100.000 FEET)
PROBLEM 207
K FACTOR AVERAGED 4 TIMES
OBSERVATION LEVEL = 0.99999999E 00
RED RACS

Fig. 34

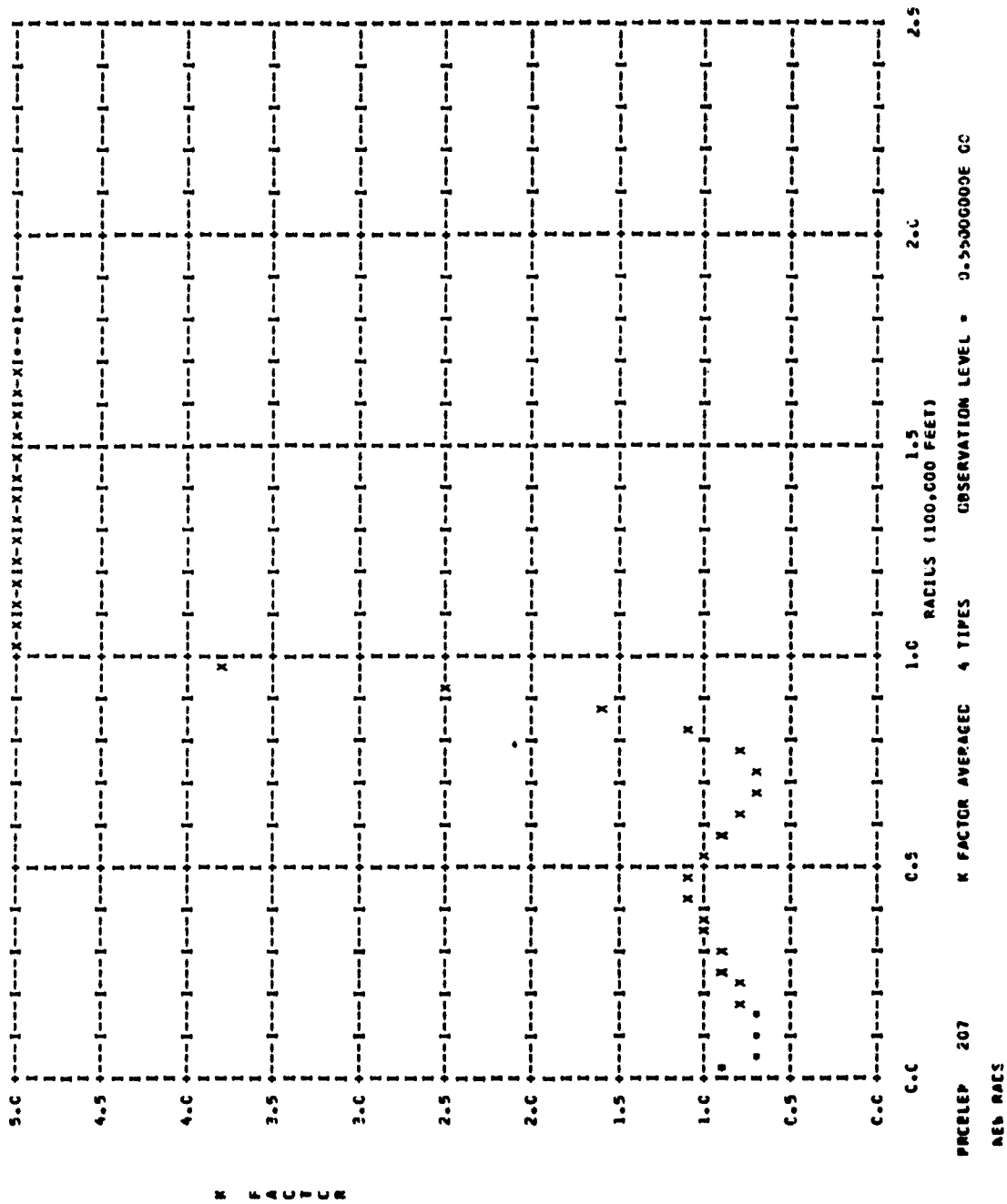
K FACTOR
5.0
4.5
4.0
3.5
3.0
2.5
2.0
1.5
1.0
0.5
0.0
0.5
1.0
1.5
2.0
2.5
RADIUS (100,000 FEET)
PRELEP 207 K FACTOR AVERAGED 4 TIMES OBSERVATION LEVEL = 0.500000E 00
RED RACE

Fig. 35

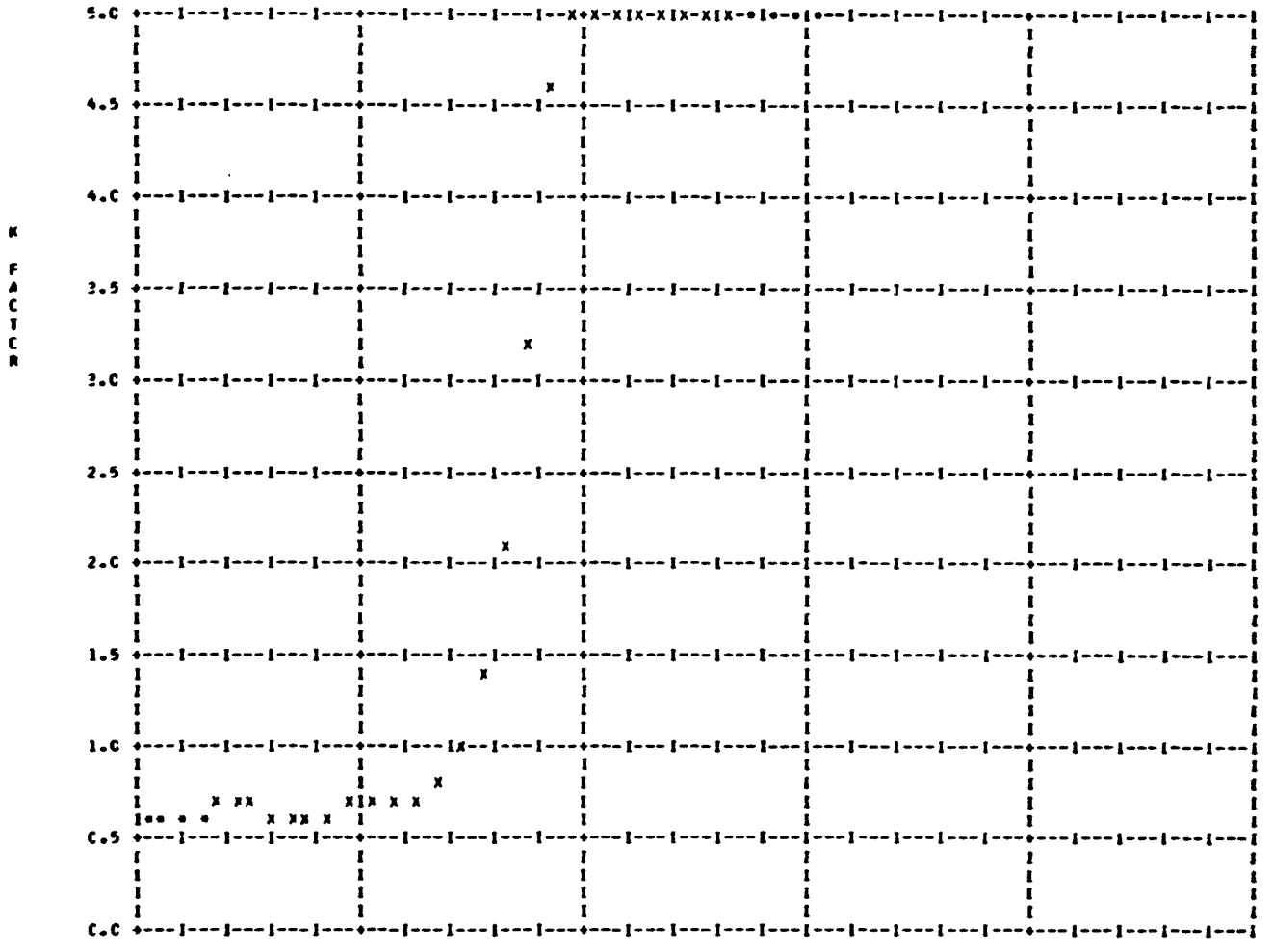

PROFILE 207 K FACTOR AVERAGED 4 TIMES OBSERVATION LEVEL = 0.960000007 G

REV RADS

Fig. 36

NOTE FOR FIG. 37

The same note as given on page 54 for the 200,000 foot source height applies to the 40,000 foot observation level results shown here.

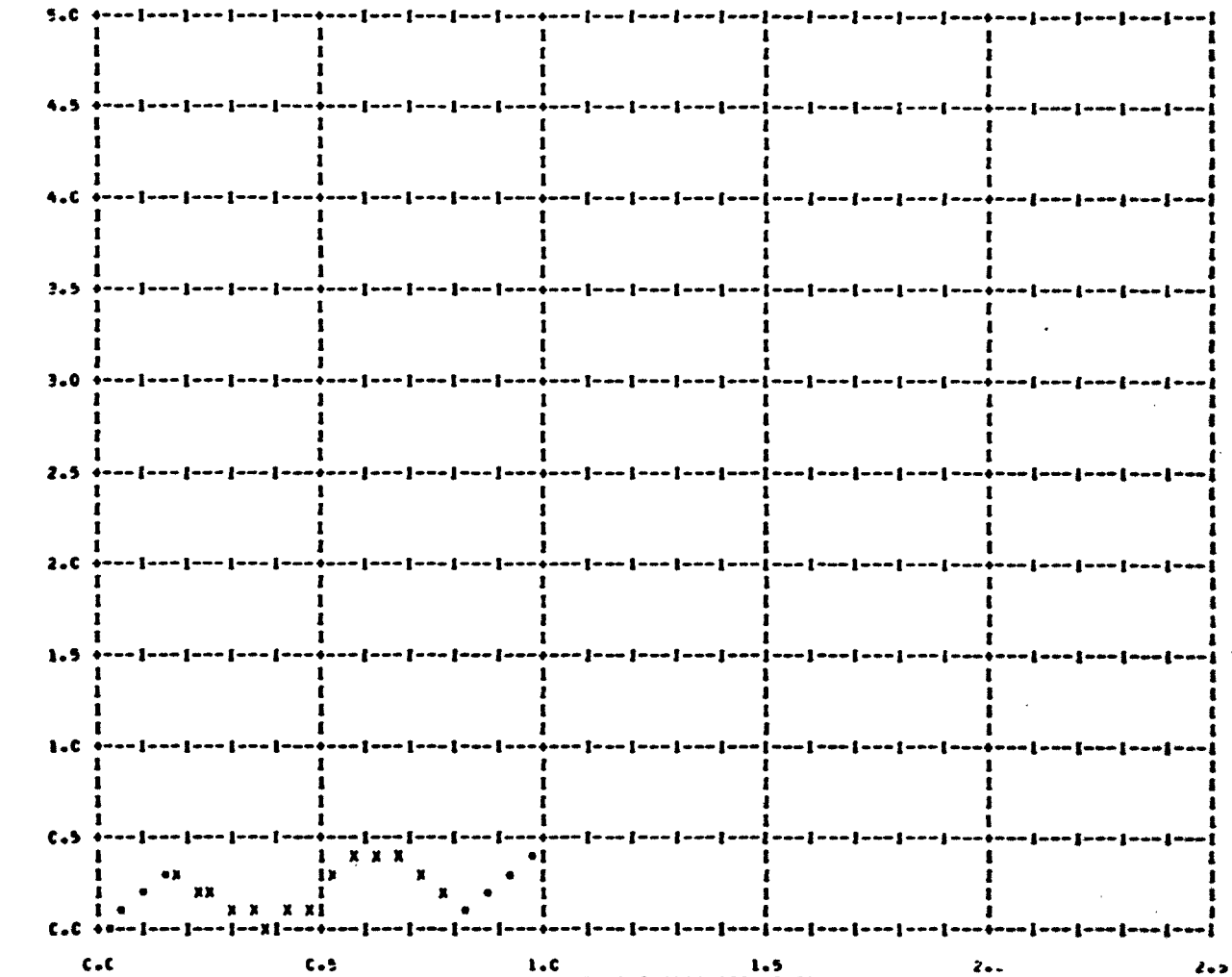

PROBLEM 207 K FACTOR AVERAGED 4 TIMES CONSERVATION LEVEL = [illegible]

RED RACE

Fig. 37

NOTES FOR FIGS. 38 THROUGH 59

These figures are all for the 14 Mev source on the air-ground interface. The input parameters are given on page 64. The observation level given on each graph is in units of 100,000 feet. The abscissa is the $\log_{10}$ of the horizontal $u_o r$, also called the adjusted $u_o r$ defined on page 36.

On the higher levels, the small close-in bins suffer from statistical inaccuracy. Thus in Fig. 38 for the 3000 foot observation level, the K factor for radii of less than $u_o r = 0.25$ are not meaningful. When the 20 foot burst altitude is reached (Fig. 43) the K factor is meaningful down to about $u_o r = .005$. On the ground level K is statistically significant all the way to the origin which is at $u_o r = .001$. This was the reason for the inclusion of the multitude of small radial bins close to the origin. There is no reason to include these bins on the higher levels, but the Monte Carlo code is now arranged so that the radial bins on all observation levels must be the same. For values of $u_o r$ greater than 8 or so the results again become bad on most observation levels due to statistics.

The density of the air at the 0 observation level or sea level in this problem is 0.00122 gms/cm^3. The mean free path of 14 Mev neutrons is 402 feet at sea level. Below the density interface, the density is 2.0 and the mean free path is 2.94 inches.

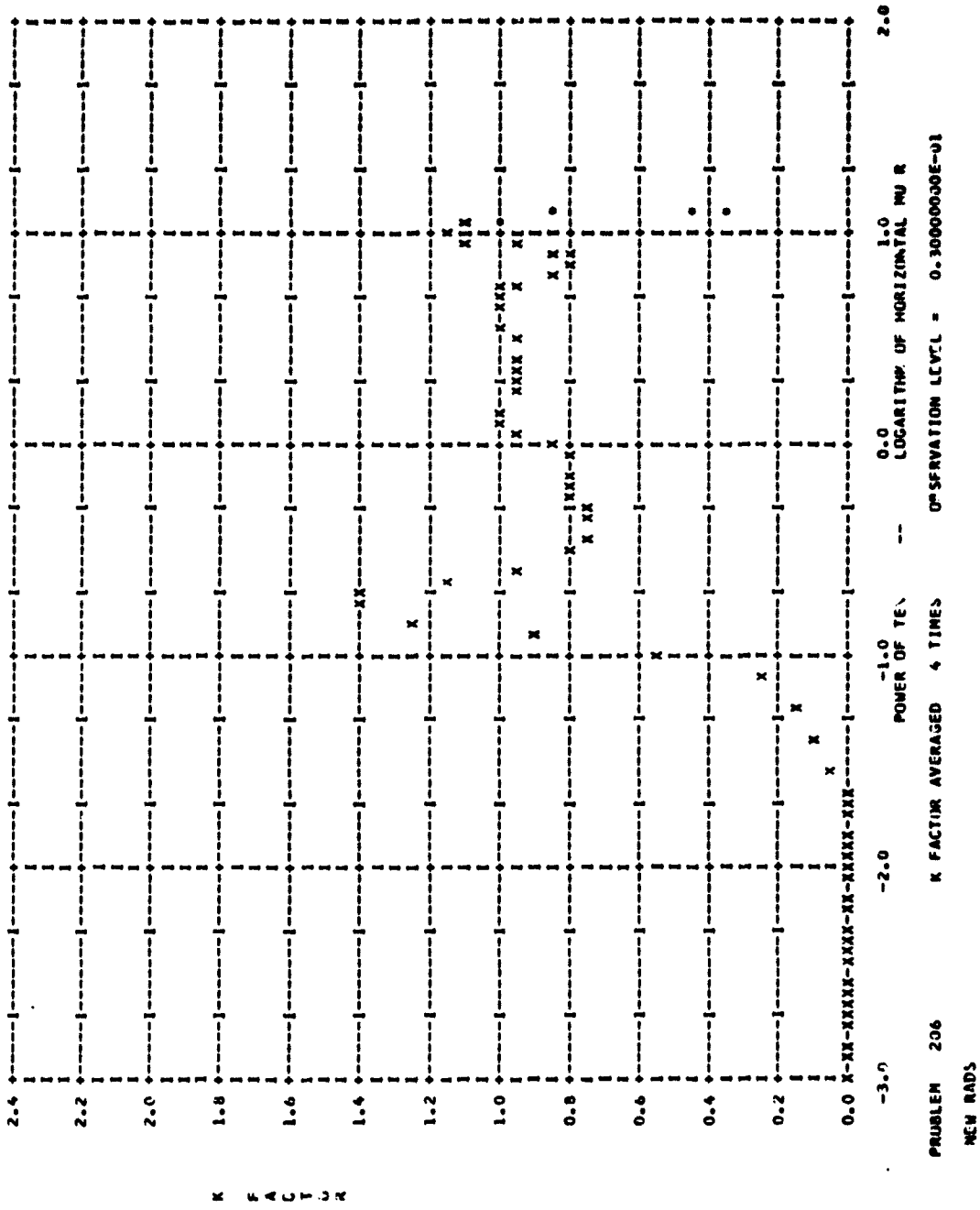
K FACTOR
2.4
2.2
2.0
1.8
1.6
1.4
1.2
1.0
0.8
0.6
0.4
0.2
0.0
-3.0
-2.0
-1.0
0.0
1.0
2.0
POWER OF TEN
LOGARITHM OF HORIZONTAL MU R
PROBLEM 206
K FACTOR AVERAGED 4 TIMES
OBSERVATION LEVEL = 0.30000000E+01
NEW RADS

Fig. 38

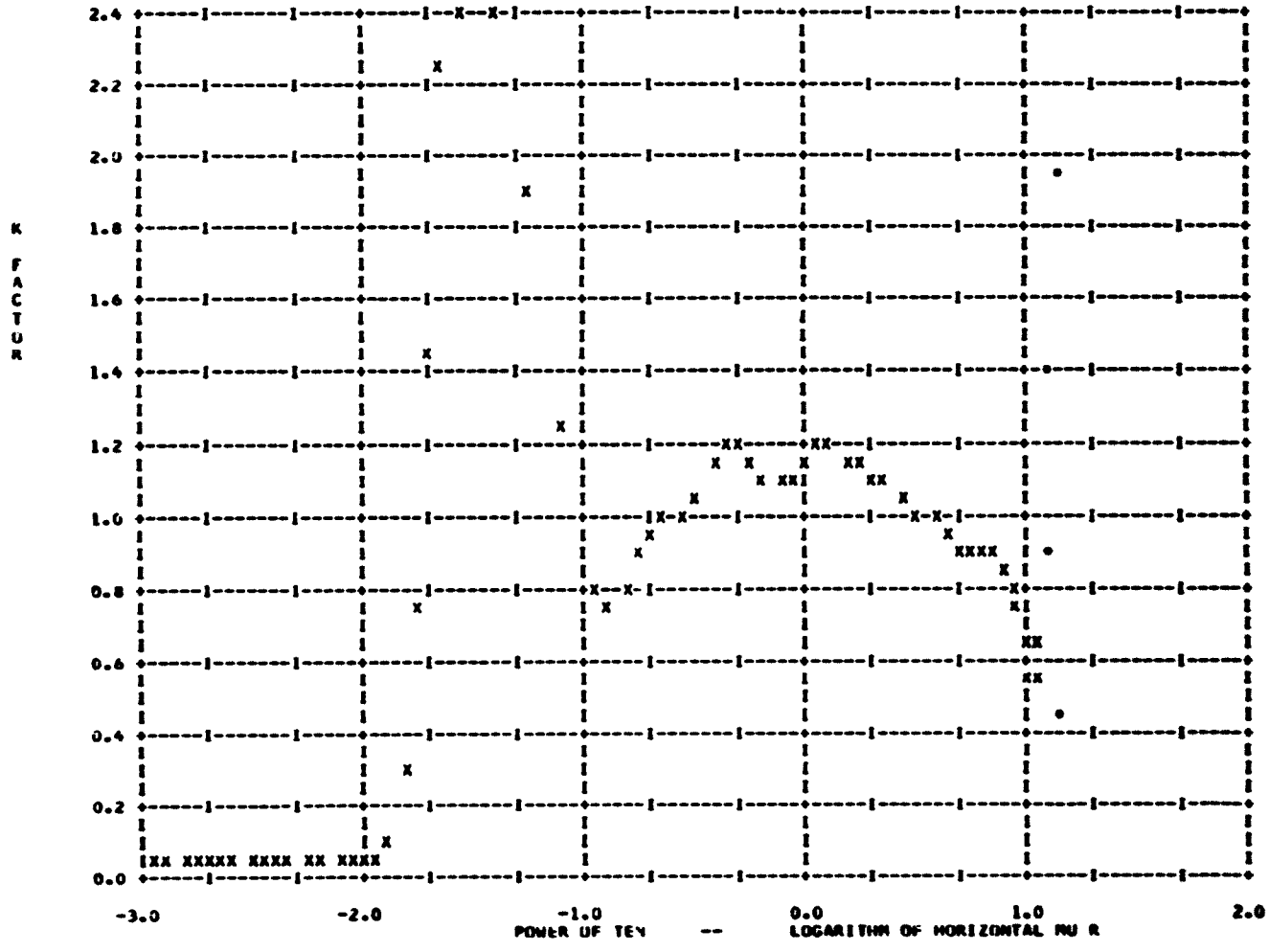

PROBLEM 206 K FACTUR AVERAGED 4 TIMES OBSERVATION LEVEL = 0.15000000E-01

NEW RADS

FIG. 39

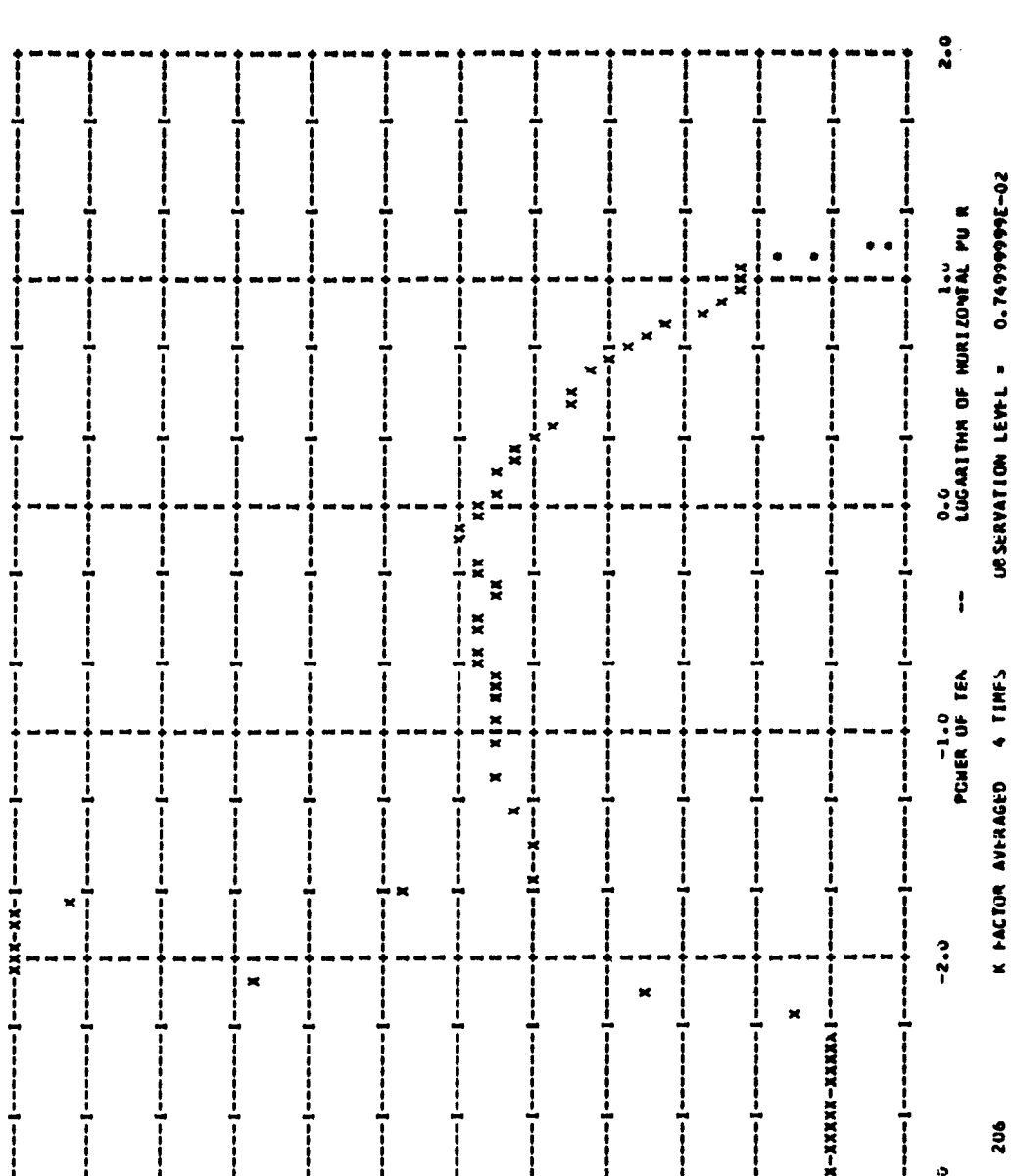
2.4
2.2
2.0
1.8
1.6
1.4
1.2
1.0
0.8
0.6
0.4
0.2
0.0
-3.0
-2.0
-1.0
0.0
1.0
2.0
POWER OF TEN
LOGARITHM OF HORIZONTAL PU R
PROBLEM 206
K FACTOR AVERAGED 4 TIMES
OBSERVATION LEVEL = 0.749999999E-02
NEW RADS

Fig. 40

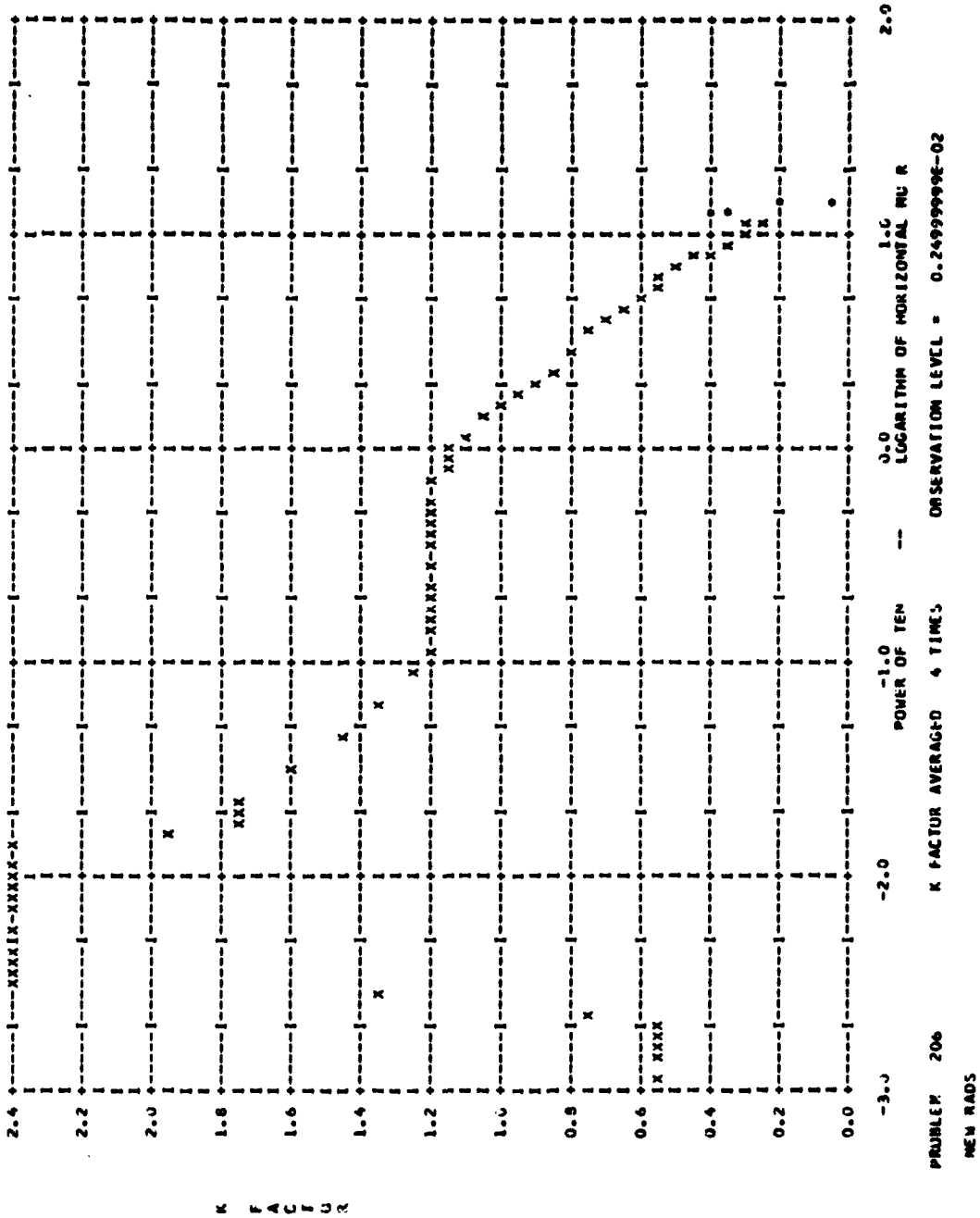
K FACTOR
2.4
2.2
2.0
1.8
1.6
1.4
1.2
1.0
0.8
0.6
0.4
0.2
0.0
-3.0
-2.0
-1.0
0.0
1.0
2.0
POWER OF TEN
LOGARITHM OF HORIZONTAL RU R
PROBLEM 206
K FACTOR AVERAGED 4 TIMES
OBSERVATION LEVEL = 0.249999999E-02
NEW RADS

Fig. 41

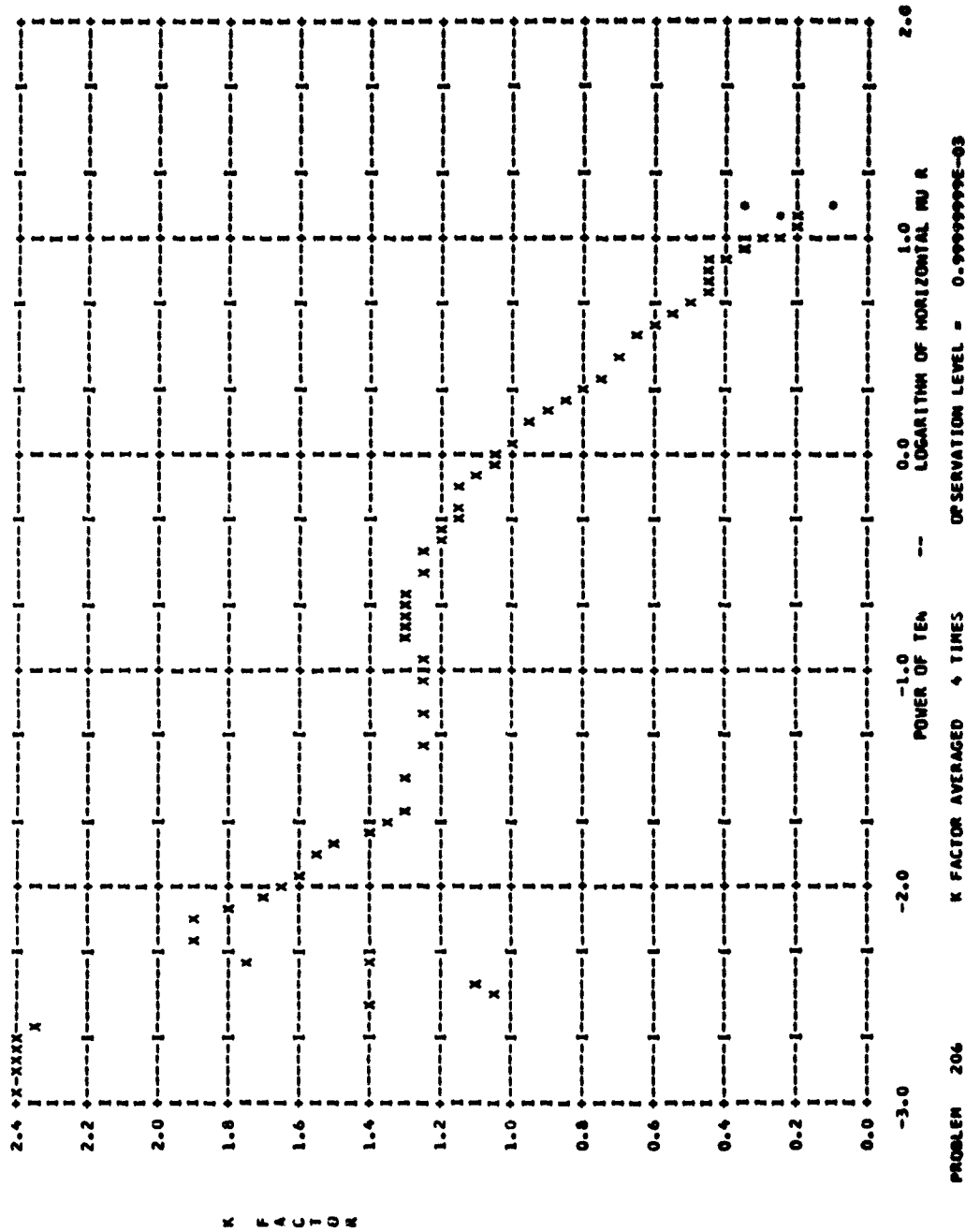
K FACTOR
2.4
2.2
2.0
1.8
1.6
1.4
1.2
1.0
0.8
0.6
0.4
0.2
0.0
-3.0
-2.0
-1.0
0.0
1.0
2.0
POWER OF TEN -- LOGARITHM OF HORIZONTAL RU R
PROBLEM 204 K FACTOR AVERAGED 4 TIMES OBSERVATION LEVEL = 0.99999999E-03
MEN RADS

Fig. 42

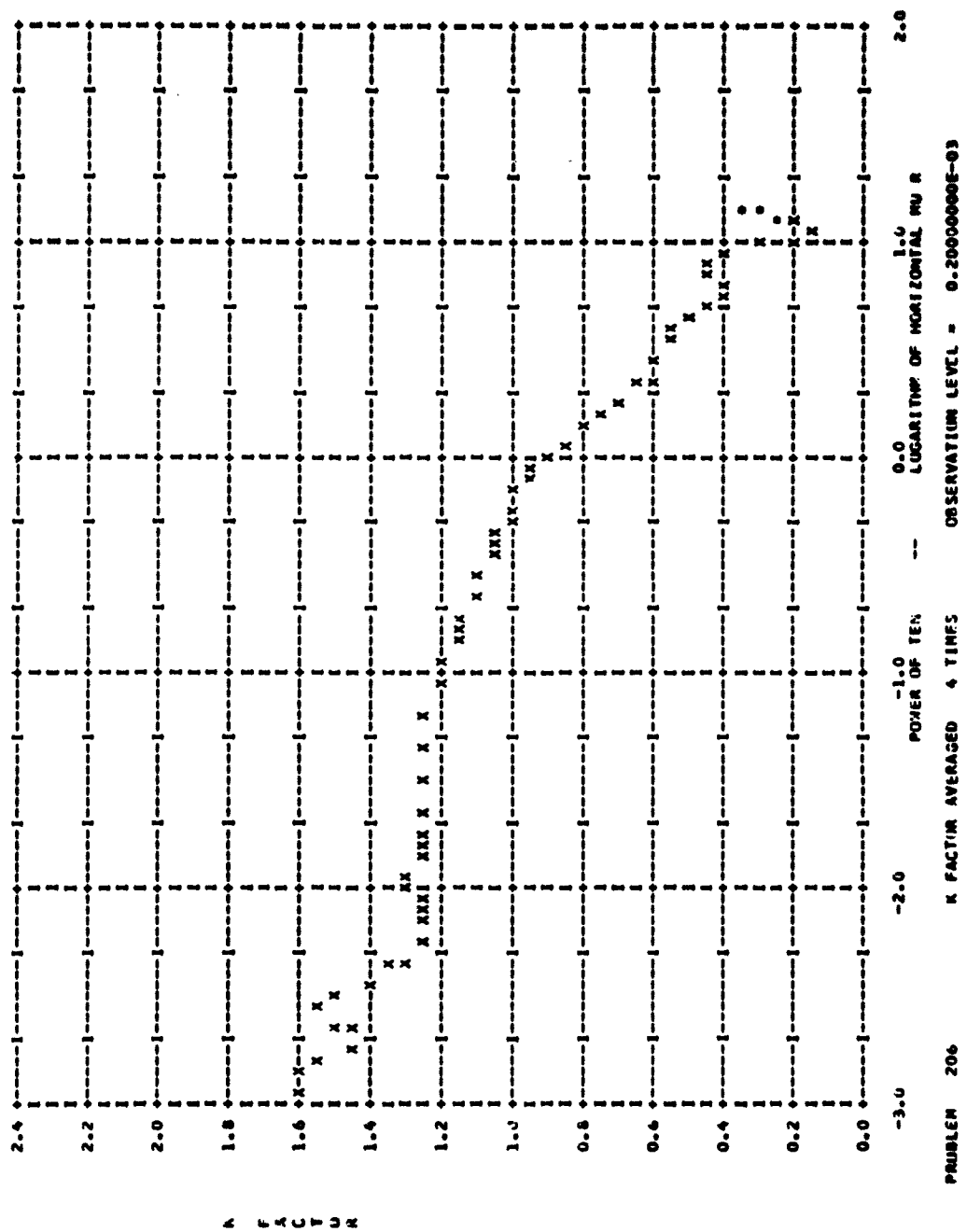
K FACTOR
2.4
2.2
2.0
1.8
1.6
1.4
1.2
1.0
0.8
0.6
0.4
0.2
0.0
-3.0
-2.0
-1.0
0.0
1.0
2.0
POWER OF TEN
LOGARITHM OF HORIZONTAL RU R
PROBLEM 206
K FACTOR AVERAGED 4 TIMES
OBSERVATION LEVEL = 0.20000000E-03
NEW RADS

Fig. 43

FOR 0' OBSERVATION LEVEL SEE FIG. 51

NOTES FOR FIGS. 44 AND 45

These observation levels are 1/2 and 1 foot below the density interface. The abscissae here are in mean free paths in the dense medium. Note that the same effect prevails here that was noted and explained for the very high altitude source on page 74, namely the rapid increase in K after several mean free paths. Here the neutrons simply go out into the air and then shine back down into the dense medium in the vicinity of the observation point. In gamma ray propagation this effect is known as "sky shine."

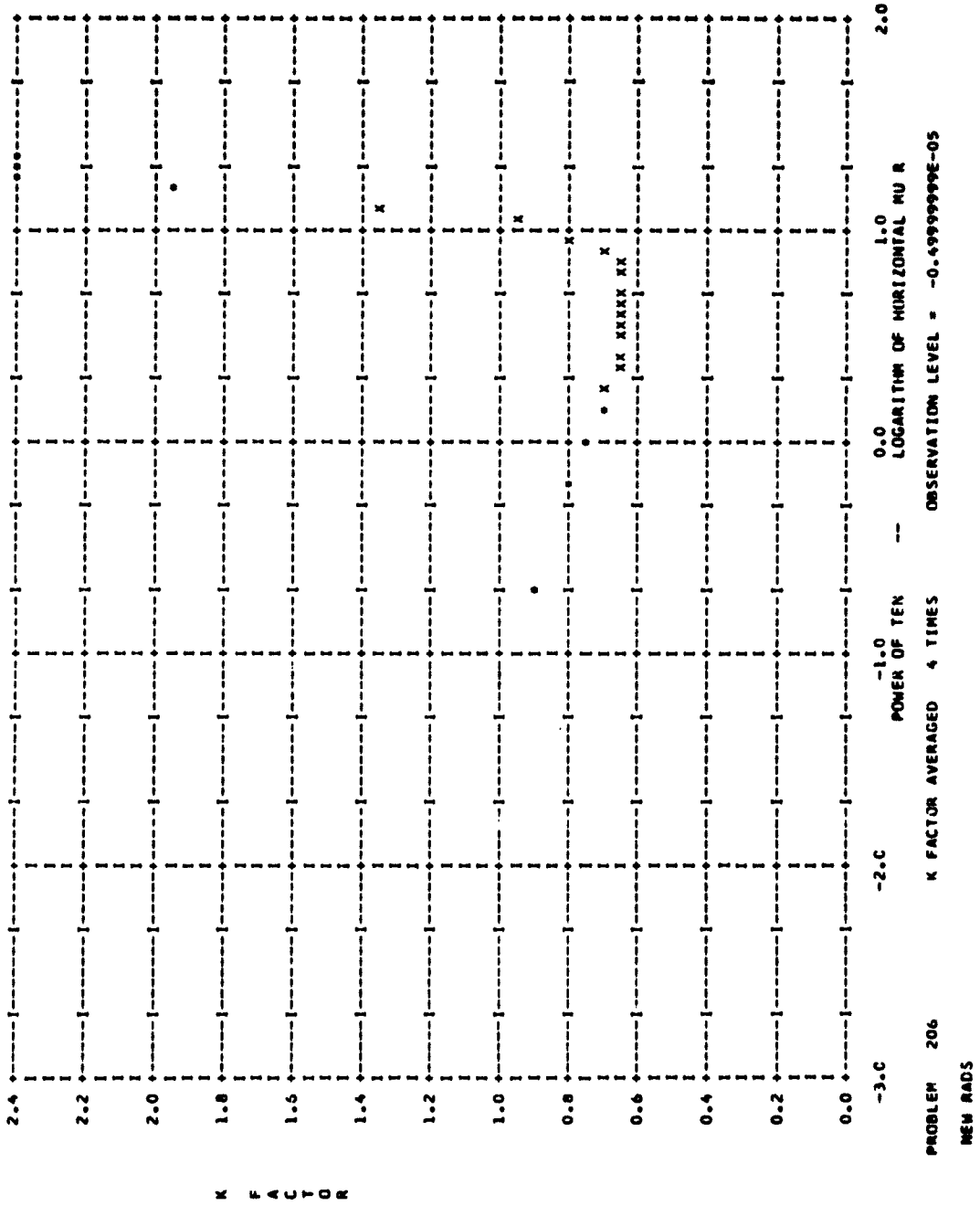
K FACTOR
2.4
2.2
2.0
1.8
1.6
1.4
1.2
1.0
0.8
0.6
0.4
0.2
0.0
-3.0
-2.0
-1.0
0.0
1.0
2.0
POWER OF TEN -- LOGARITHM OF HORIZONTAL MU R
PROBLEM 206 K FACTOR AVERAGED 4 TIMES OBSERVATION LEVEL = -0.49999999E-05
MEM RADS

Fig. 44

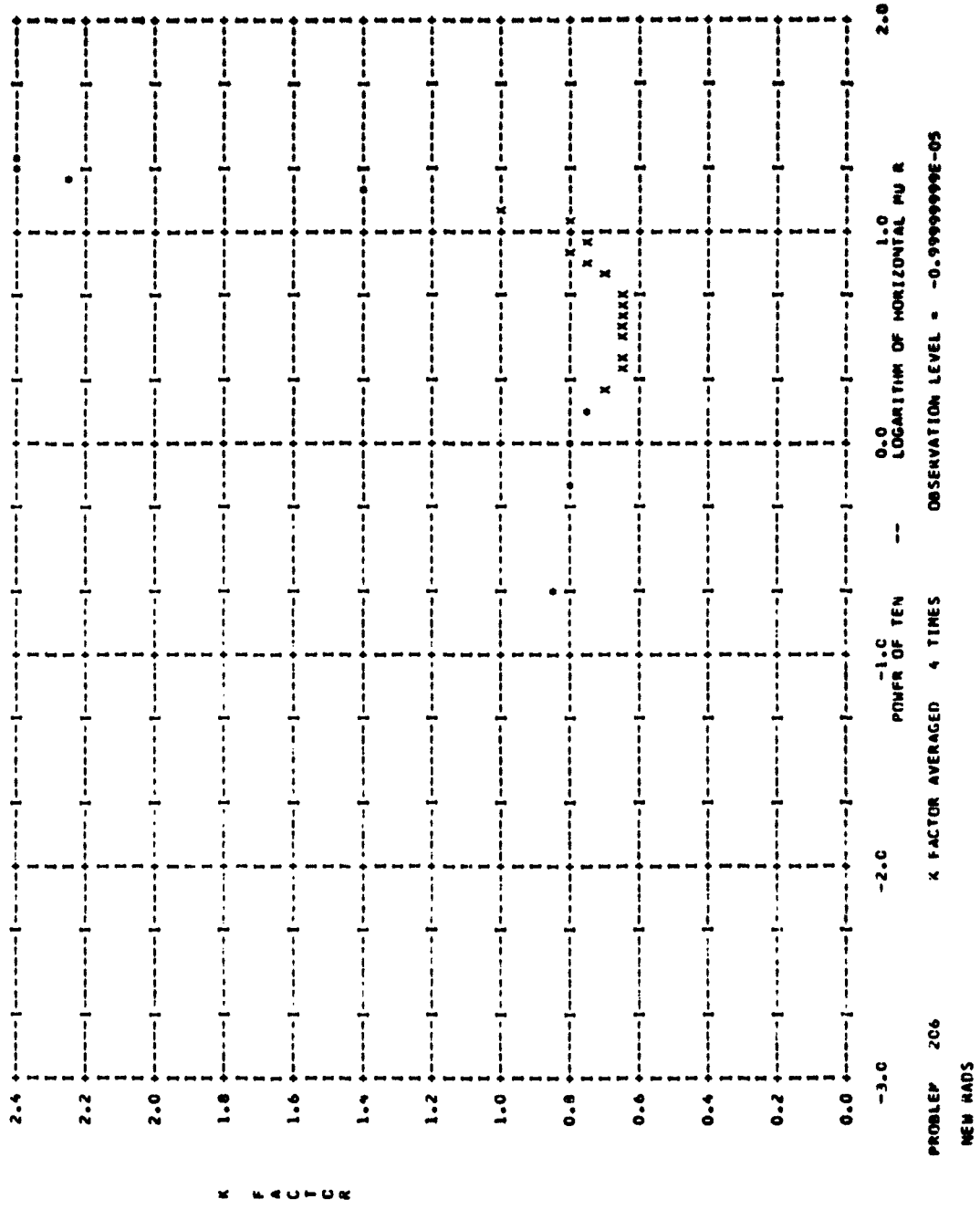
K FACTOR
2.4
2.2
2.0
1.8
1.6
1.4
1.2
1.0
0.8
0.6
0.4
0.2
0.0
-3.0
-2.0
-1.0
0.0
1.0
2.0
POWER OF TEN
LOGARITHM OF HORIZONTAL FLU R
PROBLEM 206
K FACTOR AVERAGED 4 TIMES
OBSERVATION LEVEL = -0.99999999E-05
NEW RADS

Fig. 45

NOTES FOR FIGS. 46 AND 47

The results in these two figures are not statistically significant since the two observation levels are 8 and 12 mean free paths below the ground level.

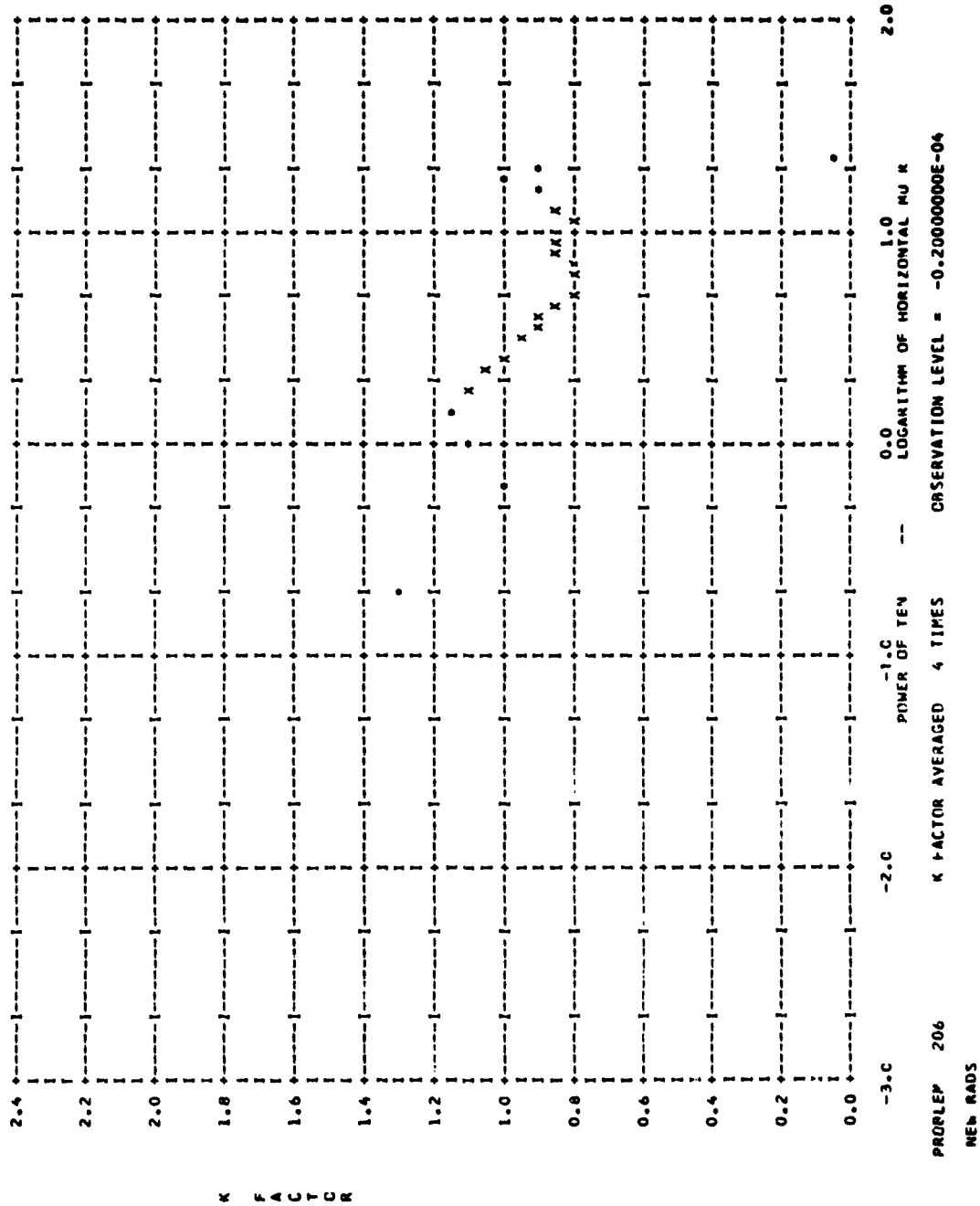
K FACTOR
2.4
2.2
2.0
1.8
1.6
1.4
1.2
1.0
0.8
0.6
0.4
0.2
0.0
-3.0
-2.0
-1.0
0.0
1.0
2.0
POWER OF TEN
LOGARITHM OF HORIZONTAL MU R
PROBLEM 206
K FACTOR AVERAGED 4 TIMES
OBSERVATION LEVEL = -0.20000000E-04
MEM RADS

Fig. 46

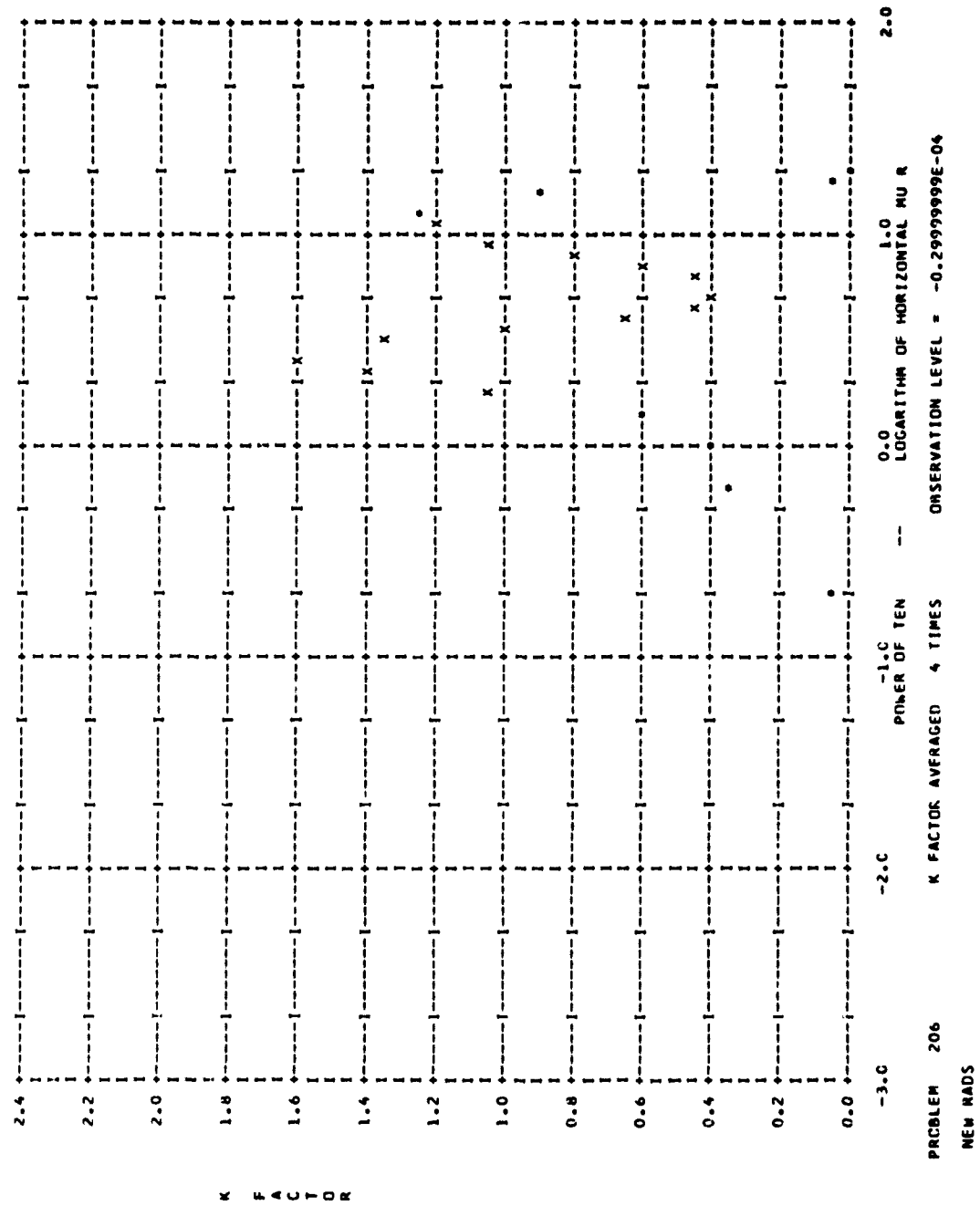
K FACTOR
2.4
2.2
2.0
1.8
1.6
1.4
1.2
1.0
0.8
0.6
0.4
0.2
0.0
-3.0
-2.0
-1.0
0.0
1.0
2.0
POWER OF TEN
LOGARITHM OF HORIZONTAL MU R
PROBLEM 206
K FACTOR AVERAGED 4 TIMES
OBSERVATION LEVEL = -0.29999999E-04
NEW RADS

Fig. 47

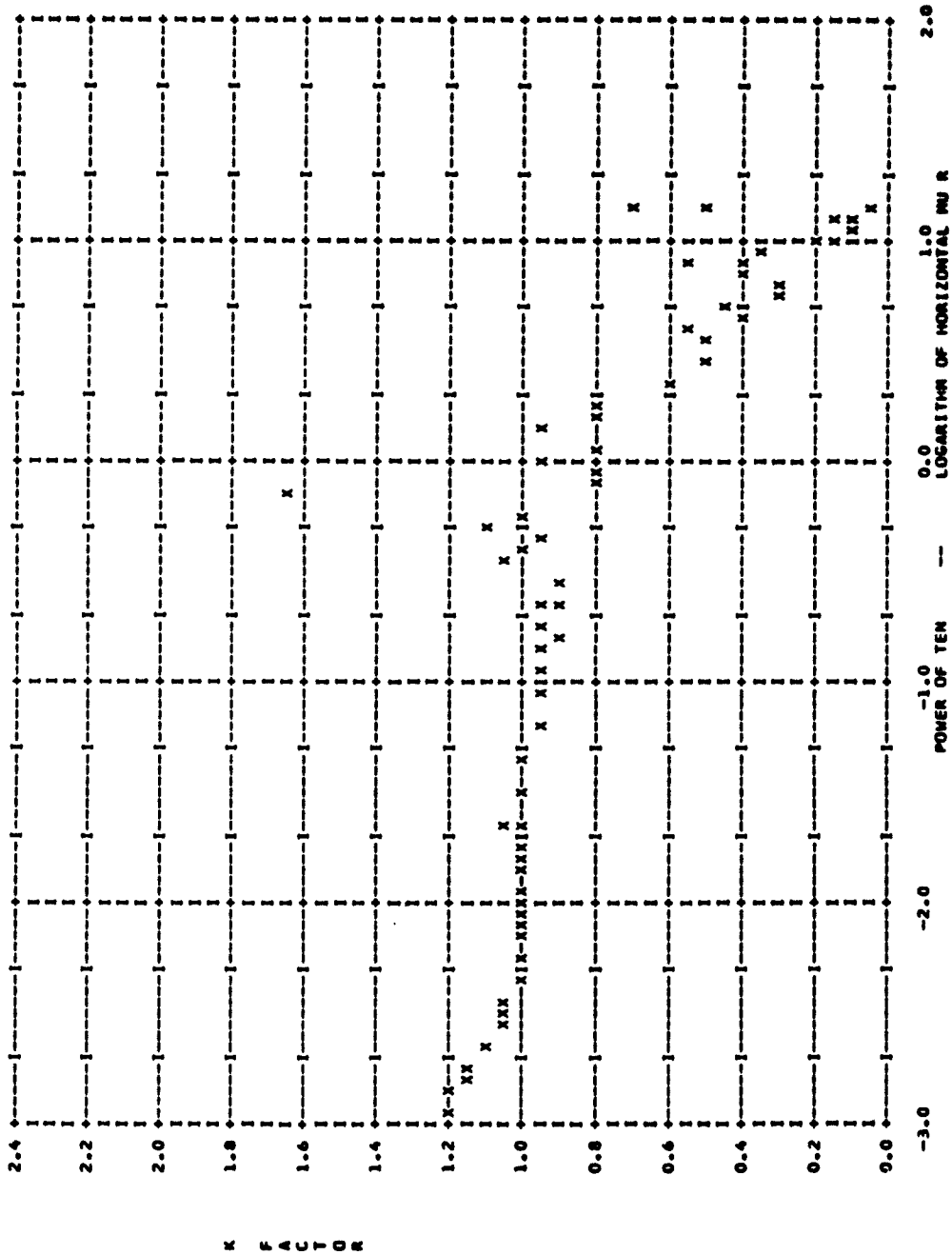
K FACTOR
2.4
2.2
2.0
1.8
1.6
1.4
1.2
1.0
0.8
0.6
0.4
0.2
0.0
-3.0
-2.0
-1.0
0.0
1.0
2.0
POWER OF TEN
LOGARITHM OF HORIZONTAL MU R
PROBLEM 206
K FACTOR AVERAGED 0 TIMES
OBSERVATION LEVEL = 0.
NEW RADS

Fig. 48

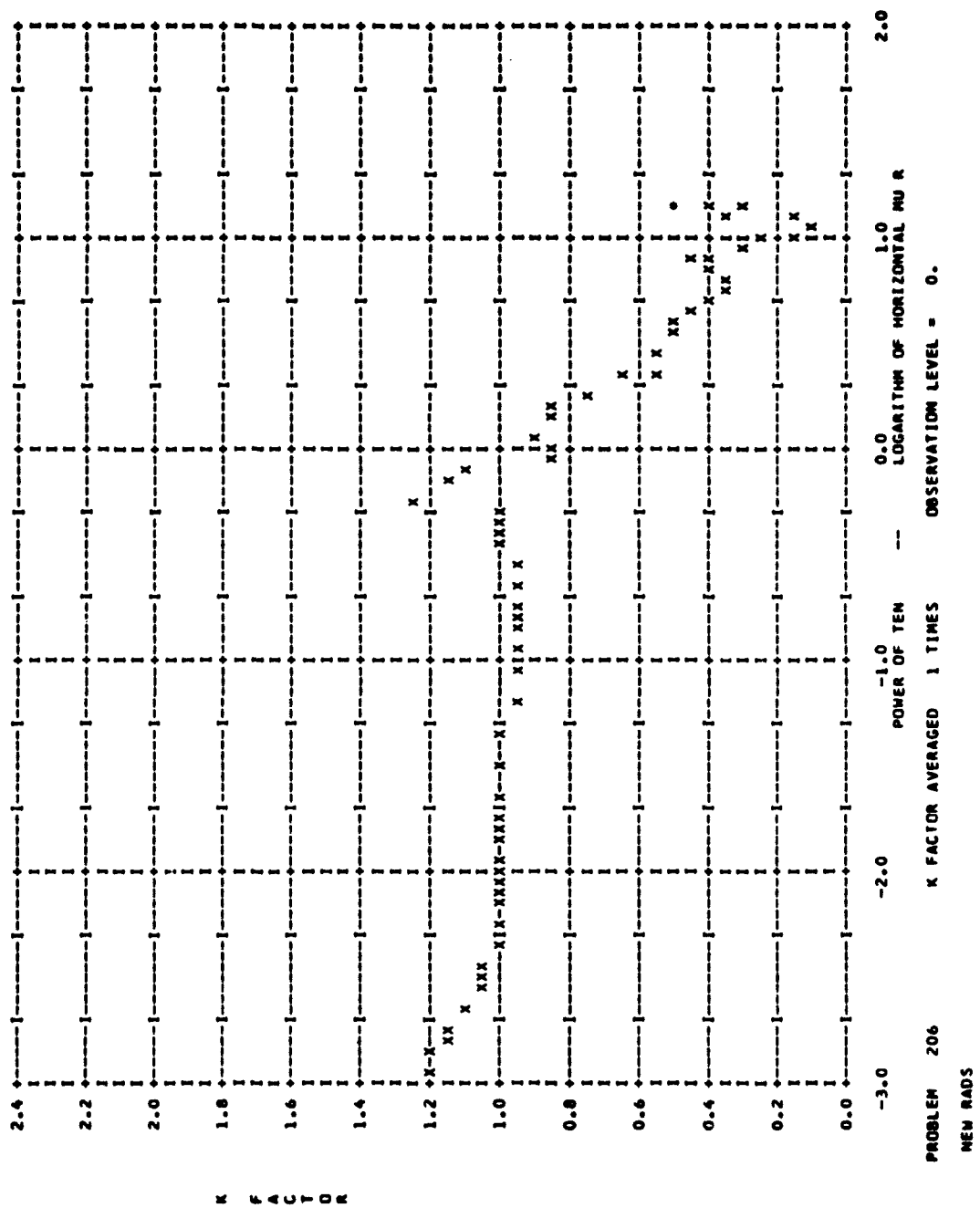
K FACTOR
2.4
2.2
2.0
1.8
1.6
1.4
1.2
1.0
0.8
0.6
0.4
0.2
0.0
-3.0
-2.0
-1.0
0.0
1.0
2.0
POWER OF TEN
--
LOGARITHM OF HORIZONTAL MU R
PROBLEM 206
K FACTOR AVERAGED 1 TIMES
OBSERVATION LEVEL = 0.
NEW RADS

Fig. 49

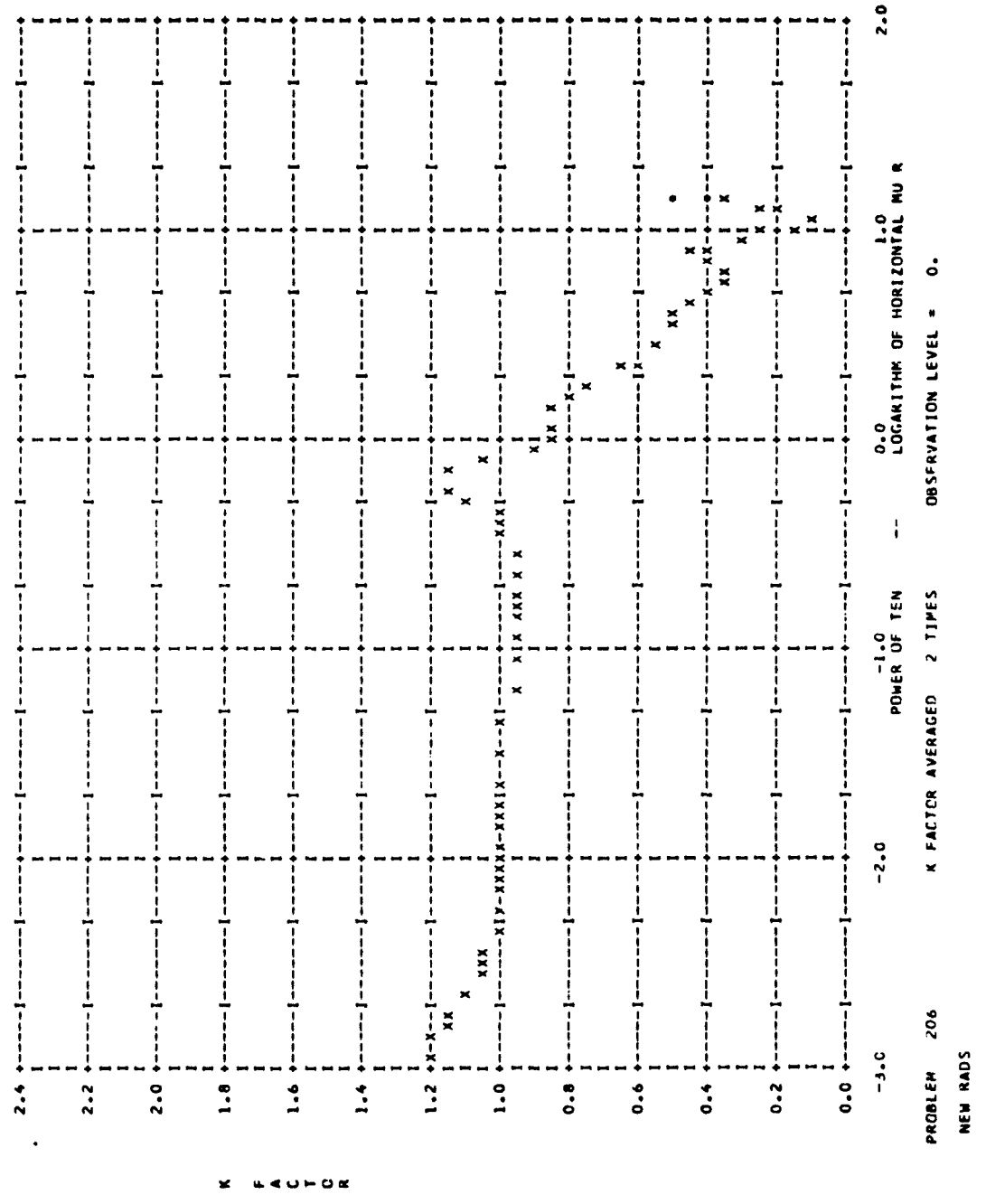
K FACTOR
2.4
2.2
2.0
1.8
1.6
1.4
1.2
1.0
0.8
0.6
0.4
0.2
0.0
-3.0
-2.0
-1.0
0.0
1.0
2.0
POWER OF TEN
LOGARITHM OF HORIZONTAL MU R
PROBLEM 206
K FACTOR AVERAGED 2 TIMES
OBSERVATION LEVEL = 0.
NEW RADS

Fig. 50

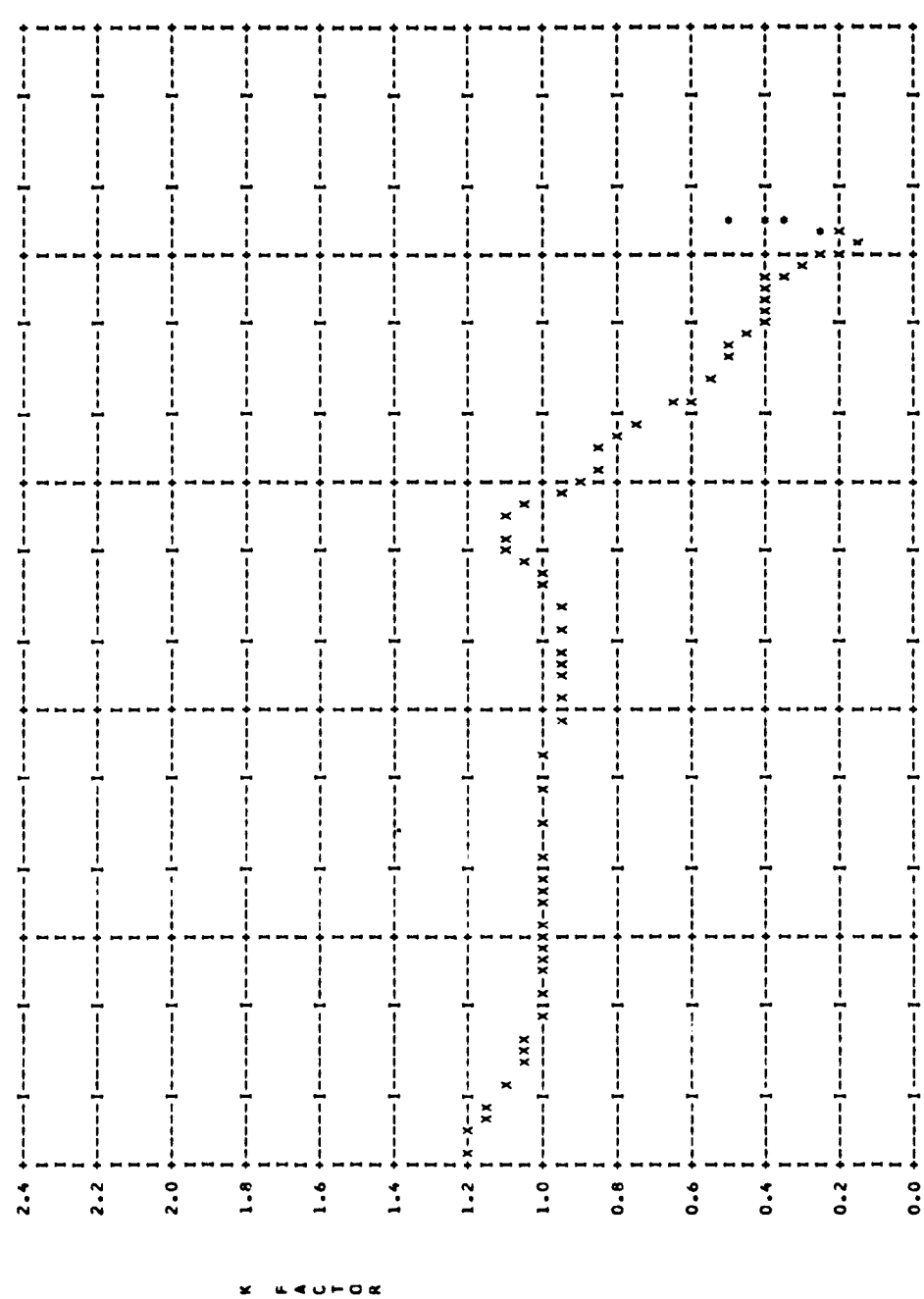
K FACTOR
2.4
2.2
2.0
1.8
1.6
1.4
1.2
1.0
0.8
0.6
0.4
0.2
0.0
-3.0
-2.0
-1.0
0.0
1.0
2.0
POWER OF TEN --
LOGARITHM OF HORIZONTAL MU R
PROBLEM 206
K FACTOR AVERAGED 4 TIMES
OBSERVATION LEVEL = 0.
NEW RADS

Fig. 51

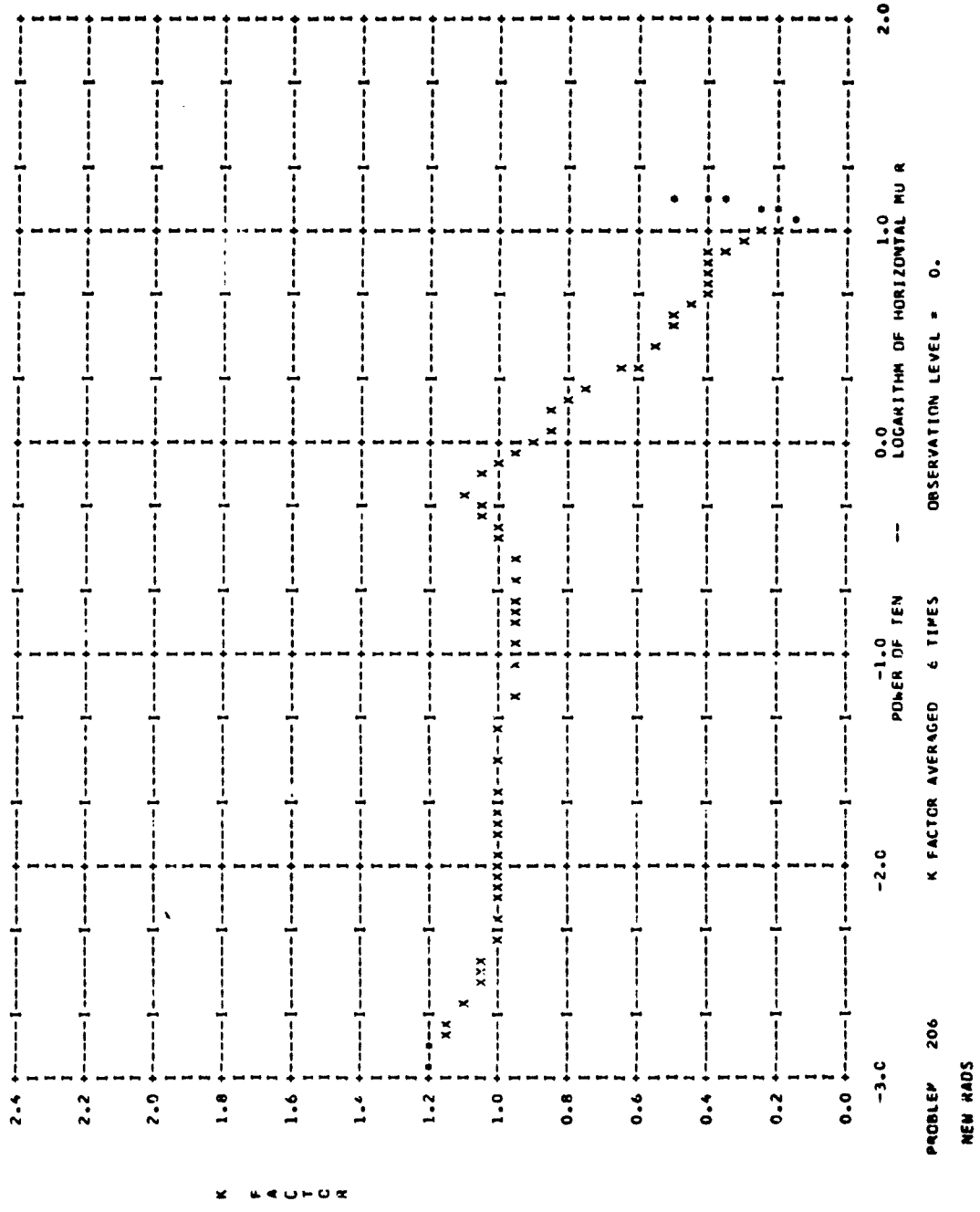
K FACTOR
2.4
2.2
2.0
1.8
1.6
1.4
1.2
1.0
0.8
0.6
0.4
0.2
0.0
-3.0
-2.0
-1.0
0.0
1.0
2.0
POWER OF TEN -- LOGARITHM OF HORIZONTAL MU R
PROBLEM 206 K FACTOR AVERAGED 6 TIMES OBSERVATION LEVEL = 0.
NEW RADS

Fig. 52

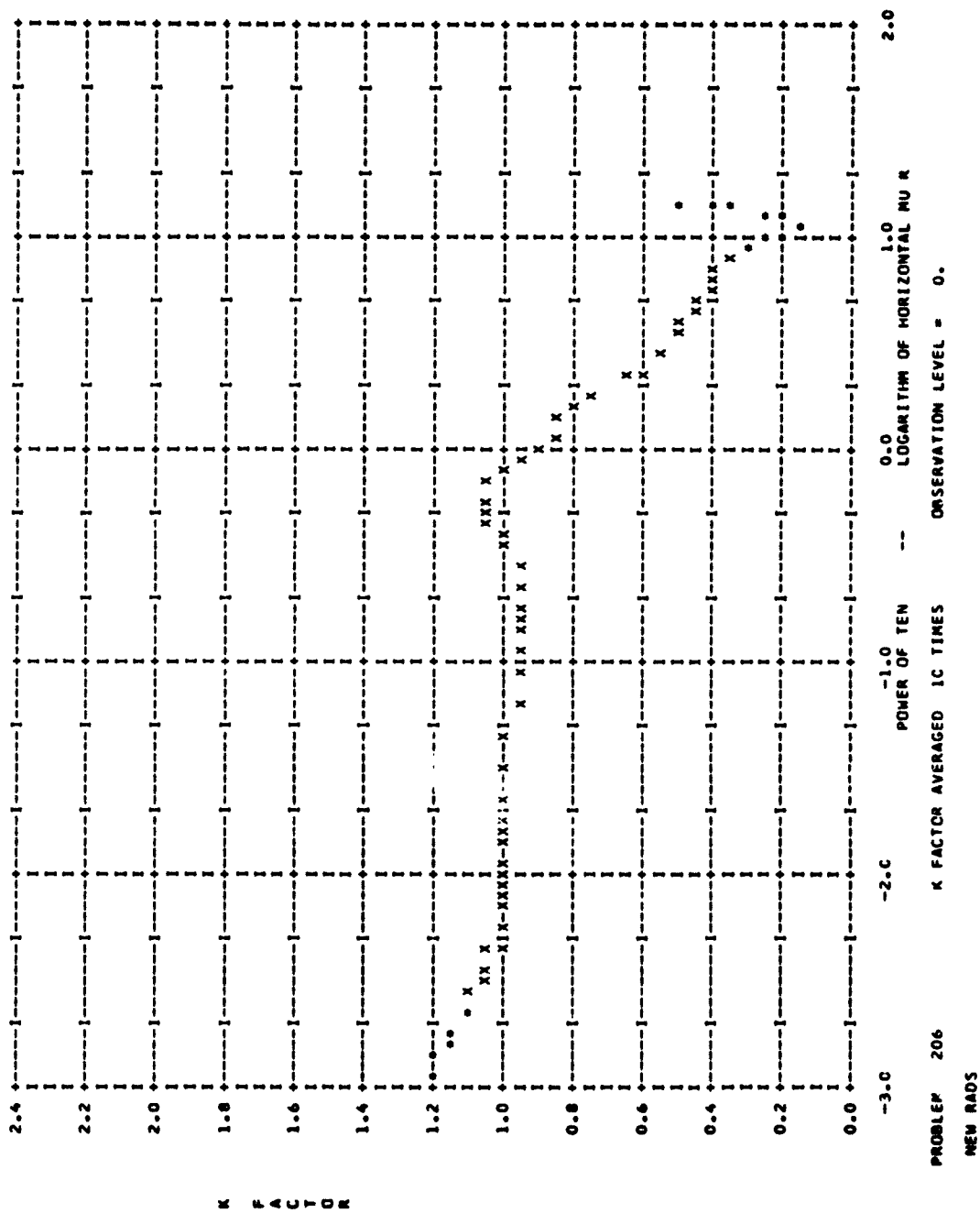
K FACTOR
2.4
2.2
2.0
1.8
1.6
1.4
1.2
1.0
0.8
0.6
0.4
0.2
0.0
-3.0
-2.0
-1.0
0.0
1.0
2.0
POWER OF TEN
LOGARITHM OF HORIZONTAL NU R
PROBLEM 206
K FACTOR AVERAGED 10 TIMES
OBSERVATION LEVEL = 0.
NEW RADS

Fig. 53

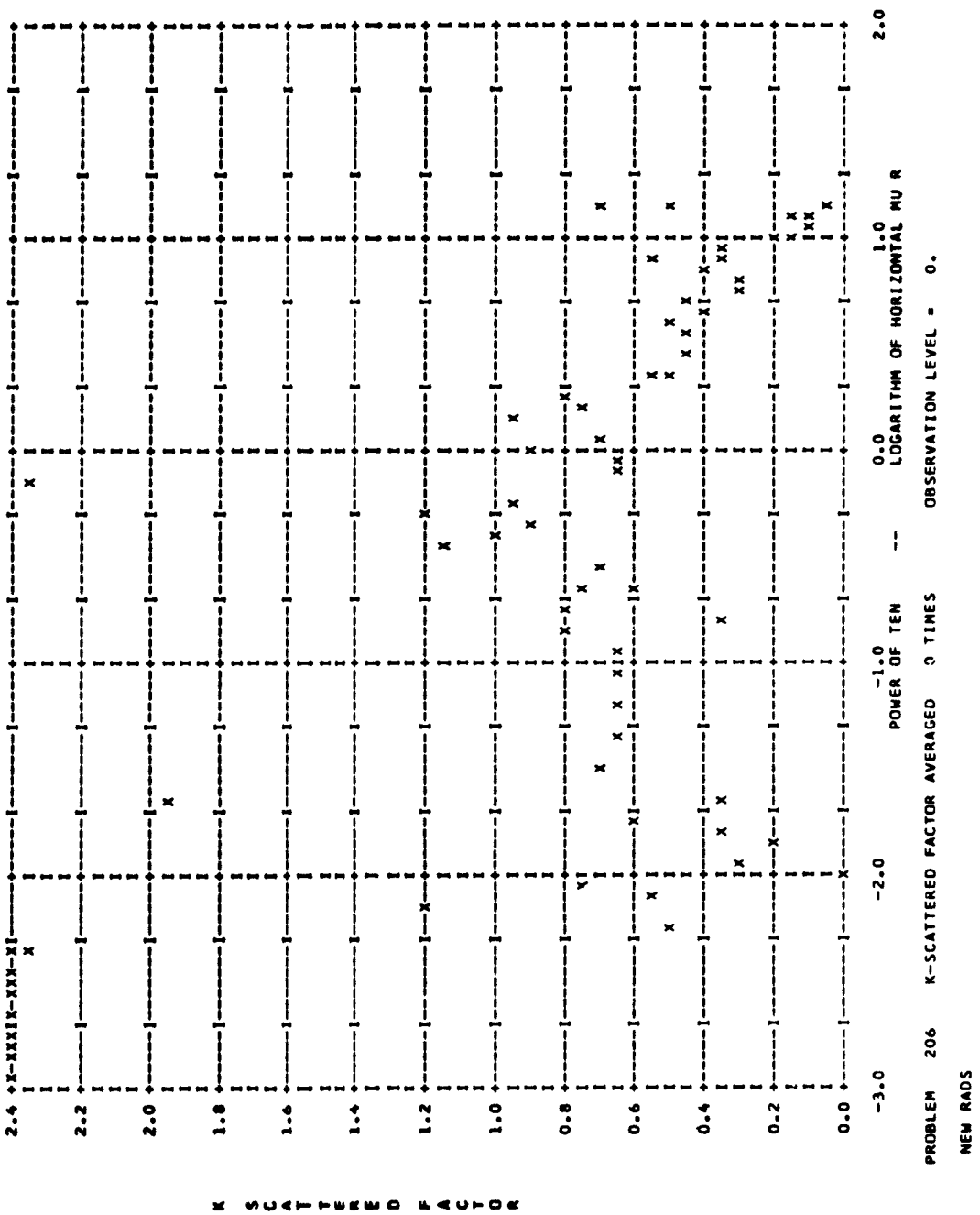
K SCATTERED FACTOR
2.4
2.2
2.0
1.8
1.6
1.4
1.2
1.0
0.8
0.6
0.4
0.2
0.0
-3.0
-2.0
-1.0
0.0
1.0
2.0
POWER OF TEN
--
LOGARITHM OF HORIZONTAL MU R
PROBLEM 206 K-SCATTERED FACTOR AVERAGED 0 TIMES OBSERVATION LEVEL = 0.
NEW RADS

Fig. 54

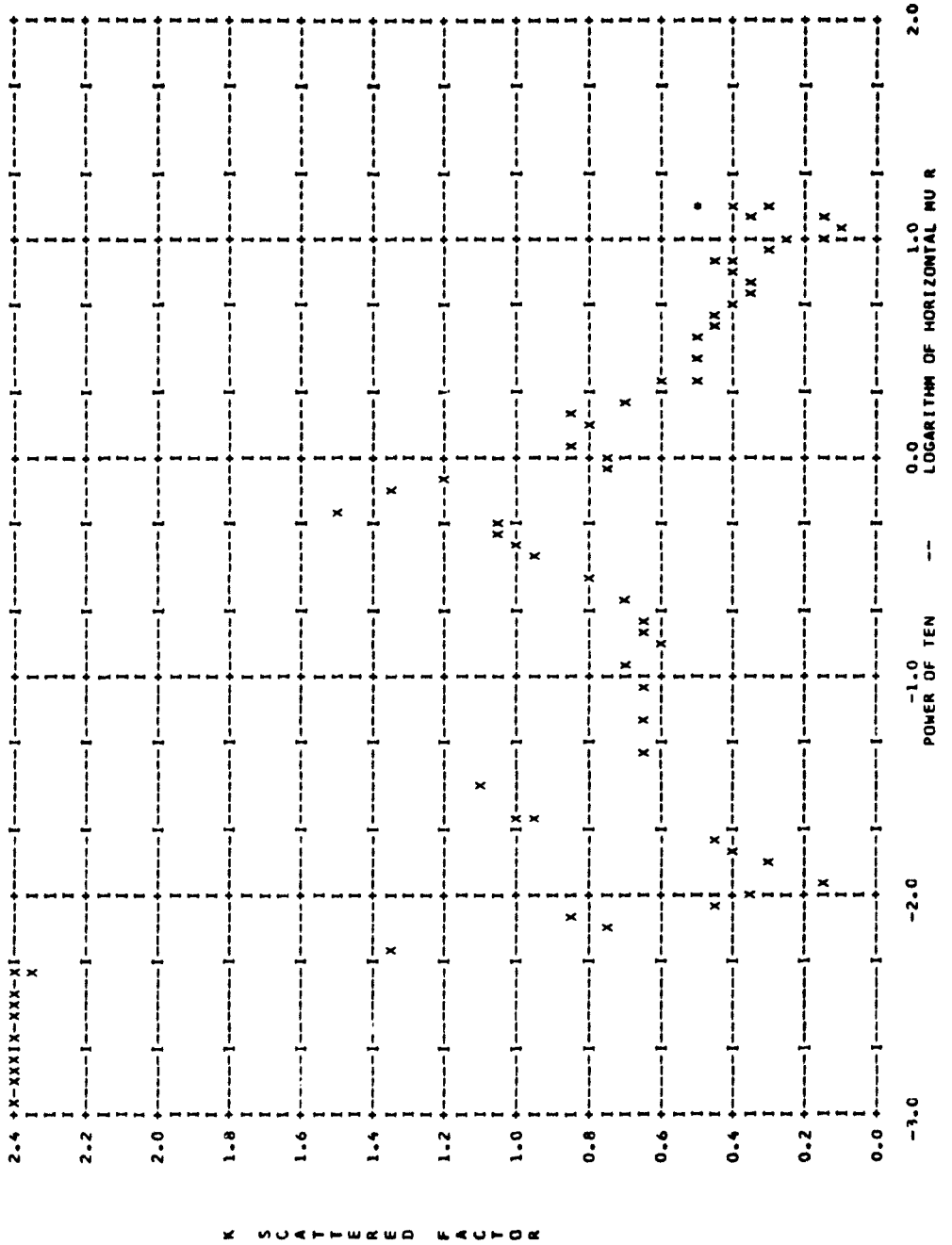
K SCATTERED FACTOR
2.4
2.2
2.0
1.8
1.6
1.4
1.2
1.0
0.8
0.6
0.4
0.2
0.0
-3.0
-2.0
-1.0
0.0
1.0
2.0
POWER OF TEN
LOGARITHM OF HORIZONTAL MU R
PROBLEM 206 K-SCATTERED FACTOR AVERAGED 1 TIMES OBSERVATION LEVEL = 0.
NEW RADS

Fig. 55

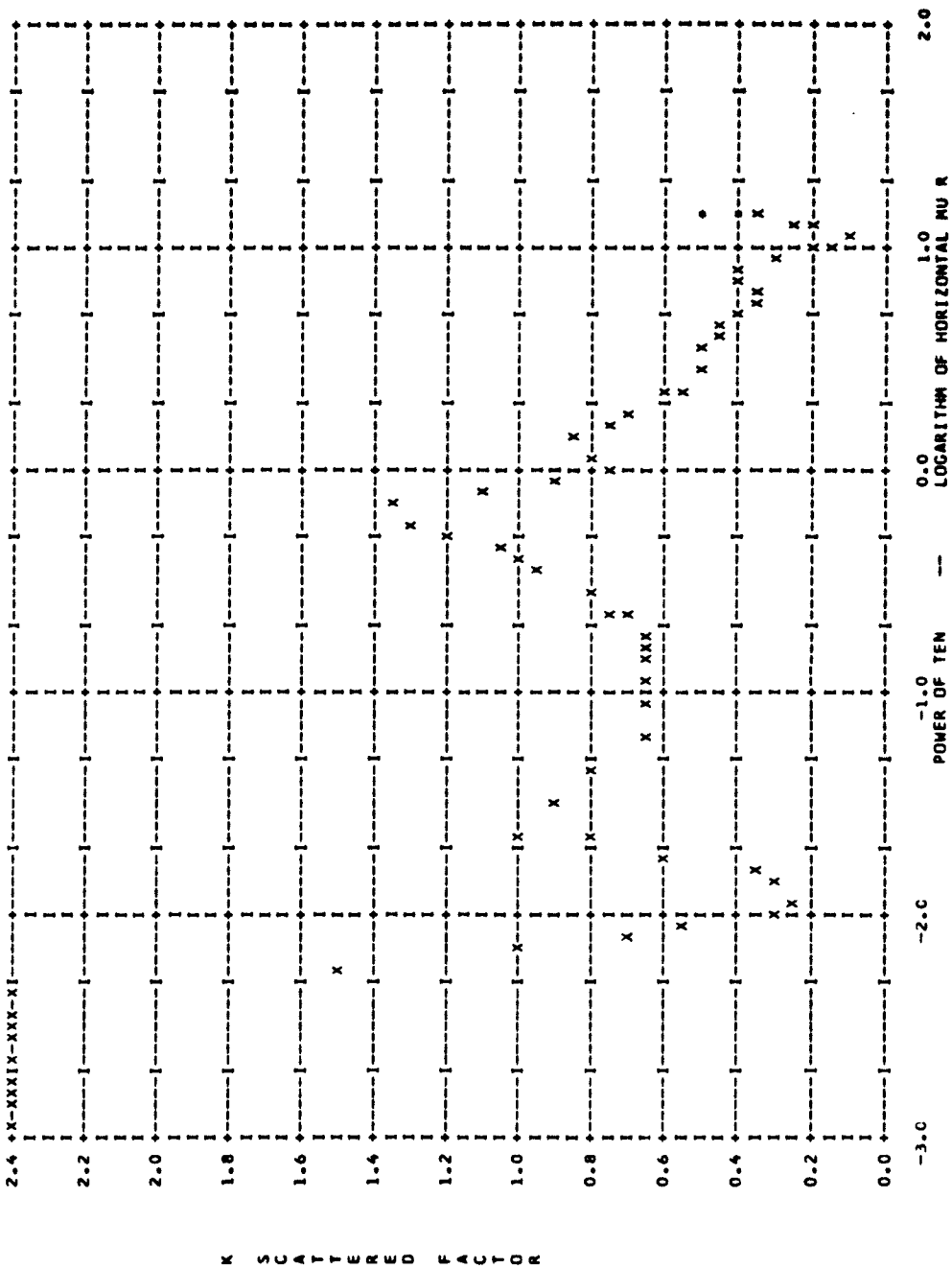
K SCATTERED FACTOR
2.4
2.2
2.0
1.8
1.6
1.4
1.2
1.0
0.8
0.6
0.4
0.2
0.0
-3.0
-2.0
-1.0
0.0
1.0
2.0
POWER OF TEN
LOGARITHM OF HORIZONTAL MU R
PROBLEM 206 K-SCATTERED FACTOR AVERAGED 2 TIMES OBSERVATION LEVEL = 0.
NEW RADS

Fig. 56

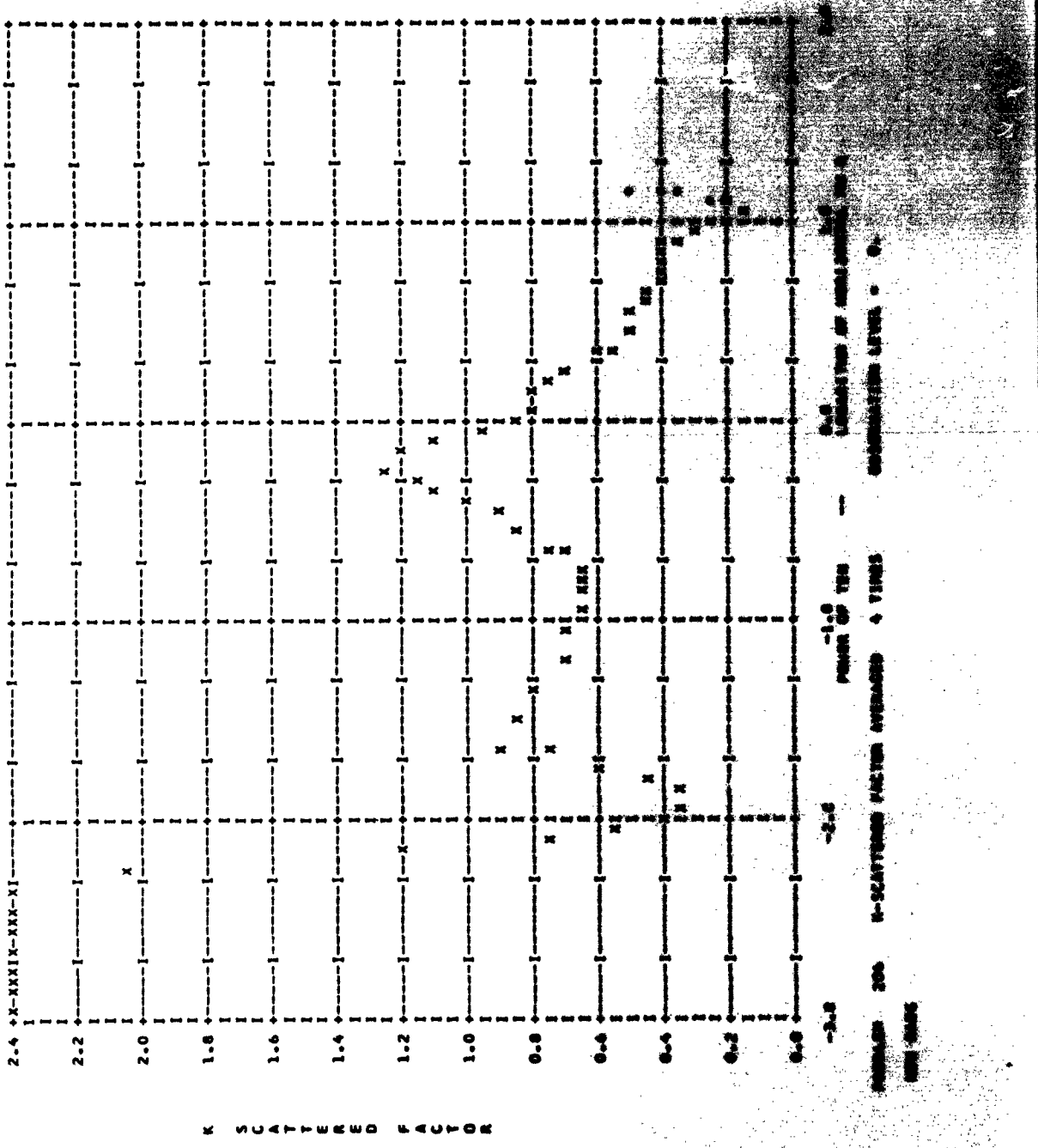

Fig. 57

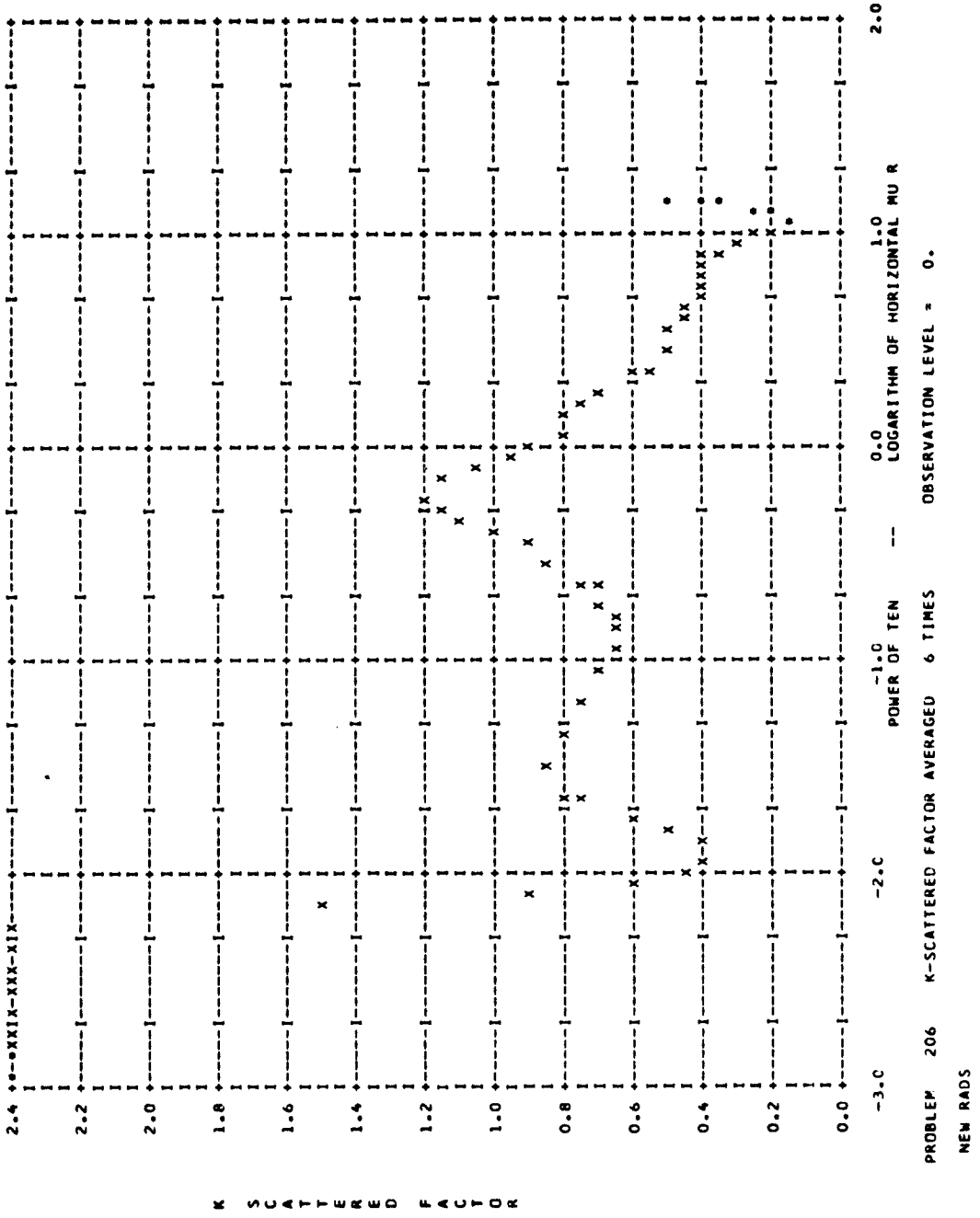
K SCATTERED FACTOR
2.4
2.2
2.0
1.8
1.6
1.4
1.2
1.0
0.8
0.6
0.4
0.2
0.0
-3.0
-2.0
-1.0
0.0
1.0
2.0
POWER OF TEN
LOGARITHM OF HORIZONTAL MU R
PROBLEM 206 K-SCATTERED FACTOR AVERAGED 6 TIMES OBSERVATION LEVEL = 0.
NEW RADS

Fig. 58

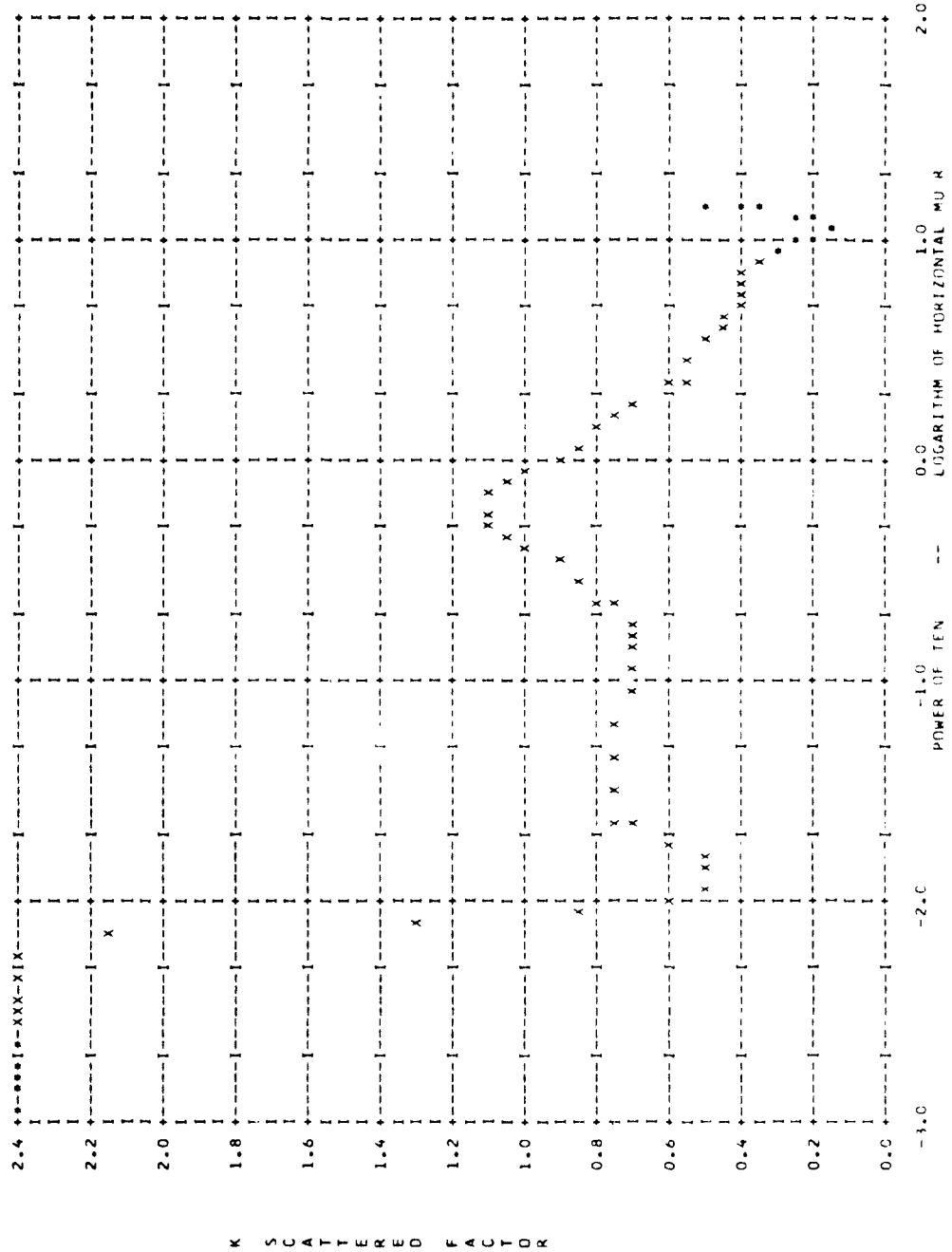
K SCATTERED FACTOR AVERAGED
2.4
2.2
2.0
1.8
1.6
1.4
1.2
1.0
0.8
0.6
0.4
0.2
0.0
-3.0
-2.0
-1.0
0.0
1.0
2.0
POWER OF TEN
LOGARITHM OF HORIZONTAL MU R
PROBLEM 206 K-SCATTERED FACTOR AVERAGED 10 TIMES
OBSERVATION LEVEL = 0.
NEW RADS

Fig. 59

12. Woodward, Kent T., G. M. McDonnel, P. S. Harris, W. J. Kirkland and J. N. Shively, "The Response of Swine after Exposure to the Gamma-Neutron Flux of a Nuclear Detonation," The American Journal of Roentgenology Radium Therapy and Nuclear Medicine, Vol. 85, January 1961.

13. Control Studies Performed in the United States and Eniwetok, Parts I, II, IV, and VI, Operation GREENHOUSE, Scientific Director's Report Annex 2.2, WT-18, pp. 123-143.

14. Effects of Very-Low-Yield Bursts on Biological Specimens (Swine and Mice), (U), Operation HARDTACK, ITR-1663, Headquarters Field Command, Defense Atomic Support Agency, June 8, 1959, (Secret Restricted Data).

15. Bond, V. P., R. E. Carter, J. S. Robertson, P. H. Seymour and H. H. Hechter, "The Effects of Total-body Fast Neutron Irradiation in Dogs," Rad. Res., Vol. 4, pp. 139-153 (1956).

16. Alpen, H. L., O. S. Shill and B. Tochilin, "The Effects of Total-body Irradiation of Dogs with Simulated Fission Neutrons," Rad. Res., Vol. 12, pp. 237-250, (1960).

17. Bond, V. P. and J. L. Bateman, Relative Biological Effectiveness, BNL-4864, Medical Research Center, Brookhaven National Laboratory, May 24, 1960.

18. Allen, R. G., F. A. Brown, L. C. Logie, D. R. Rovner, S. G. Wilson, Jr., and R. W. Zellmer, "Acute Effects of Gamma Radiation in Primates," Rad. Res., Vol. 12, May 1960, p. 532.

19. Alpen, E. L., and S. J. Baum, "Autologous Bone-Marrow Implantation After Fast Neutron Irradiation of Dogs," Rad. Res., Vol. 11, September 1959, p. 383.